Stochastic Coverage and Connectivity in Heterogeneous Wireless Sensor Networks

Thesis submitted in fulfillment of the requirements
for the degree of

Doctor of Philosophy

by

Hari Prabhat Gupta

Under the guidance of

S. V. Rao and T. Venkatesh

Department of Computer Science and Engineering
INDIAN INSTITUTE OF TECHNOLOGY GUWAHATI
Guwahati 781039, India
October 2014

Dedicated to

My parents

Declaration

I certify that

1. The work contained in this thesis is original and has been done by myself and the general supervision of my supervisors.

2. The work has not been submitted to any other Institute for any degree or diploma.

3. Whenever I have used materials (data, theoretical analysis, results) from other sources, I have given due credit to them by citing them in the text of the thesis and giving their details in the references.

4. Whenever I have quoted written materials from other sources, I have put them under quotation marks and given due credit to the sources by citing them and giving required details in the references.

Place: IIT Guwahati
Date:

Hari Prabhat Gupta
Ph.D. Student
Department of Computer Science and Engineering,
Indian Institute of Technology Guwahati,
Guwahati, Assam, INDIA 781039.

Certificate

*This is to certify that the work contained in this thesis entitled "**Stochastic Coverage and Connectivity in Heterogeneous Wireless Sensor Networks**" being submitted by **Hari Prabhat Gupta** (**Roll No. 10610101**), carried out in the Department of Computer Science and Engineering, Indian Institute of Technology Guwahati, is a bona fide research work of our supervision and is worthy of consideration for the award of the degree of Doctor of Philosophy of the Institute.*

Place: IIT Guwahati
Date:

Prof. S. V. Rao
Department of Computer Science and Engineering,
Indian Institute of Technology Guwahati,
Guwahati, Assam, INDIA 781039.

Dr. T. Venkatesh
Assistant Professor
Department of Computer Science and Engineering,
Indian Institute of Technology Guwahati,
Guwahati, Assam, INDIA 781039.

Acknowledgments

I would like to express my sincere gratitude to my supervisors Prof. S. V. Rao and Dr. T. Venkatesh for their valuable guidance, inspiration, and advice. Their support and encouragement generously paved the way for my development as a research scientist. I benefited greatly from many fruitful discussions with my supervisors, which has changed my personality, ability and nature in many ways. I feel very privileged to have had the opportunity to learn from, and work with them. I am highly grateful to my Doctoral Committee members, Prof. Diganta Goswami, Dr. Sonali Chouhan, and Dr. Saswata Shannigrahi. Their comments and suggestions have truly deepened and widened my understanding of the problems I had worked on.

I am thankful to TATA Consultancy Services, India for awarding me the research fellowship that gave me extremely good opportunities to broaden my research activities and interact with eminent researchers in the world, both from the industry as well as from the academia.

I would also like to express my heartfelt gratitude to the director, the deans and other management of IIT Guwahati whose collective efforts have made this institute a place for world-class education and research. I am thankful to all the faculty members and the staff of the Department of Computer Science and Engineering for extending their cooperation in terms of technical and official support. I am obliged to the research scholars, M. Tech and B. Tech students of this institute with whom I had closely worked.

I am indebted to all my friends, only to name a few, Tanima Dutta, Shrishendu Das, Debanjan Sadhukhan, and Rohit Tripathi with whom I have enjoyed my student life. Last but not the least, I would like to express my gratitude to my parents for their constant support and encouragement. Their motivation, assistance and guidance helped me to find the path for my future life.

Place: IIT Guwahati

Date: **Hari Prabhat Gupta**

Abstract

A wireless sensor network (WSN) consists of several tiny battery-powered sensors that can communicate with each other to monitor a Field of Interest (FoI). Coverage is acknowledged as an important metric to measure the quality of service of WSNs. It specifies how well a FoI is monitored by the WSN. Network connectivity is complementary to coverage and it indicates how well the sensory data can be communicated by the sensors to the sink. This thesis studies coverage and connectivity problems in WSNs with stochastic deployment of sensors and demonstrates their applications.

The main challenge in deployment of sensors is to make sure that a minimum number of sensors are used to provide the desired level of coverage and connectivity in the FoI. The first contribution of this thesis is to estimate the critical sensor density required for the desired coverage ratio under border effects in WSNs. This work can be used to accurately determine the sensors required in any convex polygon-shaped FoI. In some applications of WSNs, the sensors cannot be deployed directly inside the FoI to be monitored. For example, in canal water monitoring project, existing coverage solutions cannot be used because, the sensors cannot be deployed on the water surface. In the second contribution, we consider the sensors to be deployed uniformly at random outside the FoI near the boundary and estimate the minimum number of sensors required for desired level of coverage and connectivity. We also illustrate an application of this work to develop a traffic information acquisition system. The third contribution of this thesis is to consider a case when the sensors have only directional

sensing capability and may have heterogeneity in terms of the sensing range, communication range, and/or probability of being alive. For such heterogeneous directional WSNs, we derive probabilistic expressions for k-coverage and m-connectivity that are used to optimize the cost of random deployment.

Minimising the energy consumed while ensuring the desired level of coverage of a FoI is an important factor to be considered to extend the lifetime of WSNs because the batteries may not be accessible for replacement. In the last contribution, we derive an expression to determine the probability of a sensor, with a set of heterogeneous neighbours, being redundant for the desired coverage ratio of the FoI. We propose a distributed scheduling protocol to put the redundant sensors to sleep yet maintaining the k-coverage of the FoI in three-dimensional heterogeneous WSNs. We extend the protocol for partial coverage in two-dimensional heterogeneous WSNs. The proposed protocol is fully distributed and does not use any geographical information but, gathers information only about the number of neighbours and their type with periodic control messages.

Contents

List of Figures

List of Tables

List of Symbols

Symbol	Description
Ψ	Field of Interest (FoI)
Ω	Boundary region of a FoI
b	Width of a region Ω
l	Length of a region Ω
$\|xy\|$	Euclidean distance between points x and y
$\alpha(\overrightarrow{v_1}, \overrightarrow{v_2})$	Angle between vectors $\overrightarrow{v_1}$ and $\overrightarrow{v_2}$
$\|\|R\|\|$	Volume of the region R
$E[x]$	Expected value of x
$M_{x,y}$	Minimum value between x and y
η	Coverage ratio of a FoI
η_{th}	Desired coverage ratio of a FoI
η_k	k-coverage ratio of a FoI, $k \geq 1$
γ	Connectivity probability of a WSN
γ_m	m-connectivity probability of a WSN, $m \geq 1$
In homogeneous WSNs	
S	Sensing range of a sensor
C	Communication range of a sensor
ϕ	Sensing region of a sensor
ζ	Communication region of a sensor

Φ	Effective sensing region of a sensor
Υ	Effective communication region of a sensor
θ	Cone-of-view angle of a sensor

In heterogeneous WSNs

s_i	A type i sensor
S_i	Sensing range of a type i sensor
C_i	Communication range of a type i sensor
p_i	Liveness fraction of a type i sensor
$Cost_i$	Cost of a type i sensor
ϕ_i	Sensing region of a type i sensor
ζ_i	Communication region of a type i sensor
Φ_i	Effective sensing region of a type i sensor
Υ_i	Effective communication region of a type i sensor
θ_i	Cone-of-view angle of a type i sensor
ξ_i	Redundancy degree of a type i sensor for partial coverage of a FoI
ξ_i^k	Redundancy degree of a type i sensor for k-coverage of a FoI

Chapter 1

Introduction

1.1 Overview

Wireless sensor networks (WSNs) have attracted a great deal of attention due to the wide variety of their applications. A typical WSN consists of several tiny sensors powered by batteries which can communicate with each other to monitor a Field of Interest (FoI). WSNs monitoring a FoI are commonly found in applications like battlefield surveillance, environment monitoring, health care, inventory tracking, intrusion detection, and fire detection. Some of these applications use a stochastic deployment of sensors, where a large number of sensors are spread across the FoI in a random fashion. Random deployment is favoured in situations where the FoI to be monitored is hostile or inimical and this is also a popular assumption in theoretical analysis [1]. In such a deployment, all the sensors may not have the same sensing and/or communication ranges. The ranges of the different sensors might also become unequal over the time due to battery drain and imperfect sensing conditions. Such WSNs are frequently called *heterogeneous WSNs* (HWSNs) in the literature [1].

In any application of a WSN that involves monitoring a FoI, sensing coverage or simply *coverage* is acknowledged as an important metric to measure the quality of service (QoS) of the WSN. It specifies how well a FoI is monitored by the WSN.

Any event that occurs in the FoI can be detected by a sensor if the location of the event is within its sensing region [3]. Coverage can be classified into three categories: target coverage, barrier coverage, and area coverage [4]. In this thesis, we focus on area coverage, where the goal of WSNs is to deploy sensors in strategic ways, such that an optimal area coverage is achieved according to the needs of the underlying applications.

In certain applications of WSNs like intruder detection and tracking, it might be necessary to detect every intruder by at least k sensors to improve the accuracy of detection [5], where $k \geq 1$. A FoI is said to be k-covered, if each point therein is covered by at least k active sensors. In *stochastic k-coverage*, a point in the FoI is said to be *k-covered* if it falls within the sensing regions of at least k sensors [6]. In some applications of WSNs like forest fire detection and weather forecasting, the requirement of complete coverage of the FoI, may be too expensive or unnecessary. For example, in summer season the entire forest area may need to be covered while in the other seasons only part of the region may need to be covered [7]. When complete coverage is not necessary, WSNs can be made energy-efficient by relaxing the quality of coverage (QoC). *Partial coverage* refers to the relaxation in the QoC that requires only a part of the FoI to be covered. Coverage ratio is a term used in the literature to quantify the QoC. It is defined as the ratio of the area covered by the sensors to the total area of the field. In terms of the coverage ratio, partial coverage requires that the coverage ratio be no less than a pre-defined threshold (smaller than unity).

Network connectivity or simply *connectivity* is complementary to coverage and it indicates how well the data gathered can be communicated by the sensors to the sink. When a WSN is modeled as a graph with sensors as the vertices and the communication link between two sensors as an edge, a connected WSN means that the underlying graph is connected. A WSN is said to be m-connected if removal of any (m-1) sensors does not render the underlying communication graph disconnected [8],

where $m \geq 1$. As the sensors are low-cost devices with constrained resources, each sensor has only limited communication range compared with the size of the FoI. Multi-hop communication is used when a sensor cannot reach the sink directly.

In stochastic deployment of WSNs, minimising the energy consumed while ensuring the desired level of coverage of a FoI is an important factor to be considered to extend the lifetime of the WSNs because the batteries may not be accessible for replacement. On the other hand, from a cost perspective, it is often very important to maintain the desired coverage and connectivity with a minimum number of sensors. In this thesis, we focus on partial coverage, k-coverage, and m-connectivity problems in stochastic deployment of heterogeneous sensors in two-dimensional (2D) and three-dimensional (3D) FoI. By using the results in our work, one can effectively design, deploy and operate a WSN in a cost-efficient and energy-efficient manner.

1.2 Motivation of the Research Work

WSNs are often deployed to monitor a FoI and sensory data should be reported to the user whenever the need arises. The main challenge in stochastic deployment of WSNs is to make sure that a minimum number of sensors are used to ensure the desired coverage ratio of the FoI. The problem of estimating the critical sensor density (CSD) for partial coverage is complicated when the border effects are considered [8]. Due to the border effects, the sensors near the boundary of the FoI, cover a smaller area than those located deep inside the FoI. This is because, a part of the sensing disc of the sensors near the boundary might be outside the FoI (which is not of interest in coverage) [9]. The literature on determining the critical sensor density (CSD) for partial coverage assumes that the FoI is unbounded or toroidal in shape [10, 11, 12]. Although it is not a realistic assumption, it eliminates the border effects in analysis. Since the entire sensing area of the sensors near the boundary may not be useful for the coverage, the CSD estimated without the border effects is lower than the actual

value.

In most of the cases the sensors are deployed directly in the FoI to be monitored. However, in some applications, the sensors cannot be deployed directly inside the FoI. For example, in canal water monitoring application [13], the sensors cannot be deployed on the water surface. Similarly, there exist applications such as the traffic information acquisition systems (TISs), where the sensors cannot be directly deployed on the road to be monitored. Other examples where the sensors can only be deployed outside the monitored region are: railway track monitoring system [14], water transport monitoring system, and country border monitoring system [15]. In applications where the sensors cannot be deployed directly in the FoI, the existing literature to compute the number of sensors required to ensure the desired coverage and connectivity is not useful.

Estimating the number of sensors required to ensure the desired coverage is useful to optimize the cost of the stochastic deployment of WSNs. At the same time, minimising the energy consumed while ensuring the QoC is another important issue in WSNs because the batteries may not be accessible for replacement. A popular technique used for energy-efficient coverage of the FoI is to identify if there are redundant sensors and schedule them to sleep without compromising the QoC of the FoI. Determining the probability of a sensor being redundant for the desired level of coverage is complicated when the sensors are heterogeneous and no information about the geographical location or relative position is available. Unfortunately, there is no work in the literature on coverage-preserving scheduling protocols for heterogeneous WSNs that can work without the sensors using information about geographical location or relative position.

1.3 Contributions of the Thesis

In this thesis, we assume that the sensors are deployed uniformly at random independent of each other. We derive probabilistic expressions for desired coverage and connectivity that are used to optimize the cost of random deployment. We propose a coverage-preserving scheduling protocol to put the redundant sensors to sleep. The main contributions of the thesis are summarised by the following problems addressed:
Problem 1 (Partial coverage under border effects): What is the CSD required for a desired coverage ratio in a convex polygon-shaped FoI, with the sensors deployed uniformly at random by considering the border effects?

The literature on the estimation of the CSD for partial coverage considering the border effects assumed that the FoI is in the shape of either a circle, a rectangle, or a square, and the coverage ratio is derived only for that shape. In some practical applications such as, habitat monitoring, wildlife monitoring, and forest fire monitoring, the FoI will not be in a regular shape.

We derive expression for the expected value of the effective sensing area of a sensor that is useful for partial coverage of the FoI under *border effects* in WSNs. We consider the exact geometry of the FoI and the probability of a sensor being located anywhere in the FoI. We extend the analysis to derive the CSD required to maintain the desired coverage ratio in a FoI with sensors distributed uniformly at random.
Problem 2 (k-coverage and connectivity with border deployment): How many sensors are required to ensure that a FoI is k-covered by a connected WSN, when the sensors are deployed uniformly at random outside the FoI near the boundary?

The literature on WSNs assumes that the sensors are deployed directly in the FoI to be monitored. However, in some applications, the sensors cannot be deployed directly inside the FoI.

We analyze k-coverage and connectivity of a FoI when the sensors are deployed uniformly at random *outside the FoI near the boundary*. We determine the area of the

sensing and communication regions of a sensor useful for k-coverage and connectivity and calculate the minimum number of sensors required for the deployment. We also demonstrate an application of the analysis in deployment of a traffic information acquisition system based on WSNs.

Problem 3 (k-coverage and m-connectivity in 3D directional HWSNs): When a large number of heterogeneous directional sensors are deployed uniformly at random in a 3D FoI, what is the expected value of the FoI that is k-covered and the expected value of m-connectivity of the 3D HWSN?

Most of the literature on 3D WSNs assumed the omni-directional sensing model where a sensor can perfectly sense within the sphere of a given radius centred at the location of the sensor. Moreover, the literature on 3D WSNs assumed either that the probability of a sensor being alive is unity or is constant for all the sensors.

In this problem, we consider a case when the sensors have only directional sensing capability and may have heterogeneity in terms of the sensing range, communication range, and/or probability of being alive. For such 3D heterogeneous directional WSNs, we derive the expected value of the k-coverage of the 3D FoI. We also estimate the expected value of m-connectivity in a 3D HWSN which can determine the communication range and the liveness fraction required to create an m-connected HWSN. Finally, we demonstrate an application of the analysis to compute the number of sensors of each type required to ensure the desired k-coverage ratio and m-connectivity probability while optimising the network cost.

Problem 4 (Scheduling protocol for k-coverage in 3D HWSNs): How to determine the redundancy of a sensor for k-coverage of the 3D FoI without any information about the geographical location/relative position of 3D HWSNs?

The literature on coverage-preserving scheduling protocols in 3D WSNs considers the coverage problem in homogeneous WSNs using location information. The assumption of homogeneity is usually hard to maintain in large scale WSNs.

We derive an expression to determine the probability of a sensor, with a set of neighbours of different types, being redundant for a desired coverage level. We propose a distributed scheduling protocol to put the redundant sensors to sleep yet maintaining the desired level of coverage in the 3D FoI. This protocol does not require the sensor to have any information about its geographical location/relative position to discover its redundancy.

Problem 5 (Scheduling protocol for partial coverage in 2D HWSNs): When a large number of heterogeneous sensors are deployed uniformly at random in a 2D FoI, how to determine the redundancy of a sensor for partial coverage of the FoI?

The literature on coverage-preserving scheduling protocols in 2D WSNs considers the coverage problem in homogeneous WSNs. No existing work considers the partial coverage problem in 2D heterogeneous WSNs without location information.

We propose a probabilistic approach to determine the redundancy of sensors while satisfying partial coverage requirements in a HWSN. We derive an expression to evaluate the expected redundancy degree of a sensor and use it to determine if a sensor is redundant for a desired coverage ratio of the FoI. We propose a scheduling protocol to identify all the redundant sensors and schedule them to sleep while ensuring the QoC. The protocol is completely distributed, does not use any geographical information, and uses only the information gathered about the neighbours with a few control messages.

1.4 Organisation of the Thesis

The rest of the thesis is organised as follows: In next chapter, we present the state-of-the-art work with respect to the coverage and connectivity problems in WSNs. In Chapter 3, we estimate the critical sensor density required for partial coverage under border effects in WSNs. We calculate the number of sensors required for a desired level of coverage and connectivity when the sensors are deployed uniformly

at random outside the FoI near the boundary and illustrate an application of this work for traffic monitoring in Chapter 4. We derive probabilistic expressions for k-coverage and m-connectivity in 3D heterogeneous directional WSNs in Chapter 5. In Chapter 6, we derive an expression to determine the probability of a sensor, with a set of neighbours of different types, being redundant for k-coverage of a 3D FoI, and propose a distributed protocol to schedule the redundant sensors to sleep to prolong the lifetime of 3D HWSNs. In Chapter 7, we propose a scheduling protocol to identify all the redundant sensors and schedule them to sleep while satisfying partial coverage requirements in a 2D HWSN. Finally, the thesis ends with conclusions and discussion in Chapter 8.

Chapter 2

Background

In the chapter, we describe the generic components that form a WSN. We start by a brief review of the WSN operating systems, simulators, and testbeds. The remainder of this chapter contains the state-of-the-art work with respect to coverage and connectivity problems in WSNs.

2.1 Wireless Sensor Networks Hardware Systems

The main components of the physical architecture of a sensor can be classified into four major units: processing, storage, communication, and sensing. Table 2.1 lists out the main components of the architecture of some sensors [16].

• **Processing unit:** A processing unit in a sensor interacts with the components and executes the software. Sensors in WSNs have several types of processors based on their tasks, such as, microprocessors and/or microcontrollers, low power digital signal processors, communication processors, and application specific integrated circuits for certain special tasks.

• **Storage unit:** The current sensors have relatively small and low cost storage units. They most often consist of synchronous dynamic random access memory (SDRAM), electrically erasable programmable read-only memory (EEPROM), static random-

access memory (SRAM), and non-volatile (flash) memory.

• **Communication and sensing units:** The communication paradigms often associated with the current generations of WSNs are multi-hop communication. The literature in WSNs illustrates that the multi-hop communication can significantly reduce the energy consumption in large scale WSNs. Sensors in WSNs consist of sensing units, which interact with the physical world around the sensor.

Sensor	**Main components**
Tmote	• **Processing unit:** 8MHz Texas Instruments MSP430 microcontroller • **Storage unit:** 10k RAM and 48k Flash • **Communication unit:** 250kbps 2.4GHz IEEE 802.15.4 Chipcon Wireless Transceiver • **Sensing unit:** Integrated Humidity, Temperature, and Light sensors
BTnode	• **Processing unit:** Atmel ATmega128L(AVR RISC 8 MHz @ 8 MIPS) • **Storage unit:** 180 Kbyte SRAM, 128 Kbyte Flash ROM, 4 Kbyte EEPROM • **Communication unit:** Chipcon CC1000 operating in ISM Band 433-915 MHz • **Sensing unit:** UART, SPI, I2C, GPIO, ADC, Clock, Timer, LEDs Standard Molex
CSIRO Fleck	• **Processing unit:** Atmega128L, 8MHz • **Storage unit:** 512K external memory • **Communication unit:** Nordic 903 • **Sensing unit:** Temperature, Light, Screw terminal for 4X digital i/o and 2X analog
EYES	• **Processing unit:** MSP 430F149 (5 MHz @ 16 Bit) • **Storage unit:** 60 Kbytes of program memory and 4 Kbyte EEPROM • **Communication unit:** RFM TR1001 hybrid radio transceiver • **Sensing unit:** Compass, accelerometer, temperature sensor, light sensor, pressure sensor
MicaZ	• **Processing unit:** ATMEGA 128 • **Storage unit:** 4K RAM 128K Flash • **Communication unit:** 802.15.4/ZigBee compliant RF transceiver • **Sensing unit:** Large expansion connector
Telos	• **Processing unit:** Motorola HCS08 • **Storage unit:** 4K RAM • **Communication unit:** 250kbps 2.4GHz IEEE 802.15.4 • **Sensing unit:** Large expansion connector

Table 2.1 Main components of the architecture of some sensors.

2.2 Wireless Sensor Networks Operating Systems

One major challenge in a WSN is to produce low cost and tiny sensors. For network protocols to operate, an operating system that implements the protocols runs on every sensor. Operating systems for sensors in WSNs are typically lighter than general-purpose operating systems. A WSN has severe resource constraints in terms of processing power, memory size and energy. The operating system in WSNs must efficiently manage the constrained resources while providing a programming interface. In the sensor network research community, several operating systems have been developed, with each offering a different solution for the fundamental problems. In this section, we elaborate on the state-of-the-art WSNs operating systems.

• **TinyOS:** TinyOS is an open-source operating system designed for low-power and low-cost WSN devices. TinyOS is based on an event-driven programming model. TinyOS programs are composed of event handlers and tasks with run-to-completion semantics. When an external event occurs, such as an incoming data packet or a sensor reading, TinyOS signals the appropriate event handler to handle the event [17].

• **LiteOS:** LiteOS is an open source, interactive, and UNIX-like operating system designed for WSN devices. It runs on the following platforms: Windows XP/Vista/7, MicaZ as target board, and MIB510/MIB520 as programming boards [18].

• **Contiki:** Contiki is an open source operating system for networked and memory-constrained systems with a particular focus on low-power WSNs [19].

Table 2.2 illustrates a comparison between TinyOS, LiteOS, and Contiki.

2.3 Wireless Sensor Networks Simulators

A WSN simulator consists of various modules namely events, sensor, protocols, and applications. Each category is represented by an interface that defines its methods and events generated and consumed. There are many different possible platforms for

Feature	TInyOS	LiteOS	Contiki
Publication	2000	2008	2004
Language Support	nesC	LiteC++	C
Event Based Programming	Yes	Yes	Yes
Multi-Threading	Yes	Yes	Yes
Platform Support	Mica, Mica2, MicaZ, TelosB, Tmote, IRIS, Tinynode, Eyes	MicaZ, IRIS, AVR MCU	Tmote, TelosB, ESB, AVR MCU, MSP430 MCU
Simulator	TOSSIM, Power Tossim	Through AVRORA	Cooja, MSPSim, Netsim

Table 2.2 A comparison between TinyOS, LiteOS, and Contiki operating system.

simulation and testing of routing protocols for WSNs. In this section, we elaborate on the state-of-the-art WSNs simulators.

• **NS-2:** NS-2 is a discrete event simulator targeted at networking research [20]. NS-2 began as a variant of the REAL network simulator in 1989 and has evolved substantially over the past few years. It has an object-oriented design which allows for straightforward creation and use of the new protocols. The key features of NS-2 in WSNs include sensor channels, battery models, lightweight protocol stacks, hybrid simulation support, and scenario generation tools.

• **TOSSIM:** TOSSIM is a discrete event simulator for TinyOS WSNs, which was developed at UC Berkeley [21]. TOSSIM captures the behavior and interactions of networks not on the packet level but at network bit granularity. TOSSIM is designed specifically for TinyOS applications to be run on MICA Motes. TOSSIM simulates entire TinyOS applications. It works by replacing components with simulation implementations.

• **GLoMoSim:** Global Mobile Information System Simulator (GloMoSim) is a scalable simulation environment for large wireless and wired communication networks [22]. The node aggregation technique is introduced into GloMoSim to give significant bene-

fits to the simulation performance. In GloMoSim, each node represents a geographical area of the simulation. Hence the network nodes which a particular entity represents are determined by the physical position of the nodes.

2.4 Wireless Sensor Networks Testbeds

In this section, we elaborate on the state-of-the-art WSNs testbeds.

• **WISBED:** The WISEBED is a large-scale heterogeneous WSN testbed [23]. It is a joint effort of European Universities and Research Institutes. It facilitates end users and application through a variety of interfaces and unified algorithmic and software environment. WISEBED follows a hierarchical multi-hop architecture that consists sensors, gateways, portal server, and overlay network. The operating systems supported by WISEBED are Contiki and TinyOS. The WISEBED testbed provides a C++ library.

• **SensLAB:** SensLAB is a large-scale WSN testbed with a total of 1000 sensors deployed in France [24]. The main goal of SensLAB is to offer an accurate and efficient scientific tool to help in the design and development of large scale WSNs. The operating systems supported by SensLAB are Contiki and TinyOS. The SensLAB testbed provides a C++ library.

• **INDRIYA:** INDRIYA is a three-dimensional WSN deployed across three floors of the School of Computing at the National University of Singapore [25]. The testbed facilitates research in WSN programming environments, communication protocols, system design, and applications. It provides a public, permanent framework for development and testing of sensor network protocols and applications. The testbed comprises of 139 TelosB sensor. At present, more than 50% of the sensors include following sensing units: Passive and active infrared, accelerometer, magnetometer, light, temperature, and acoustic. Sensors run the TinyOS operating system and are programmed in the NesC programming language.

2.5 Coverage and Connectivity problems

2.5.1 Type of Coverage

Based on the subjects to be covered by a WSN, coverage can be classified into three categories: area coverage, point coverage, and barrier coverage [26].

• **Area coverage:** The objective of the area coverage is to monitor the FoI by a set of deployed active sensors. Fig. 2.1 illustrates an example of a random deployment of sensors to cover a given FoI, where disk represents the sensing range of a sensor.

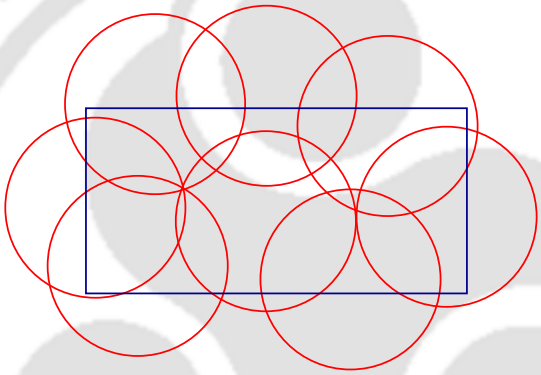

Figure 2.1 Illustration of the area coverage in the FoI.

• **Target Coverage:** Target coverage which is also known as point coverage, is to cover only a finite set of targets in the FoI. Fig. 2.2 shows an example of target coverage, where sensors s_1, s_2, and s_3 are monitoring targets T_1, T_2, T_3, T_4, and T_5. Target coverage is useful in surveillance environment data collections where fixed points or locations are required to be monitored.

• **Barrier coverage:** The main objective of barrier coverage concerns with constructing a barrier for intrusion detection. If any intrusion takes place along the barrier, then sensors can detect the intrusion. Barrier coverage is illustrated in Figure 2.3. On the basis of efficiency, barrier coverage is divided as strong barrier coverage and weak barrier coverage. Weak barrier coverage can only guarantee to detect intruders

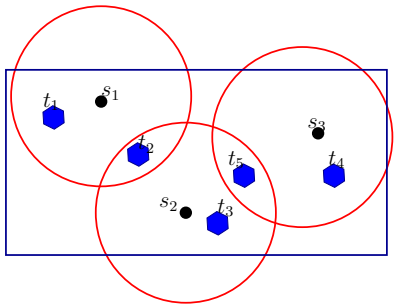

Figure 2.2 Illustration of the target coverage in the FoI.

moving along congruent paths.

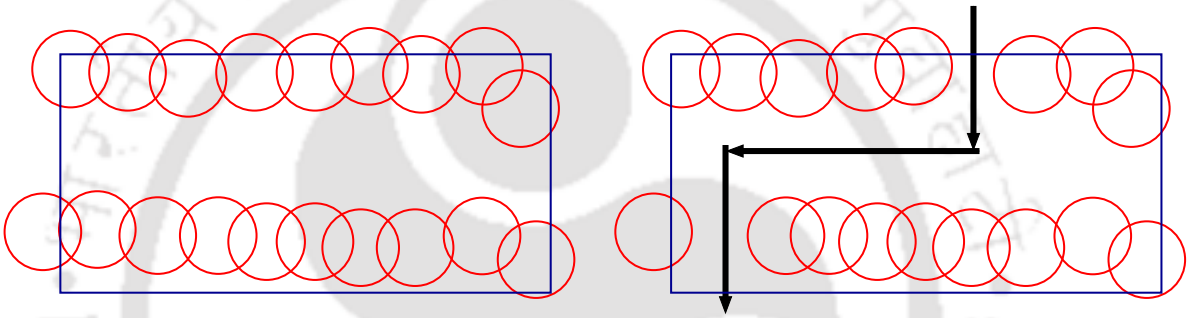

(a) Strong barrier coverage

(b) Weak barrier coverage

Figure 2.3 Illustration of the barrier coverage in the FoI.

2.5.2 Coverage and Connectivity Problems

Several different coverage formulaions arise naturally in many domains. The Art Gallery Problem determining the number of sensors necessary to cover an art gallery room such that every point in the gallery is seen by at least one sensor. The Art Gallery problem was solved optimally in 2D and 3D [27]. The coverage in WSNs is trying to answer *how well* the FoI is covered. Reference [4] provides a survey on sensor coverage techniques and algorithms in WSNs.

Maximum lifetime coverage protocols have naturally attracted a great deal of attention because the batteries may not be accessible for replacement. The maximum lifetime coverage problem can be defined as follows: *Given a WSN and a FoI, find*

a set of sensors that provides the desired level of coverage and the time duration for the set of sensors to be active, such that to maximize the network lifetime. Many solutions have been proposed for enhancing the lifetime of 3D WSNs and 2D WSNs. Most of the existing work focus on a mechanism to organize the sensors into a number of scheduling subsets such that each subset can provide the desired level of coverage in order for enhancing network lifetime. The work in [2] derives the necessary conditions to determine if a sensor is redundant. The work in [28, 29] identified if there are redundant sensors for complete coverage of the FoI. Though the work in [6] considers the heterogeneity of sensors for the coverage and connectivity problem. In [30], the authors propose a Coverage Connectivity Protocol (CCP) that guarantees both connectivity and coverage when the communication range of a sensor is at least twice its sensing range. Chapter 6 and Chapter 7 briefly discuss previous work on coverage preserving scheduling protocols in 3D WSNs and 2D WSNs, respectivey.

A low cost WSN has attracted a great deal of attention in the environment monitoring due to potentially large economic impacts. The low cost coverage and connectivity problem can be defined as follows: *Given a WSN and a FoI, estimate the CSD that provides the desired level of coverage and connectivity.* Zhang and Hou in [10] analysed the CSD required to cover a FoI when the sensors are deployed following a Poisson point process. In [11], the authors derived the sensor density for a square-shaped FoI with the sensors deployed following a Poisson point process, a uniform distribution, and a grid deployment. The authors in [12] derived an upper bound for the lifetime of a large scale WSN with a dense deployment. Lazos and Poovendran in [1] formulated the stochastic coverage problem in heterogeneous WSNs as a set intersection problem. The authors in [31] estimated critical transmitting and sensing ranges for desired coverage and connectivity in 3D homogeneous WSNs. Ammari and Das in [6] proposed the Reuleaux tetrahedron model to characterize k-coverage of a 3D FoI and investigated the minimum sensor density required when the sensors

are deployed following a uniform distribution. Recently the work in [32] studied the fundamental properties of 3D MANETs: link probability, node degree, and network coverage. Chapter 3 briefly discusses previous work on partial coverage. Chapter 5 reviews the work in the literature that addresses k-coverage and m-connectivity problems in WSNs.

Chapter 3

Critical Sensor Density for Partial Coverage under Border Effects in WSNs

3.1 Introduction

Coverage is one of the fundamental requirement in almost all WSN applications. A FoI is said to be *completely covered* if each point in the FoI lies in the sensing region of at least one active sensor. In certain applications like forest fire detection and weather forecasting, complete coverage may be expensive or unnecessary. Other real-life situation is an indoor navigation or location system, where selected regions are covered [33]. The problem of *partial coverage* refers to a relaxation in the desired QoC that requires only a part of the FoI to be covered. *Coverage ratio*, which is defined as the ratio of the area covered by the WSN to the total area of the field, is typically used to measure the QoC [8]. Typically, the partial coverage problem requires that the coverage ratio be no less than a pre-defined threshold. Note that, if the desired coverage ratio is unity, then the partial coverage problem degenerates to the complete coverage problem. In this work, we estimate the CSD required to achieve a desired

coverage ratio in a FoI with a stochastic deployment of sensors.

The problem of estimating the CSD is complicated when the *border effects* are considered [8, 34]. Due to the border effects, the sensors near the boundary of the FoI, cover a smaller area than those located deep inside the FoI. This is because, a part of the sensing disc of the sensors near the boundary might be outside the FoI (which is not of interest in coverage) [9]. When the sensor density is estimated by neglecting the border effects, it would be lower than the exact value due to the assumption that the entire sensing area of a sensor is useful for the coverage. We introduce the term *effective sensing area* to indicate the area of the sensing disc inside the FoI, which is equal to the entire sensing area for those sensors deep inside the FoI.

The literature on the estimation of the CSD for coverage considering the border effects assumed that the FoI is in the shape of either a circle, a rectangle, or a square, and the coverage ratio is derived only for that shape. In some practical applications such as, habitat monitoring [35], wildlife monitoring [36], and forest fire monitoring [37], the FoI will not be in a regular shape. A FoI is said to be *irregular* convex-shaped FoI if the sides of the FoI are not all the same length or interior angles of the vertices of the FoI do not all have the same measure. Parts (a) and (b) of Fig 3.1 illustrate regular and irregular convex-shaped FoIs, respectively.

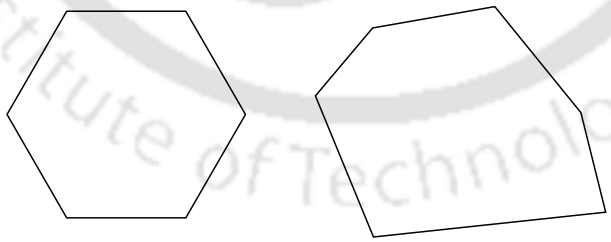

(a) Regular FoI (b) Irregular FoI

Figure 3.1 Illustration of a convex polygon shaped FoI with 6 vertices.

In this chapter, we address the problem: *what is the CSD required for a desired coverage ratio in a convex polygon-shaped FoI, with the sensors deployed uniformly*

at random by considering the border effects? We consider the exact geometry of the FoI and the probability of a sensor being located anywhere in the FoI to estimate the expected value of the effective sensing area of a sensor (that is useful for coverage). We extend the analysis to derive the CSD required to maintain the desired coverage ratio in a FoI with sensors distributed uniformly at random. Through numerical evaluation and simulation we validate the analysis and demonstrate the significance of border effects and the geometry of the FoI on the estimation of the sensor density.

The rest of the chapter is organised as follows: In the next section, we briefly discuss the literature on the estimation of sensor density for a desired coverage and present the motivation for this work. In Section 3.3, we derive the expected value of the effective sensing area of a sensor at random considering the border effects. In Section 3.4, we extend the analysis to estimate the CSD for a desired coverage ratio. Section 3.5 presents the numerical results that validate and demonstrate the impact of border effects on CSD. We conclude the chapter in Section 3.6.

3.2 Related Work

The coverage problem in WSNs has been addressed widely in the past and surveyed comprehensively in [4]. In this section, we review significant contributions in the literature on the estimation of the CSD for coverage both with and without considering the border effects.

Zhang and Hou in [10] analysed the sensor density required to cover a square-shaped FoI when the sensors are deployed following a Poisson point process. The analysis is subsequently used to derive an upper-bound for the lifetime of a WSN. The same authors in [11] derived the sensor density for a square-shaped FoI with the sensors deployed following a Poisson point process, a uniform distribution, and a grid deployment. It was concluded that the grid deployment requires the lowest density of sensors than any random deployment. The authors in [12] also derived an upper

bound for the lifetime of a large scale WSN with a dense deployment. The work done in [10, 11, 12], avoided the border effects by modelling the FoI as a torus. In a toroidal field, the sensors near one edge are assumed to also cover the region near the opposite edge of the FoI. Due to this assumption, the entire sensing area of a sensor is useful for coverage and hence, the estimated sensor density will be lower than that done with the border effects. Since it is not realistic to assume a toroidal FoI, some work in the literature considered the impact of border effects on the coverage ratio and the sensor density.

Lazos and Poovendran in [1] formulated the stochastic coverage problem (coverage under random deployment) in heterogeneous WSNs as a set intersection problem. The authors used results from integral geometry to derive the coverage ratio in a bounded FoI with any distribution of sensors. They also derived the number of sensors and the sensing range required for a desired coverage ratio. However, the analysis only considers the perimeter and the area of the FoI and not the exact geometry of the FoI. Since two regions with same area or perimeter might require different number of sensors based on their shape, ignoring the actual shape does not ensure that the sensor density is minimal.

In [9], the expected coverage ratio is derived for stochastic deployment in a rectangular-shaped FoI. The expected coverage by a sensor was estimated from the area of intersection between the sensing disk (of circular shape) and the rectangular strips of the boundary region. Though it is the closest one to our approach, it is only applicable for a rectangular region. Our analysis is applicable for any convex polygon shape. The authors in [38] derived the coverage ratio for a given sensing range and the density of sensors. They assumed that the sensors are deployed following a Poisson point process or a uniform point process in a bounded square or circular region. Jin *et al.* in [8] studied the density required for both coverage and connectivity of WSNs with border effects and proposed a location-independent routing algorithm. However,

the sensors were assumed to be uniformly deployed in a circular-shaped FoI. Wang *et. al.* in [39] also studied the sensor density for complete information coverage of a FoI with stochastic deployment. The authors derived an upper bound for the probability of an arbitrary point in the field not being information covered.

Motivation: Most of the literature except [1] assumed that the FoI is in the shape of either a circle, a rectangle, or a square, and the coverage ratio is derived only for that shape. In some practical applications such as, habitat monitoring [35], wildlife monitoring [36], and forest fire monitoring [37], the FoI will not be in a regular shape. Similarly, we believe that the exact shape of the FoI should be considered, and not just the perimeter or area to get a tighter estimate of the CSD with the border effects. These limitations in the literature motivate us to determine the CSD for an expected coverage ratio of a convex polygon shaped FoI considering the border effects. Since we derive the expected coverage ratio of a bounded convex polygon shaped FoI, the results are also applicable to any other regular shape (for *e.g.*, circle, ellipse, or rectangle). Incidentally, we demonstrate the significance of border effects for a low density deployment of sensors with a large sensing range. Though, we assume that the sensors are uniformly deployed, our analysis can be applied for any other spatial distribution with a well-known density function. We also discuss how our analysis can be applied to an irregular convex region and non-disc sensing model.

3.3 Estimation of the Effective Sensing Area

In this section, we choose a sensor at random from a convex polygon shaped FoI, and compute the expected value of its effective sensing area. Obviously if a sensor lies deep inside the region, its entire sensing region contributes to the coverage. But, if a sensor lies near the boundary, its effective sensing area is smaller than the total sensing area. We estimate the expected value of the effective sensing area of a sensor in the boundary region. We consider the exact geometry of the boundary region,

whose width is equal to the sensing range of the sensor, to estimate the effective sensing area.

We assume that the sensors are deployed uniformly at random, independent of each other, in a convex polygon-shaped FoI. Such a deployment is justified when a large number of sensors are air-dropped in a hostile environment. This is a common assumption in the literature, both for theoretical analysis [40, 41] and in real applications [42]. We assume the *binary disc sensing* model [8] in which a sensor located at a point s, can only sense perfectly within a circular region of radius S centred at s, denoted by $A(s, S)$. Any event that occurs outside $A(s, S)$ cannot be detected by the sensor at s. The area covered by a sensor at s, which is also its sensing area, is simply the area of $A(s, S)$, denoted by $\|A(s, S)\| = \pi S^2$. Due to the border effects, the sensors near the boundary can only cover an area smaller than their sensing area.

Consider a convex polygon-shaped FoI Ψ illustrated in Fig. 3.2(a). As shown in the figure, the polygon has six vertices $v_0, v_1, \ldots, v_5$, with the length of the edge (v_k, v_{k+1}) denoted by l_k. The angles at the vertices are denoted by $\theta_0, \theta_1, \ldots, \theta_5$. Let us formally define the effective sensing region of a sensor as the region of intersection between its sensing disc and the FoI, *i.e.*, $A(s, S) \cap \Psi$. Obviously, the area of this region depends on the position of the sensor. When the sensor is located deep inside Ψ, indicated as the center region C in Fig. 3.2(b), the effective sensing region is the disc $A(s, S)$ itself. However, if the sensor is at the point $s \in D$ shown in Fig. 3.2(c), which is within a distance of S from the edges of the FoI, its entire sensing region does not contribute to the coverage. It is easy to infer that the boundary region D, is simply a strip of width S, where S is the sensing range of the sensors. The boundary region is the shaded region in Fig. 3.2(c). If a sensor lies at a distance greater than S from the edge, which means that it lies in the region C, its entire sensing area contributes to the coverage. Otherwise, part of its sensing region lies outside the FoI and border effects must be considered to account for its reduced contribution to the

coverage area.

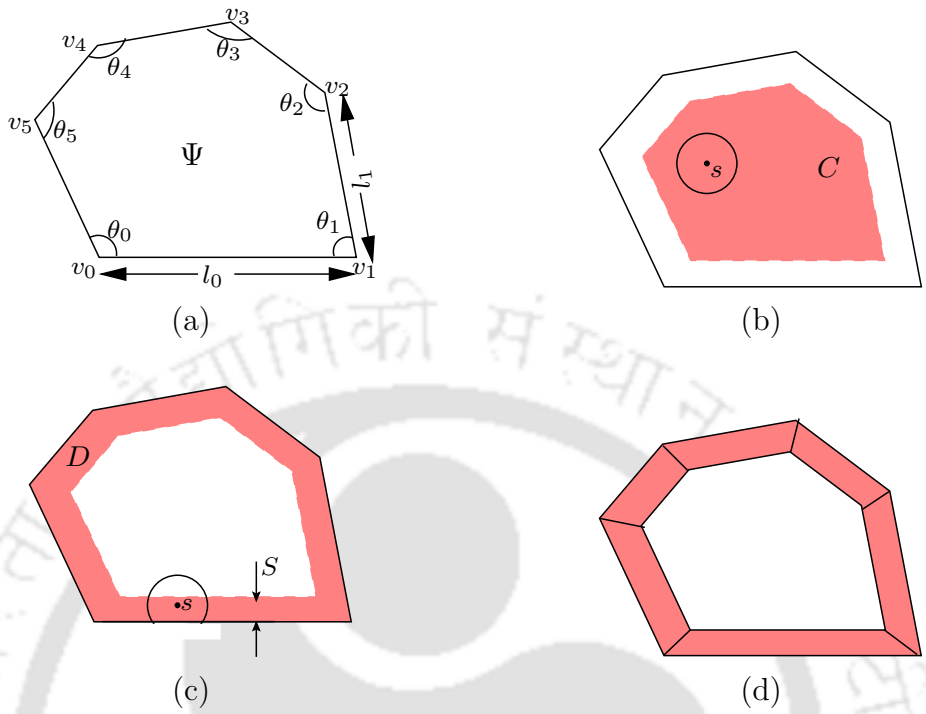

Figure 3.2 Illustration of a convex polygon shaped FoI Ψ with 6 vertices.

3.3.1 Area of the FoI and the boundary region

From Figs. 3.2(b) and 3.2(c), it can be observed that any polygon can be divided into two disjoint regions: a boundary region D of width S, and the remaining center region C. First, we determine the areas of these two regions in terms of the coordinates of the vertices, angles at the vertices, and lengths of the edges of the polygon. The area of a convex polygon Ψ with n vertices illustrated in Fig. 3.2(a) is given by

$$\|\Psi\| = \sum_{k=0}^{n-1} \left(\frac{1}{2} x_k y_{(k+1) \bmod n} - \frac{1}{2} y_k x_{(k+1) \bmod n} \right), \tag{3.1}$$

where (x_k, y_k) are the coordinates of the vertices v_k of the polygon for all $0 \leq k \leq n-1$.

As illustrated in Fig. 3.2(d), the boundary region D of a 6-vertex polygon can be

partitioned into six trapezoids. For any arbitrary polygon on n vertices, given the lengths of the edges and the angles at the vertices, the area of the boundary region D can be computed from the sum of the areas of the n trapezoids. Based on simple results from geometry, the area of the boundary region D can be expressed as

$$\|D\| = \sum_{k=0}^{n-1} \frac{S}{2} \left(2l_k - \frac{S}{\tan(\theta_k/2)} - \frac{S}{\tan(\theta_{(k+1) \bmod n}/2)} \right), \tag{3.2}$$

where l_k is the length of an edge (v_k, v_{k+1}), θ_k is the angle at v_k, and S is the width of the boundary region (also the sensing range of sensors).

3.3.2 Definition of the effective sensing area

Let c denote the event that a sensor picked at random is located in the region C and d denote the event that it is located in the region D. As mentioned earlier, the expected value of the sensing area of a sensor in C, denoted by $E[P]$, is simply equal to πS^2. Let $E[B]$ be the expected value of the sensing area of a sensor in the region D. Since the sensor lies either in C or D, the expected value of the effective sensing area of a sensor in the FoI, denoted by $E[\Phi]$, can be expressed as

$$\begin{aligned} E[\Phi] =& \mathbf{P}(c) \times E[P] + \mathbf{P}(d) \times E[B], \\ =& \left(\frac{\|C\|}{\|C\| + \|D\|} \right) E[P] + \left(\frac{\|D\|}{\|C\| + \|D\|} \right) E[B], \\ =& \frac{\big(\|\Psi\| - \|D\| \big) \pi S^2 + \|D\| \, E[B]}{\|\Psi\|}, \end{aligned} \tag{3.3}$$

where $\|R\|$ denotes the area of a region R. The areas $\|\Psi\|$ and $\|D\|$ are defined by Eq. 3.1 and Eq. 3.2, respectively. In the rest of this section, we derive $E[B]$ by evaluating the area of intersection between the sensing disc of a sensor and different segments of the boundary region.

3.3.3 Effective sensing area near boundary

It can be observed from Fig 3.2(c) that, the effective sensing area of a sensor in the boundary strip (useful for coverage) is the area of intersection between its sensing disc and the boundary strip. As shown in Fig. 3.3, we divide the boundary region into n disjoint regions, denoted by $D_0, D_1, \ldots, D_{n-1}$, such that $\|D\| = \sum_{k=0}^{n-1} \|D_k\|$. This is done to simplify the calculation of the area of intersection between the sensing disc and the boundary region.

Let d_k denote the event that the sensor lies in the region D_k, $0 \leq k \leq n-1$. Let B_k be the effective sensing region of a sensor in the region D_k. That is, $B_k = A(s, S) \cap \Psi$, when $s \in D_k$. Since the sensor could be located anywhere in D, with the probability of a sensor being in D_k given by $\mathbf{P}(d_k)$, the expected value of the effective sensing area of a sensor in the region D can be expressed as

$$\begin{aligned} E[B] =& \mathbf{P}(d_0) \times E[B_0] + \cdots + \mathbf{P}(d_{n-1}) \times E[B_{n-1}], \\ =& \frac{\|D_0\|}{\|D\|} \times E[B_0] + \cdots + \frac{\|D_{n-1}\|}{\|D\|} \times E[B_{n-1}], \end{aligned} \tag{3.4}$$

where $\|D_k\|$ is the area of D_k and $E[B_k]$ is the expected value of the effective sensing area of a sensor in D_k.

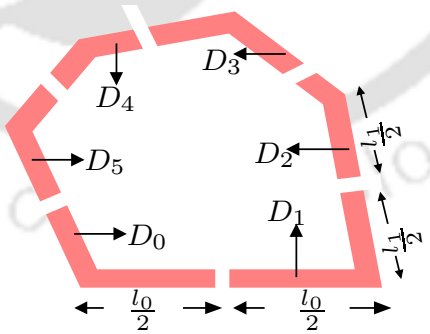

Figure 3.3 Illustration of the boundary region D of a 6-vertex polygonal FoI being divided into six disjoint regions.

Eq. 3.4 shows that $E[B]$ depends on $E[B_k]$ which in turn depends on the area of intersection between the sensing disc and the boundary region. It can be observed

from the geometry of the regions D_k, $k = 0, 1, \ldots, 5$ that $E[B_k]$ depends on the angle at the vertices $0 < \theta_k < \pi$. For a given angle θ_k that characterizes the shape of the region D_k, and the location of the sensor, the effective sensing region B_k can be determined. Different values of the angle θ_k lead to different cases in evaluating $E[B_k]$ as explained below:

Case 1 : $\theta_k \leq \pi/2$: We consider the case when the sensor lies in one of the regions D_k for which the angle at the vertex is less than or equal to a right angle. The shape of the effective sensing region of the sensor depends on its position. To determine various regions of intersection possible, we partition one region D_k, (for example D_1) into four disjoint regions: $D_{k,1}$, $D_{k,2}$, $D_{k,3}$, and $D_{k,4}$, such that $\|D_k\| = \sum_{j=1}^{4} ||D_{k,j}||$ as illustrated in Fig. 3.4(b) which are also shown separately in Figs. 3.4(b1)-(b4). Figs. 3.4(a1)-(a4) illustrate the four possible regions (shown as shaded regions) where a sensor could be located that give rise to different shapes of the effective sensing region. It may be noted that these are the only possible locations for the sensor. For example, Fig. 3.4(a1) shows the case when a sensor is within a distance of S from v_k. As shown in Fig. 3.4(c1), the effective sensing region in this case is a union of the triangle $\triangle sp_2v_k$, the triangle $\triangle sv_kp_1$, and the sector $\widehat{sp_1p_2}$. Similarly, Figs. 3.4(a2)-(a4) illustrate the cases where a sensor could be at various other points in the region D_k. The effective sensing regions for these cases are shown in Figs. 3.4(c2)-(c4). Figs. 3.4(b1)-(b4) explicitly show the regions $D_{k,j}$, $j = 1, 2, 3, 4$, where the sensor could be located.

For different locations of a sensor in $D_{k,j}$, illustrated in Fig. 3.4(b0), let $B_{k,j} = A(s, S) \cap \Psi$ denote the effective sensing regions, illustrated in Figs. 3.4(c1)-(c4). Let $d_{k,j}$ denote the event that a sensor is in the region $D_{k,j}$. The expected value of the effective sensing area can be expressed as

$$E[B_k] = \mathbf{P}(d_{k,1}) \times E[B_{k,1}] + \cdots + \mathbf{P}(d_{k,4}) \times E[B_{k,4}],$$
$$= \frac{\|D_{k,1}\|}{\|D_k\|} \times E[B_{k,1}] + \cdots + \frac{\|D_{k,4}\|}{\|D_k\|} \times E[B_{k,4}]. \quad (3.5)$$

In the rest of this section, we evaluate $E[B_{k,j}]$ for $1 \leq j \leq 4$ by estimating the effective sensing areas.

Case 1.1 : $E[B_{k,1}]$: As illustrated in Fig. 3.4(a1), this case occurs when the sensor is located within a distance of S from the vertex of D_k. It can be seen that the sensing disc intersects the edges of the FoI at points p_1 and p_2. From Fig. 3.4(c1), it may be observed that the effective sensing region when the sensor is at s, is the union of the $\triangle sp_2v_k$, the $\triangle sv_kp_1$, and the $\widehat{sp_1p_2}$ so that the effective sensing area is simply,

$$F^{(x,y)} = \|\triangle sp_2v_k\| + \|\triangle sv_kp_1\| + \left\|\widehat{sp_1p_2}\right\|. \quad (3.6)$$

Eq. 3.6 gives the effective sensing area of a sensor located at (x, y). But, we need to consider all the possible locations for a sensor in the region $D_{k,1}$. As shown in Fig. 3.4(b1), $D_{k,1}$ consists of two parts which can be formally defined as $\{(x,\, y) \mid 0 \leq x \leq a_x,\, 0 \leq y \leq x \tan\theta_k\} \cup \{(x,\, y) \mid a_x \leq x \leq b_x,\, 0 \leq y \leq \sqrt{S^2 - x^2}\}$, where $a_x = S\cos\theta_k$ and $b_x = S$ are the x coordinates of points a and b, respectively and θ_k is the angle at v_k. After determining the (x, y) coordinates for the region $D_{k,1}$, the expected value of the effective sensing area when a sensor lies in $D_{k,1}$ can be obtained by simply integrating Eq. 3.6 over $D_{k,1}$. Therefore,

$$
\begin{aligned}
E[B_{k,1}] =& \frac{1}{\|D_{k,1}\|} \iint_{(x,y)\in D_{k,1}} F^{(x,y)}\, dD_{k,1} = \frac{1}{\|D_{k,1}\|}\Bigg(\int_0^{a_x} \int_0^{x\tan(\theta_k)} F^{(x,y)} dydx + \int_{a_x}^{b_x} \int_0^{\sqrt{S^2-x^2}} F^{(x,y)} dydx \Bigg), \\
=& \frac{1}{\|D_{k,1}\|}\Bigg(\int_0^{S\cos(\theta_k)} \int_0^{x\tan(\theta_k)} y(x+\sqrt{S^2-y^2}) dydx + \frac{S^2}{2} \int_0^{S\cos(\theta_k)} \int_0^{x\tan(\theta_k)} \Bigg(2\pi - \\
& \tan^{-1}\frac{x}{y} - \Big(\frac{\pi}{2} - \theta_k + \tan^{-1}\frac{y}{x}\Big) - \cos^{-1}\frac{y}{S} - \cos^{-1}\Big(\frac{\sqrt{x^2+y^2}\sin(\theta_k - \tan^{-1}\frac{y}{x})}{S}\Big)\Bigg) dydx \\
& + \frac{S^2}{2} \int_{S\cos(\theta_k)}^{S} \int_0^{\sqrt{S^2-x^2}} \Bigg(2\pi - \tan^{-1}\frac{x}{y} - \Big(\frac{\pi}{2} - \theta_k + \tan^{-1}\frac{y}{x}\Big) - \cos^{-1}\frac{y}{S} - \cos^{-1}\Big(\\
& \frac{\sqrt{x^2+y^2}\sin(\theta_k - \tan^{-1}\frac{y}{x})}{S}\Big)\Bigg) dydx + \int_{S\cos(\theta_k)}^{S} \int_0^{\sqrt{S^2-x^2}} y(x+\sqrt{S^2-y^2}) dydx \Bigg), \\
=& \frac{1}{\|D_{k,1}\|} \times \frac{S^4}{8}\left(4\theta_k^2 + \frac{\theta_k}{\tan(\theta_k)} - \cos(2\theta_k) \right). \qquad (3.7)
\end{aligned}
$$

Case 1.2 : $E[B_{k,2}]$: This case occurs when the sensor is at a distance greater than S from v_k at any point in the region $D_{k,2}$ (shaded in Fig. 3.4(a2)). The sensing disc intersects the edges of the FoI at points p_1, p_2, q_1, and q_2 and the effective sensing region in this case, as shown in Fig. 3.4(c2), is a union of the $\triangle sq_1q_2$, the $\triangle sp_1p_2$, the $\widehat{sp_1q_1}$, and the $\widehat{sq_2p_2}$. The effective sensing area in this case is therefore,

$$
F^{(x,y)} = \|\triangle sq_1q_2\| + \|\triangle sp_1p_2\| + \left\|\widehat{sp_1q_1}\right\| + \left\|\widehat{sq_2p_2}\right\|. \qquad (3.8)
$$

Similar to the previous case, the expected value of the effective sensing area when the sensor lies in $D_{k,2}$ can be obtained by simply integrating Eq. 3.8 over the region $D_{k,2}$. Fig. 3.4(b2) shows the region $D_{k,2}$ divided into four parts that can be formally defined by $\{(x,\, y) \mid a_x \le x \le c_x,\ \sqrt{S^2-x^2} \le y \le x\tan\theta_k\} \cup \{(x,\, y) \mid c_x \le x \le b_x,\ \sqrt{S^2-x^2} \le y \le S\} \cup \{(x,\, y) \mid b_x \le x \le d_x,\ 0 \le y \le S\} \cup \{(x,\, y) \mid d_x \le x \le e_x,\ x\tan\theta_k - S\sec\theta_k \le y \le S\}$, where $a_x = S\cos\theta_k$, $b_x = S$, $c_x = S\cot\theta_k$, $d_x = S\csc\theta_k$, $e_x = S\cot(\theta_k/2)$, and θ_k is the angle at v_k. Therefore, the expected value of the

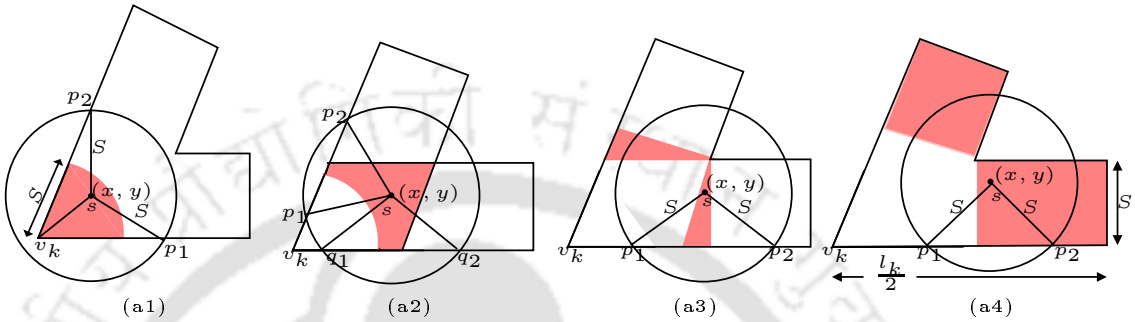

(a) Illustration of the cases when a sensor lies in the regions $D_{k,j}$, $1 \leq j \leq 4$.

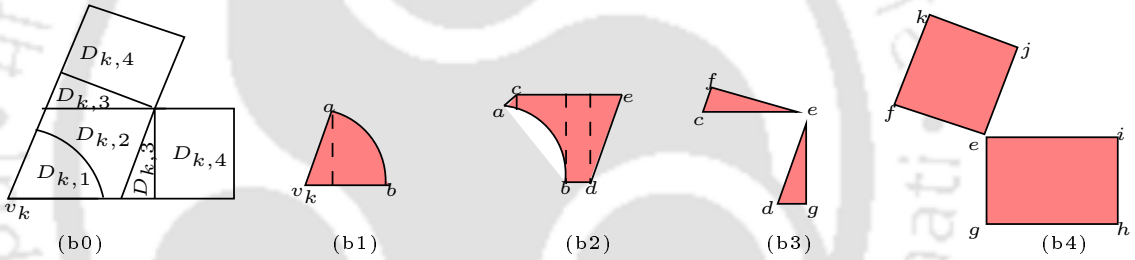

(b) Illustration of the regions $D_{k,j}$, $1 \leq j \leq 4$ and $D_k = \bigcup_{j=1}^{4} D_{k,j}$.

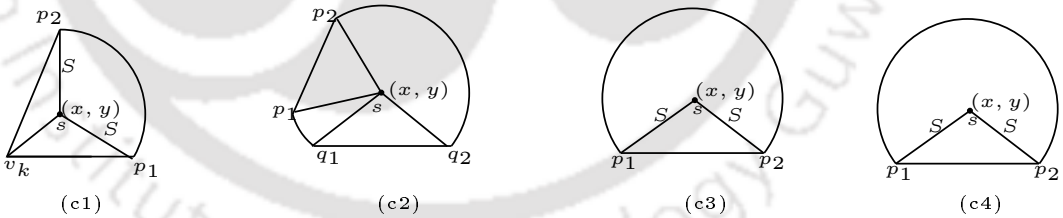

(c) Illustration of the effective sensing regions when the sensor lies in the regions $D_{k,j}$, $1 \leq j \leq 4$.

Figure 3.4 Illustration of the regions $D_{k,j}$ and effective sensing regions $B_{k,j}$, for $1 \leq j \leq 4$ and $\theta_k \leq \pi/2$.

effective sensing area of a sensor in $D_{k,2}$ is given by

$$E[B_{k,2}] = \frac{1}{\|D_{k,2}\|} \iint\limits_{(x,y)\in D_{k,2}} F^{(x,y)}\, dD_{k,2} = \frac{1}{\|D_{k,2}\|}\Bigg(\int\limits_{a_x}^{c_x} \int\limits_{\sqrt{S^2-x^2}}^{x\tan\theta_k} F^{(x,y)} dydx + \int\limits_{c_x}^{b_x} \int\limits_{\sqrt{S^2-x^2}}^{S} F^{(x,y)} dydx$$
$$+ \int\limits_{b_x}^{d_x} \int\limits_{0}^{S} F^{(x,y)} dydx + \int\limits_{d_x}^{e_x} \int\limits_{x\tan\theta_k - S\sec\theta_k}^{S} F^{(x,y)} dydx \Bigg),$$
$$= \frac{1}{\|D_{k,2}\|}\Bigg(\int_{S\cos(\theta_k)}^{S\cot(\theta_k)} \int_{\sqrt{S^2-x^2}}^{x\tan(\theta_k)} \Big(2y\sqrt{S^2-y^2} + \pi S^2 - \frac{S^2}{2}\cos^{-1}(y/S)\Big) dydx + \int_{S\cot(\theta_k)}^{S}$$
$$\int_{\sqrt{S^2-x^2}}^{S} \Big(2y\sqrt{S^2-y^2} + \pi S^2 - \frac{S^2}{2}\cos^{-1}(y/S)\Big) dydx + \int_{S}^{\frac{S}{\sin(\theta_k)}} \int_{0}^{S} \Big(2y\sqrt{S^2-y^2} + \pi S^2 - \frac{S^2}{2}$$
$$\cos^{-1}(y/S)\Big) dydx + \int_{\frac{S}{\sin(\theta_k)}}^{\frac{S}{\tan(\theta_k/2)}} \int_{\frac{x}{\cot(\theta_k)} - \frac{S}{\cos(\theta_k)}}^{S} \Big(2y\sqrt{S^2-y^2} + \pi S^2 - \frac{S^2}{2}\cos^{-1}(y/S)\Big) dydx \Bigg),$$
$$= \frac{S^4}{\|D_{k,2}\|}\left(\frac{3\,\pi - 4}{3\,sin(\theta_k)} - \frac{\theta_k}{4\,\tan(\theta_k)} - \frac{(sin^{-1}(cos(\theta_k)) - \frac{\pi}{2})^2}{2} + \frac{\cos^2(\theta_k)}{3} \right). \tag{3.9}$$

Case 1.3 : $E[B_{k,3}]$: This case is illustrated in Fig 3.4(a3). The sensing region of a sensor at point s intersects with an edge of the FoI at points p_1 and p_2. From Fig. 3.4(c3), the effective sensing region of a sensor at (x, y) is a union of the $\triangle sp_1p_2$ and the $\widehat{p_2p_1s}$ with an area of

$$F^{(x,y)} = \|\triangle sp_1p_2\| + \left\|\widehat{p_2p_1s}\right\|. \tag{3.10}$$

From Figs. 3.4(b0) and 3.4(b3), it can be seen that the region $D_{k,3}$ is composed of two equal-sized triangles in which the $\triangle edg$ can be formally defined as $\{(x,\, y) \mid d_x \le x \le g_x,\, 0 \le y \le x\tan\theta_k - S\sec\theta_k\}$, where the x coordinates of points d and g, are $d_x = S\csc\theta_k$ and $g_x = S\cot\theta_k/2$, respectively. The expected value of the effective sensing area of a sensor in the region $D_{k,3}$ is obtained by simply integrating

Eq. 3.10 over $D_{k,3}$. Therefore,

$$E[B_{k,3}] = \frac{2}{\|D_{k,3}\|} \iint\limits_{(x,y)\in D_{k,3}} F^{(x,y)}\, dD_{k,3} = \frac{2}{\|D_{k,3}\|} \int\limits_{d_x}^{g_x} \int\limits_{0}^{x\tan\theta_k - S\sec\theta_k} \Big(\|\triangle s p_1 p_2\| + \big\|\widehat{p_2 p_1 s}\big\| \Big) dy dx,$$

$$= \frac{2}{\|D_{k,3}\|} \int_{\frac{S}{\sin(\theta_k)}}^{\frac{S}{\tan(\theta_k/2)}} \int_0^{x\tan(\theta_k) - \frac{S}{\cos(\theta_k)}} \Big(y\sqrt{S^2 - y^2} + \pi S^2 - S^2 \cos^{-1}(y/S) \Big) dy dx,$$

$$= \frac{S^4}{\|D_{k,3}\| \tan(\theta_k)} \Big(\frac{9\pi}{8} - \frac{4}{3} \Big). \tag{3.11}$$

Case 1.4 : $E[B_{k,4}]$: Fig 3.4(a4) illustrates this case when a sensor lies in the region $D_{k,4}$ (shown in Fig. 3.4(b0)). The sensing disc intersects an edge of the FoI at points p_1 and p_2. From Fig 3.4(c4), the effective sensing area of a sensor at (x, y) is given by

$$F^{(x,y)} = \|\triangle s p_1 p_2\| + \big\|\widehat{p_2 p_1 s}\big\|. \tag{3.12}$$

Fig. 3.4(b4) shows that the region $D_{k,4}$ is composed of two rectangles which can be formally defined as
$\{(x,\ y) \mid g_x \le x \le h_x,\ 0 \le y \le S\} \cup \{(x,\ y) \mid g_x \le x \le l_{k-1}/2,\ 0 \le y \le S\}$, where $g_x = S\cot(\theta_k/2)$ and $h_x = l_k/2$, are the x coordinates of the points g and h, respectively. The expected value of the effective sensing area of a sensor located anywhere in $D_{k,4}$ can be obtained by integrating Eq. 3.12 over $D_{k,4}$. Therefore,

$$E[B_{k,4}] = \frac{1}{\|D_{k,4}\|} \iint\limits_{(x,y)\in D_{k,4}} F^{(x,y)}\, dD_{k,4} = \frac{1}{\|D_{k,1}\|} \Big(\int_{g_x}^{h_x} \int_0^S F^{(x,y)} dy dx + \int_{g_x}^{l_{k-1}/2} \int_0^S F^{(x,y)} dy dx \Big),$$

$$= \frac{1}{\|D_{k,4}\|} \Big(\int_{\frac{S}{\tan(\theta_k/2)}}^{l_k/2} \int_0^S \Big(y\sqrt{S^2 - y^2} - S^2\cos^{-1}(y/S) + \pi S^2 \Big) dy dx + \int_{\frac{S}{\tan(\theta_k/2)}}^{l_{k-1}/2} \int_0^S$$

$$\Big(y\sqrt{S^2 - y^2} + \pi S^2 - S^2\cos^{-1}(y/S) \Big) dy dx \Big),$$

$$= \frac{S^3}{\|D_{k,4}\|} \Big(\pi - \frac{2}{3} \Big) \Big(\frac{l_k + l_{k-1}}{2} - \frac{2S}{\tan(\theta_k/2)} \Big). \tag{3.13}$$

In summary, the expected value of the effective sensing area of a sensor in D_k can be obtained by substituting $E[B_{k,j}]$, $1 \leq j \leq 4$ from Eqs. 3.7, 3.9, 3.11, and 3.13 into Eq. 3.5. Therefore,

$$\begin{aligned} E[B_k] =& \frac{\|D_{k,1}\|}{\|D_k\|} \times E[B_{k,1}] + \cdots + \frac{\|D_{k,4}\|}{\|D_k\|} \times E[B_{k,4}], \\ =& \frac{S^4}{\|D_k\|}\left(\frac{\pi}{\sin\theta_k} - \frac{4}{3\sin\theta_k} - \frac{\theta_k}{8\tan\theta_k} + \frac{cos^2\theta_k}{3} + \frac{\theta_k^2}{2} - \frac{(\sin^{-1}(\cos\theta_k) - \frac{\pi}{2})^2}{2} - \frac{\cos(2\theta_k)}{8}\right. \\ &\left. + \frac{9\pi}{8\tan\theta_k} - \frac{4}{3\tan\theta_k} + \frac{3\pi - 2}{3S}\left(\frac{l_{k-1} + l_k}{2} - \frac{2S}{\tan(\theta_k/2)}\right)\right). \end{aligned} \tag{3.14}$$

Note that the terms $\|D_{k,j}\|$, $1 \leq j \leq 4$ in various expressions get canceled and need not be evaluated at all.

Case 2 : $\theta_k > \pi/2$: In this case the geometry of the region D_k is such that the angle at the vertex v_k is an obtuse angle. This is the only other case possible for a convex polygon. For this case, the regions of intersection between the sensing disc and the FoI with different locations of the sensor are shown in Fig. 3.5. Based on the location of the sensor, the region D_k is again divided into four disjoint regions:$D_{k,j}$, $1 \leq j \leq 4$ and for each region, the expected value of the effective sensing area is computed using the area of intersection. Due to the high symmetry involved in the derivation, we do not show the steps. The final expressions of $E[B_{k,j}]$, $1 \leq j \leq 4$ and $\theta_k > \pi/2$, are given by Eqs. 3.15, 3.16, 3.17, and 3.18, respectively.

$$\begin{aligned} E[B_{k,1}] &= \frac{1}{\|D_{k,1}\|} \iint\limits_{(x,y)\in D_{k,1}} F^{(x,y)}\, dD_{k,1} = \frac{1}{\|D_{k,1}\|}\left(\int_0^{\pi/2}\int_0^{S} F^{(x,y)} dydx + \int_{\pi/2}^{\theta_k}\int_0^{S} F^{(x,y)} dydx\right), \\ &= \frac{1}{\|D_{k,1}\|} \times \frac{S^4}{8}\left(1 - \pi^2 - \frac{\theta_k - \pi}{\tan(\theta_k)} + 4\,\theta_k\pi\right). \end{aligned} \tag{3.15}$$

$$
\begin{aligned}
E[B_{k,2}] =& \frac{1}{\|D_{k,2}\|} \iint\limits_{(x,y)\in D_{k,2}} F^{(x,y)}\, dD_{k,2}, \\
=& \frac{1}{\|D_{k,2}\|}\Bigg(\int_0^{S\, cot\frac{\theta_k}{2}} \int_{\sqrt{(S^2-x^2)}}^{S} \Big(2y\sqrt{S^2-y^2} + \pi S^2 - \frac{S^2}{2}\cos^{-1}(y/S)\Big) dydx + \\
& \int_{S\cot\frac{\theta_k}{2}}^{S\sin\theta_k} \int_{\sqrt{(S^2-x^2)}}^{x\tan\theta_k - \frac{S}{\cos\theta_k}} \Big(\pi S^2 + 2y\sqrt{S^2-y^2} - \frac{S^2}{2}\cos^{-1}(y/S)\Big) dydx\Bigg), \\
=& \frac{S^4}{\|D_{k,2}\|}\left(\frac{\cos^2(\theta_k)-16}{12} + \frac{\cos(\theta_k)\,\sin^{-1}(-\cos(\theta_k))}{4\sin(\theta_k)} + \frac{8\,\theta_k - \pi}{8\,\tan(\theta_k)} + \frac{\pi}{\sin(\theta_k)} + \frac{\theta_k\,(\theta_k-\pi)}{2}\right).
\end{aligned} \tag{3.16}
$$

$$
\begin{aligned}
E[B_{k,3}] =& \frac{2}{\|D_{k,3}\|} \iint\limits_{(x,y)\in D_{k,3}} F^{(x,y)}\, dD_{k,3}, \\
=& \frac{2}{\|D_{k,3}\|}\Bigg(\int_{\frac{S}{\tan(\theta_k/2)}}^{S\sin(\theta_k)} \int_{S}^{x\,\tan(\theta_k) - \frac{S}{\cos(\theta_k)}} \Big(y\sqrt{S^2-y^2} + \pi S^2 - S^2\cos^{-1}(y/S)\Big) dydx + \\
& \int_{S\sin(\theta_k)}^{S} \int_{S}^{\sqrt{S^2-x^2}} \Big(\pi S^2 + y\sqrt{S^2-y^2} - S^2\cos^{-1}(y/S)\Big) dydx\Bigg), \\
=& \frac{S^4}{\|D_{k,3}\|}\Bigg(2\pi - \frac{\theta_k^2}{2} + \frac{\pi^2}{8} - \frac{\sin^{-1}(-\cos(\theta_k))}{4\tan(\theta_k)} + \frac{2\pi}{\sin(2\theta_k)} + \frac{\pi}{8\tan(\theta_k)} - \frac{\cos^2(\theta_k)}{12} - \\
& \frac{\theta_k}{\tan(\theta_k)} + \pi\tan(\theta_k) - \frac{2\pi\cot(\theta_k/2)}{\cos(\theta_k)}\Bigg).
\end{aligned} \tag{3.17}
$$

$$
\begin{aligned}
E[B_{k,4}] =& \frac{2}{\|D_{k,4}\|} \iint\limits_{(x,y)\in D_{k,4}} F^{(x,y)}\, dD_{k,4}, \\
=& \frac{1}{\|D_{k,4}\|}\Bigg(\int_S^{l_k/2} \int_0^S \Big(y\sqrt{S^2-y^2} - S^2\cos^{-1}(y/S) + \pi S^2\Big) dydx + \int_S^{l_{k-1}/2} \int_0^S \\
& \Big(y\sqrt{S^2-y^2} + \pi S^2 - S^2\cos^{-1}(y/S)\Big) dydx\Bigg), \\
=& \frac{S^3}{\|D_{k,4}\|}\Big(\pi - \frac{2}{3}\Big)\left(\frac{l_k + l_{k-1}}{2} - 2S\right).
\end{aligned} \tag{3.18}
$$

Finally, substituting Eqs. 3.15, 3.16, 3.17, and 3.18 into Eq. 3.5, the expected value

of the effective sensing area of a sensor in D_k for $\theta_k > \pi/2$ is given by

$$E[B_k] = \frac{S^4}{\|D_k\|}\left(\frac{2\pi}{\sin(2\theta_k)} + \frac{\pi}{\cot\theta_k} - \frac{2\pi\cot(\frac{\theta_k}{2})}{\cos\theta_k} + \frac{\pi}{\sin\theta_k} + \frac{1}{8} + \frac{\pi-\theta_k}{8\tan\theta_k} + \frac{3\pi-2}{3S}\left(\frac{l_{k-1}+l_k}{2}\right)\right). \tag{3.19}$$

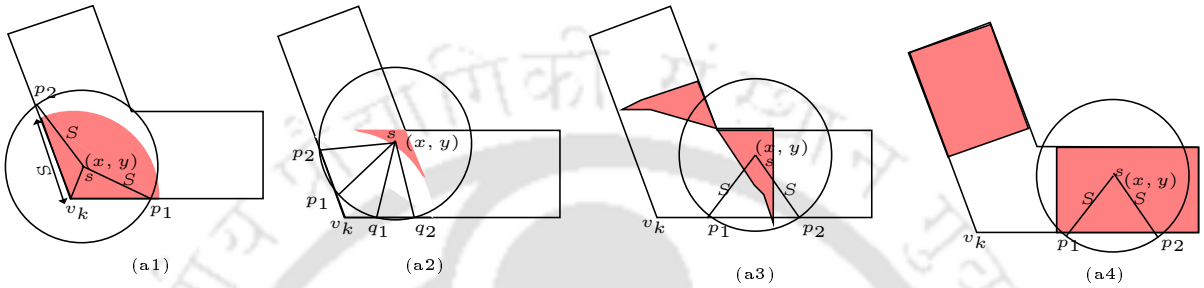

(a) Illustration of the cases when a sensor lies in the regions $D_{k,j}$, $1 \le j \le 4$.

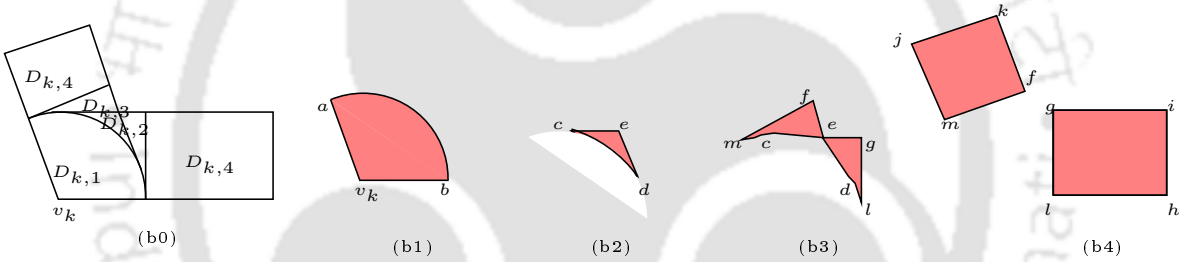

(b) Illustration of the regions $D_{k,j}$, $1 \le j \le 4$ and $D_k = \bigcup_{j=1}^{4} D_{k,j}$.

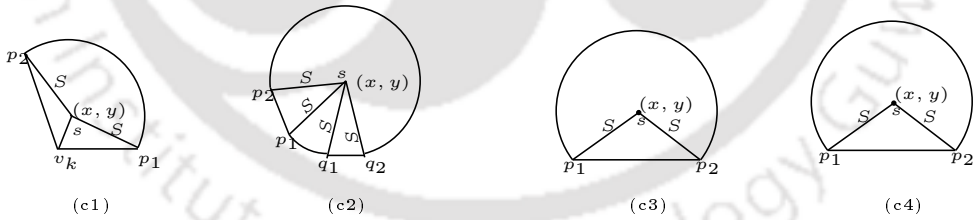

(c) Illustration of the effective sensing regions when the sensor lies in the regions $D_{k,j}$, $1 \le j \le 4$.

Figure 3.5 Illustration of the regions $D_{k,j}$ and effective sensing regions $B_{k,j}$, for $1 \le j \le 4$ and $\theta_k > \pi/2$.

3.3.4 Expected value of the effective sensing area

Now, we are ready to calculate the expected value of the effective sensing area of a sensor in the FoI. By substituting $\|\Psi\|$, $\|D\|$, and $E[B]$ from Eqs. 3.1, 3.2, and 3.4,

respectively in Eq. 3.3 gives

$$E[\Phi] = \frac{\big(\,\|\Psi\| - \|D\|\,\big)\pi S^2 + \|D\|\,E[B]}{\|\Psi\|}, \tag{3.20}$$

where $\|\Psi\| = \sum_{k=0}^{n-1} \left(\frac{1}{2}x_k y_{(k+1)\bmod n} - \frac{1}{2}y_k x_{(k+1)\bmod n}\right)$, $E[B] = \frac{\sum_{k=0}^{n-1}\|D_k\|E[B_k]}{\|D\|}$,

$\|D\| = \sum_{k=0}^{n-1} \frac{S}{2}\left(2l_k - \frac{S}{\tan(\theta_k/2)} - \frac{S}{\tan(\theta_{(k+1)\bmod n}/2)}\right)$, and $E[B_k] = \begin{cases} \text{Eq.3.14} & \textbf{if}(\theta_k \le \pi/2) \\ \text{Eq.3.19} & \textbf{otherwise}. \end{cases}$

3.4 Critical Sensor Density for Partial Coverage

In the previous section, we estimated the expected value of the effective sensing area of a sensor located anywhere in a convex polygon-shaped bounded FoI. In this section, we estimate the CSD for a desired coverage ratio of the FoI using the effective sensing area. Let N sensors be deployed uniformly at random, independent of each other in the FoI Ψ. Let $C(X)$ denote the event that a point X in the FoI Ψ falls within the sensing region of a sensor. Assuming a uniform distribution of sensors, the probability of this event is given by

$$\mathbf{P}(C(X)) = \frac{E[\Phi]}{\|\Psi\|}, \text{ where } E[\Phi] \text{ is given by Eq. 3.20.} \tag{3.21}$$

From the definition of point coverage, a point in the FoI is said to be covered if it falls within the sensing region of at least one sensor. Let $D(X)$ denote the event that the point X in the FoI Ψ is covered by at least one sensor, the probability of which is given by

$$\mathbf{P}(D(X)) = 1 - (1 - \mathbf{P}(C(X)))^N = 1 - \left(1 - \frac{E[\Phi]}{\|\Psi\|}\right)^N. \tag{3.22}$$

The expected area of the FoI covered by at least one sensor can be obtained by simply integrating $\mathbf{P}(D(X))$ over Ψ. The expected value of the coverage ratio of the FoI, denoted by $E[\eta]$, is the ratio of the expected area of FoI covered by at least one

sensor to the area of the FoI. Therefore,

$$E[\eta] = \frac{1}{\|\Psi\|} \iint_{\Psi} \mathbf{P}(D(X))d\Psi = 1 - \left(1 - \frac{E[\Phi]}{\|\Psi\|}\right)^{N}. \tag{3.23}$$

The expected coverage ratio of the FoI can be interpreted as follows: If $E[\eta] = 0.80$, when we pick several points from the FoI randomly, 80% of them are covered by at least one sensor.

Theorem 3.1 *Given a convex polygon shaped FoI Ψ, with sensors deployed uniformly and an expected coverage ratio $E[\eta]$, the critical sensor density required to ensure the desired coverage ratio is*

$$\rho = \frac{\ln(1 - E[\eta])}{\|\Psi\| \ln\left(1 - \frac{E[\Phi]}{\|\Psi\|}\right)}, \textit{where } E[\Phi] \textit{ is given by Eq. 3.20.} \tag{3.24}$$

Proof: From Eq. 3.23, the number of sensors required to obtain a desired coverage ratio is given by $N = \ln(1 - E[\eta])/\ln(1 - \frac{E[\Phi]}{\|\Psi\|})$. The critical sensor density is then simply the minimal number of sensors per unit area of the FoI required for a desired coverage ratio, *i.e.*, $\rho = N/\|\Psi\|$ which proves the theorem. □

Example 1: Consider a parallelogram-shaped FoI as illustrated in Fig. 3.6 in which sensors with a sensing range of $100m$ are uniformly deployed at random. We want to compute the minimal number of sensors to be deployed in the FoI such that 90% of the points selected at random are covered by at least one sensor. Alternatively, we want to find the CSD required for $E[\eta] \geq 0.90$.

Using Eq. 3.20, we obtain $\|\Psi\| = 2 \times 10^6 m^2$, $\|\Psi - D\| = 1.28 \times 10^6 m^2$, and $\sum_{k=0}^{3} \|D_k\| E[B_k] = 1.7439 \times 10^{10} m^4$. The expected value of the effective sensing area of a sensor under border effects calculated using Eq. 3.20 is $E[\Phi] = 2.8825 \times 10^4 m^2$. Substituting for $E[\Phi]$, $E[\eta]$, and $\|\Psi\|$ in Theorem 3.1, we get $\rho = 7.93 \times 10^{-5}/m^2$ and

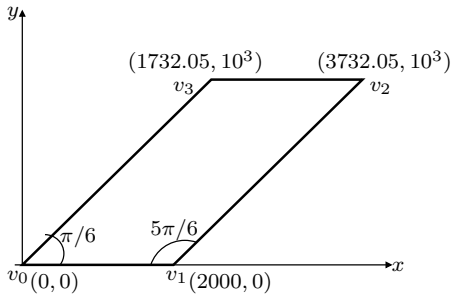

Figure 3.6 Parallelogram-shaped FoI.

N=159. That is, if we deploy 159 sensors uniformly in the FoI, we can ensure that 90% of the area is covered.

Example 2: Consider a convex polygon-shaped FoI as illustrated in Fig. 3.7 in which sensors with a sensing range of $100m$ are uniformly deployed at random. We want to compute the minimal number of sensors required for $E[\eta] \geq 0.90$. Using Eq. 3.20, we obtain $\|\Psi\| = 368 \times 10^4 m^2$ and $E[\Phi]= 3.0017 \times 10^4 m^2$. Substituting for $E[\Phi]$, $E[\eta]$, and $\|\Psi\|$ in Theorem 3.1, we get $N = 282$.

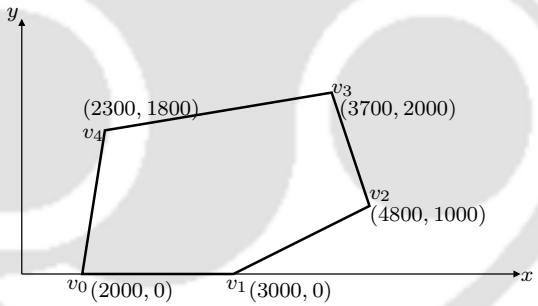

Figure 3.7 Convex polygon-shaped FoI.

• **Validation of the analysis:** To verify the expressions for the CSD and the expected coverage ratio under border effects, we evaluate Eq. 3.23 numerically for the FoI in Fig. 3.6, and compare it with that obtained in a simulation. We consider the same scenario described in Example 1 for the validation of the analysis. For the simulation results a Monte Carlo simulation is conducted which is used to estimate probability from a large number of experiments. In each Monte Carlo experiment conducted to determine the coverage ratio, several tests are performed to check if a

point is covered. In each test, a point in the FoI is picked at random to see if it is covered. The test is termed *successful* if the point is covered, otherwise it is termed *unsuccessful*. The number of such tests conducted (in each experiment) is equal to the integer value nearest to the area of the FoI. We repeat the experiment 100 times by changing the seed for selecting the points. The expected coverage ratio of the FoI is computed as the ratio of the number of tests successful to the total number of tests conducted. The simulation results are with 95% confidence level though the error bars are not visible in the plots.

Fig. 3.8 shows the expected coverage ratio of the FoI obtained with both simulation and numerical evaluation, for different densities of the sensors deployed. It can be observed that the expected coverage ratio of the FoI evaluated using Eq. 3.23 matches with that obtained from the simulation. The results also show that the expected coverage ratio is over-estimated when the border effects are not considered. This is because, the entire sensing area of a sensor is considered to be useful for the coverage.

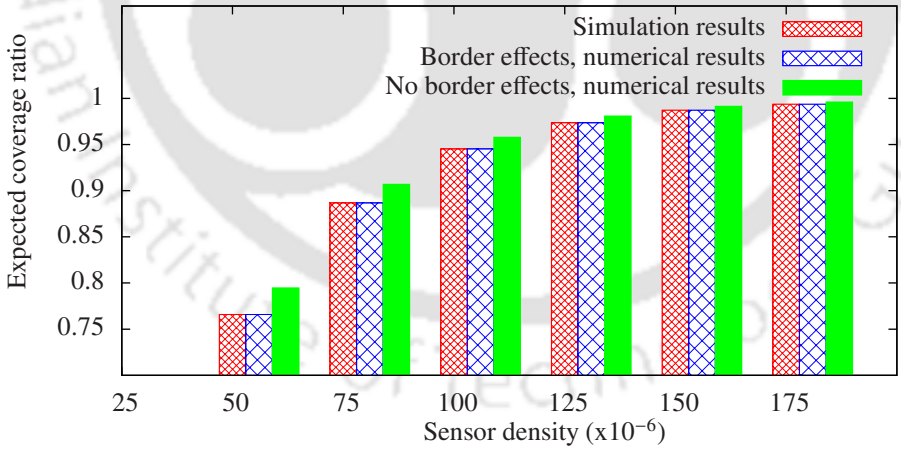

Figure 3.8 Variation in the expected coverage ratio of the FoI for different sensor densities.

3.5 Numerical Results

In this section, we present results based on numerical evaluation of the expressions derived in this chapter. We study the effect of perimeter of the FoI and the sensing range of sensors on the CSD and the coverage ratio under border effects. We also demonstrate that the sensor density obtained with our analysis is lower than that obtained using the analysis in [1].

• **Impact of the area of the FoI:** Next, we study the impact of the area of the FoI on the number of sensors required for two different sensing ranges. The sensors are uniformly deployed in a parallelogram-shaped FoI illustrated in Fig. 3.6. *Extra Sensors* in Table 3.1 shows the percentage increase in the number of sensors when the border effects are considered. An interesting observation from this result is that for a higher value of the ratio of the sensing range to the area of the FoI, the border effects are significant. This result shows that for a given area of the FoI, the border effects are significant for a larger sensing range. We conclude that considering the ratio of the sensing range to the area of the FoI and not just the area of the FoI gives a better understanding of the border effects.

Table 3.1 Impact of the sensing range and the area of the FoI on the number sensors required for a desired coverage ratio of 0.9.

$\|\mathbf{\Psi}\|$ $(\times\mathbf{10^4})$	25	30	35	40	45
S$/\|\mathbf{\Psi}\|(\times\mathbf{10^{-5}})$, **S=10m**	4	3.33	2.86	2.5	2.22
S=10m, Extra Sensors	2.65%	2.34%	2.12%	1.95%	1.82%
S$/\|\mathbf{\Psi}\|(\times\mathbf{10^{-5}})$, **S=50m**	20	16.67	14.29	12.5	11.11
S=50m, Extra Sensors	15.38%	12.9%	12.5%	10.84%	9.68%

• **Impact of the perimeter of the FoI:** We study the relationship between coverage ratio, CSD, and the size of the field. We choose a parallelogram-shaped FoI with an area of $2 \times 10^6 m^2$ deployed with sensors of $100m$ sensing range. Fig. 3.9 shows the variation in the CSD as the perimeter of the FoI is increased, for the desired coverage ratios of 0.8 and 0.9. Obviously as the size of the region increases, a larger number of

sensors are required to maintain the desired coverage ratio. Interestingly, when the border effects are ignored, the sensor density does not increase with the perimeter since the area is constant. On the other hand, a FoI with a larger perimeter has a larger boundary region, and for all the sensors near the boundary, a part of their sensing region falls outside the FoI. This result shows that the border effects are too important to be neglected in a FoI with a large perimeter, when the desired coverage ratio is high.

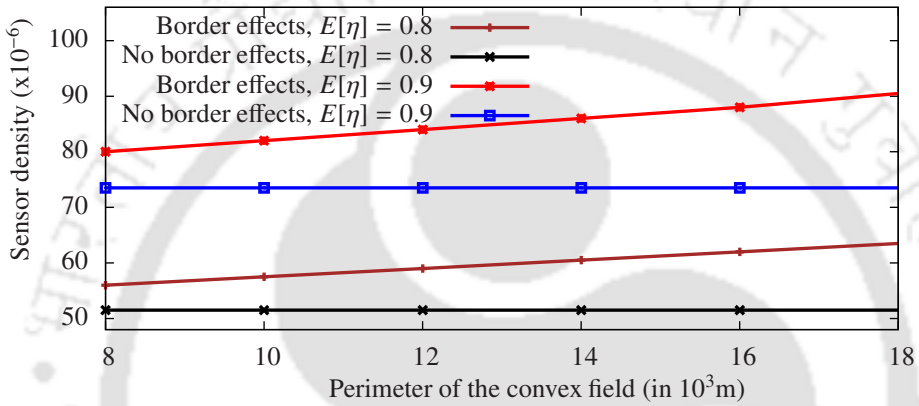

Figure 3.9 Relationship between the sensor density and the perimeter of the FoI for a desired coverage ratio under border effects.

• **Impact of sensing range:** We study the impact of the sensing range on the coverage ratio for two different densities of deployment in a FoI. The sensors are uniformly deployed in a FoI with an area of $4 \times 10^6 m^2$ and a perimeter of $12 \times 10^3 m$. Fig. 3.10 shows an increase in the expected coverage ratio with the sensing range for two different densities of deployment. Obviously, as the sensing range of the sensors increases, the coverage ratio increases but rapidly for a larger density. An interesting observation from this result is that for a lower density of sensors, the border effects are prominent. Similar to the results in the previous section, we observe that the border effects are important for a higher coverage ratio with a low density of sensors. Thus, some work in the literature avoids border effects by considering dense deployment of sensors in the FoI. This result also shows that the border effects are prominent for larger sensing ranges because, when such sensors are located closer to the boundary,

they tend to have a smaller effective sensing area. The results in Figs. 3.9 and 3.10 show that the border effects are negligible in the case of a smaller perimeter and a lower ratio of the sensing range to the area of the FoI.

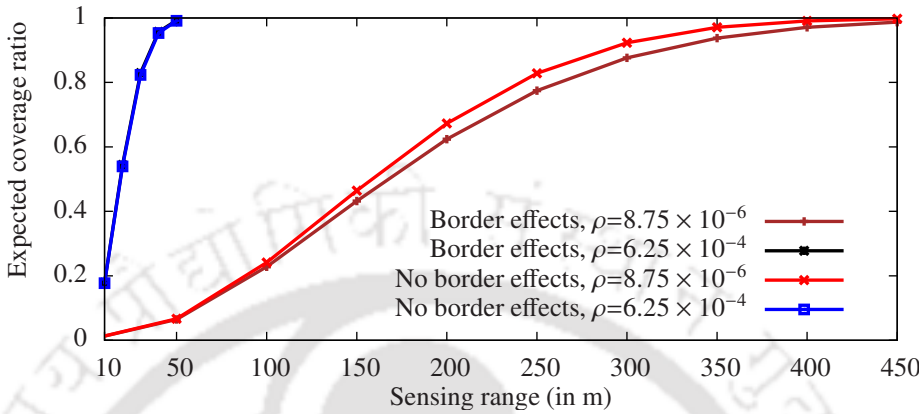

Figure 3.10 Relationship between the expected coverage ratio and the sensing range of sensors.

• **Comparison with sensor density computed in [1]:** Finally, we compare the CSD estimated in this work with that obtained in [1]. As mentioned earlier, the work in [1] does not consider the exact geometry of the FoI but considers only the area and the perimeter. Due to this, the number of sensors computed with their analysis is not necessarily minimal. For the scenario described in Example 1, we compute the sensor density for a given coverage ratio, using both Eq. 3.24 and the results in [1]. The sensing range, perimeter, and the area of the FoI are $100m$, $6 \times 10^3 m$, and $10^6 m^2$, respectively. Fig. 3.11 compares the sensor densities for different coverage ratios. It can be seen that the sensor density estimated with our analysis is always lower than that obtained in [1]. The difference in the estimated sensor density is significant for higher coverage ratio. Thus, we conclude that our approach estimates the sensor density better and hence lowers the cost of stochastic deployment of WSNs. The results in Figs. 3.9 and 3.11 show that considering the geometry of the FoI and not just the area estimates the CSD better.

• **Impact of a rectangular boundary over the FoI:** We study the impact of a rectangular boundary over the FoI. We compare the required number of sensors

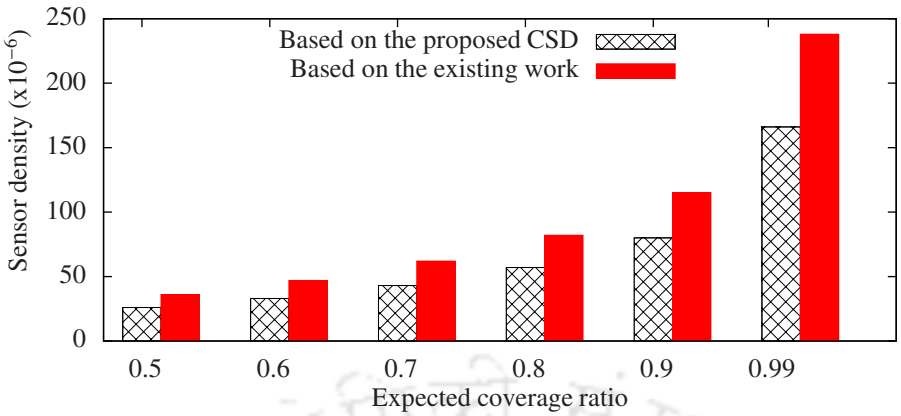

Figure 3.11 Comparison of the sensor density obtained with Eq. 3.24 and that in [1] for different coverage ratios.

estimated in this work with that obtained using a rectangular boundary over the FoI. We compute the required number of sensors for a given coverage ratio, using Eq. 3.24. We create a rectangular boundary over the FoI and compute the required number of sensors for the given coverage ratio as shown in Fig. 3.12. The sensing range of the sensors is $100m$. Fig. 3.13 compares the required number of sensors for different coverage ratios. It can be seen that the required sensors estimated with our analysis is always lower than that obtained using a rectangular boundary over the FoI. The difference in the estimated sensors is significant for higher coverage ratio. Thus, we conclude that our approach estimates the number of sensors better and hence lowers the cost of stochastic deployment of WSNs.

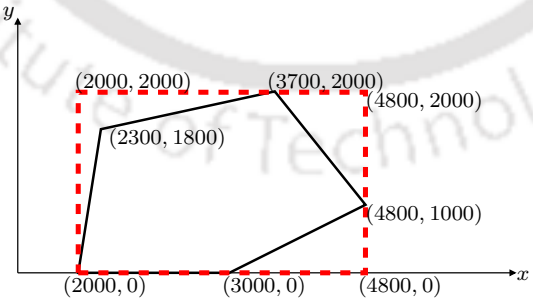

Figure 3.12 A rectangular boundary over a convex polygon shaped FoI.

• **Impact of irregular geometry and sensing model:** In our work, we made some assumptions on the geometry of the FoI and the sensing model which are not

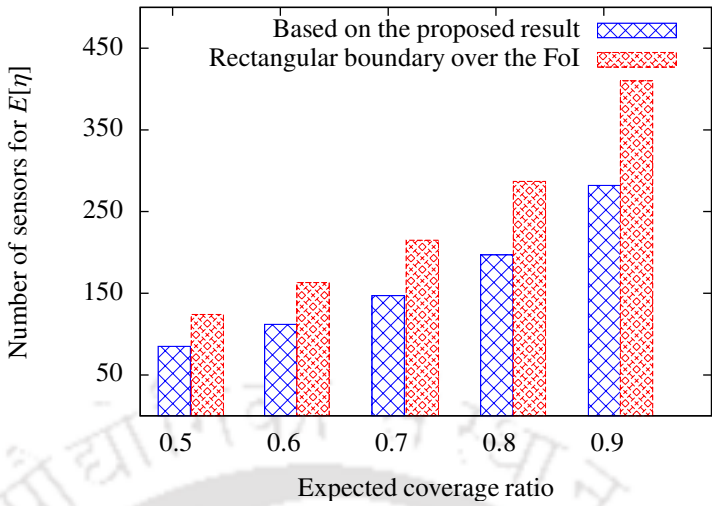

Figure 3.13 Comparison of the required number of sensors obtained with Eq. 3.24 and a rectangular boundary over the FoI for different coverage ratios.

very realistic. We discuss how the analysis proposed in our work can be extended when the assumptions are not valid.

When the FoI is not in the shape of a polygon but is in an irregular shape, it is hard to estimate the effective sensing area exactly. An irregular-shaped region can be approximated with a polygonal shape and then our analysis can be applied. Circumscribing an irregular shaped FoI with a polygon can be done efficiently by using the algorithms proposed in [43]. With this approach, our analysis for the CSD can be used for even an irregular-shaped FoI.

Similarly, our analysis is based on the assumption that the sensing region of a sensor is circular. In practice, the sensing region may not be a perfect disc. A few other sensing models are described in [4]. The work in [44] estimated the inner radius of a non-disc region by inscribing a circle inside the region. Once the inner radius is estimated it can be used in our analysis for other sensing models.

3.6 Conclusion

In this chapter, we studied the coverage problem in WSNs considering the border effects and derived the CSD required to ensure the QoC. Unlike earlier work in the literature, we used the exact geometry of the FoI instead of the area and the perimeter, to compute the effective sensing area of a sensor located at the boundary. The expected value of the effective sensing area was used to calculate the CSD required for a desired coverage ratio. The analysis was validated with simulations and the numerical results demonstrated its benefit. The results demonstrated that the geometry of the FoI should be considered to compute the CSD, particularly for a large region with a low density of sensors. Our results also demonstrated that for larger sensing ranges, boundary effects need to be considered in estimating the coverage ratio, and that the CSD computed with our analysis is lower than that obtained from a previous work. Our work can be used for cost effective deployment of sensors in any convex polygon-shaped FoI.

In this chapter, we assumed that the sensors are deployed in a FoI. However, in some applications, the sensors cannot be deployed directly inside the FoI to be monitored. For example, in canal water monitoring project, the sensors cannot be deployed on the water surface. In the next chapter, we assume that the sensors are deployed uniformly at random outside the FoI near the boundary. For such WSNs, we analyze the CSD for desired level of coverage and connectivity probability using exact geometry of the FoI.

Chapter 4

Analysis of k-Coverage and Connectivity in WSNs with Boundary Deployment

4.1 Introduction

The literature on WSNs typically addresses the problems of coverage and connectivity in either two-dimensional surface coverage [1, 39, 40] or three-dimensional volume coverage [45, 46, 47]. In most of these studies the sensors are deployed directly in the FoI to be monitored. However, in some applications, the sensors cannot be deployed directly inside the FoI. For example, in canal water monitoring application [13] (Fig 4.1(a)), the sensors cannot be deployed on the water surface. Similarly, there exist applications such as the traffic information acquisition systems (TISs), where the sensors cannot be directly deployed on the road to be monitored. Other examples where the sensors can only be deployed outside the monitored region are: railway track monitoring system [14], water transport monitoring system, and country border monitoring system [15](see parts (b) and (c) of Fig 4.1).

In applications where the sensors cannot be directly deployed in the FoI, the

existing results on coverage cannot be applied. Further, most of the existing TISs have focused on the deterministic deployment of sensors on the road or along the edges of the road, which requires excavation of road surface and leads to traffic disruption during the installation [48, 49, 50, 51, 52, 53]. In this work, we consider a deployment scenario in which the sensors are randomly deployed outside the FoI to be monitored.

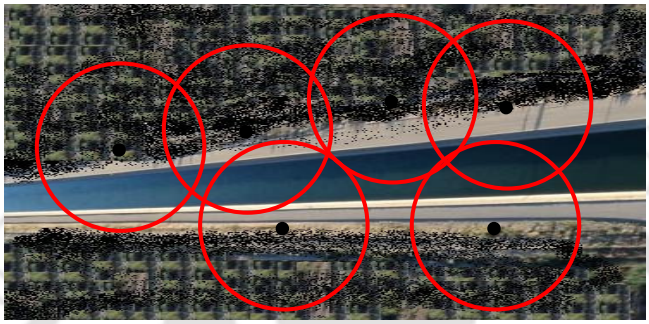

(a) Canal water monitoring.

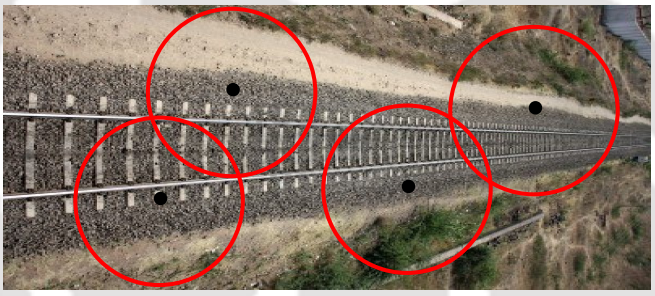

(b) Railway track monitoring.

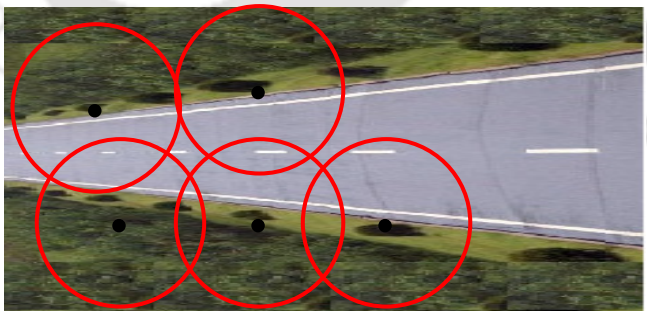

(c) Road surface monitoring.

Figure 4.1 Examples of the coverage of FoIs with sensors deployed outside the edges.

In this chapter, we address the problem: *how many sensors are required to ensure that a FoI is k-covered and the WSN is connected, when the sensors are deployed*

uniformly at random outside the FoI near the boundaries? To address this problem, we first derive the expected k-coverage ratio (stochastic coverage measure) and connectivity probability for a scenario of deployment with sensors randomly deployed outside the FoI.

Major Contributions: To the best of our knowledge, this is the first work to address the problem of determining k-coverage and connectivity in WSNs when a large number of sensors are deployed uniformly at random outside the FoI near the boundary. We estimate the expected values of the effective sensing area and communication area of a sensor located outside the FoI near the boundary. We demonstrate the utility of the analysis in the estimation of the minimum number of sensors required for a desired level of coverage and connectivity. We also illustrate an application of this work for developing a **T**raffic **I**nformation acquisition system based on the wireless sensor **NET**work called TINet.

The rest of this chapter is organised as follows. In the next section, we state the assumptions and define the terms used in this work. In Sections 4.3 and 4.4, we derive the expressions for the expected value of k-coverage and connectivity probability, respectively, with sensors deployed uniformly at random outside the FoI near the boundaries. Section 4.5 presents the results on the minimum number of sensors required for a desired level of coverage and connectivity. We illustrate the application of this work to deploy TINet in Section 4.6 and conclude the chapter in Section 4.7.

4.2 Preliminaries

In this section, we state the assumptions and define the terms used in this work.

Assumptions: We assume that the shape of FoI Ψ is rectangular with a width d and length l as illustrated in Fig. 4.2. We assume that the sensors are deployed uniformly at random independent of each other along the boundaries of the FoI (indicated by Ω in the figure). We assume that n sensors are deployed on both sides of Ψ ($n/2$ on

each side) across strips of length l and width b. We assume the *binary disc sensing* model [8] in which a sensor located at a point $s \in \Omega$, can only sense perfectly within a disc of radius S centered at s, denoted by $A(s, S)$. Any event that occurs outside $A(s, S)$ cannot be detected by the sensor s. The sensing area of a sensor is simply the area of $A(s, S)$, denoted by $\|A(s, S)\| = \pi S^2$. The communication region of a sensor is modeled by the *binary disc communication model*. The communication disc is the region over which a sensor can communicate with other sensors. The area of the communication region of a sensor at s is nothing but the area of the communication disc given by $\|A(s, C)\| = \pi C^2$, where C is the communication range. We discuss the effect of irregularity in the sensing and communication regions on our analysis in Section 4.5.2.

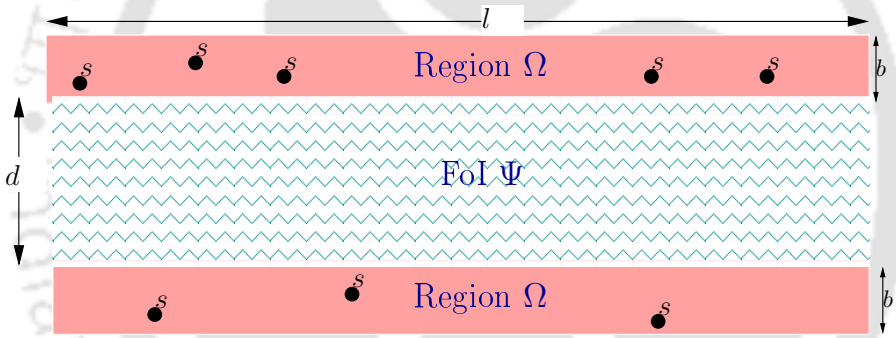

Figure 4.2 Illustration of sensors deployed uniformly at random in the boundary region Ω to monitor a FoI Ψ.

Definition 1: For any sensor at a point $s \in \Omega$, $\|A(s, S) \cap \Psi\| > 0$, $\|A(s, C) \cap \Omega\| > 0$, and $\|\Omega \cap \Psi\| = 0$.

Definition 2: *k-coverage ratio* of the FoI is defined as the fraction of the area of the FoI in which each point is almost surely k-covered. In WSNs with stochastic deployment, the FoI is said to be *k-covered* only if the expected value of the k-coverage ratio is equal to unity with probability one.

Definition 3: If two sensors i and j are such that the distance between them is less than C, then they are said to be *neighbours*.

Definition 4: A WSN can be modelled as a graph G=(V, E), where $V = \{v_1, ..., v_{n/2}\}$

and $E = \{e_1, \ldots, e_m\}$ are the sets of $n/2$ sensors and the bi-directional wireless links between them, respectively. The number of neighbours of a sensor, say s, is called the *sensor degree*, denoted by $d(s)$. The *minimum sensor degree* in a communication graph G is given by $d(G)=\min_{s \in V} d(s)$.

Definition 5: A WSN is said to be *node-connected* or simply *connected* if, for each pair of sensors in the communication graph G, there is at least one path connecting them [54]. The *connectivity probability*, denoted by γ is defined as the fraction of the sensors that are connected to the others.

4.3 Analysis of the k-Coverage with Boundary Deployment

In this section, we derive an expression for the expected value of k-covered area of a FoI when the sensors are deployed uniformly at random along the boundaries of the FoI. We choose a sensor at random from the boundary region Ω and compute the expected value of its effective sensing area, which is the area of the sensing region useful for the k-coverage of Ψ. Since the sensors are not deployed directly in the FoI, they can only cover an area smaller than their total sensing area. We define the effective sensing region of a sensor, denoted by Φ, as the region of intersection between its sensing region and the FoI, *i.e.*, $\Phi = A(s, S) \cap \Psi$. For a given width d of the FoI Ψ, the location of the sensor $s \in \Omega$, and its sensing range S, the effective sensing region Φ is determined. Without any loss of generality, we assume $d < 2S$ so that the entire FoI is covered with the sensors on each side.

We evaluate the expected value of the area of Φ for two possible cases given below:

Case 1) $S \leq d$: In this case, the sensing range of a sensor is smaller than or equal to the width of the region Ψ. As illustrated in Fig. 4.3(a), it can be seen that the sensing disc intersects the region Ψ at points p_1 and p_2. Fig. 4.3(c) shows the effective sensing region (dark shaded region) for this case (with the sensor at s) whose area

can be expressed as

$$F^{(x,y)} = \left\|\widehat{sp_1p_2}\right\| - \|\triangle p_1sp_2\|\,. \tag{4.1}$$

While the above equation gives the effective sensing area of a sensor at the point $s = (x, y)$, we need to consider all the possible locations of a sensor in the region Ω formally defined by $\{(x,\ y) \mid 0 \leq x \leq b,\ 0 \leq y \leq l\}$. It can be observed from Fig. 4.3(a) that, $F^{(x,y)}$ depends on b and S, *i.e.*, $F^{(x,y)} > 0$ **if** $0 \leq x < M_{b,S}$, where $M_{b,S}$ is the minimum of b and S.

The expected value of the effective sensing area when a sensor lies in Ω can be obtained by simply integrating Eq. 4.1 over Ω, *i.e.*,

$$\begin{aligned}
E[\|\Phi\|] =& \frac{2}{\|\Omega\|}\iint\limits_{(x,y)\in\Omega} F^{(x,y)}\,d\Omega,\\
=& \frac{1}{lb}\int\limits_0^l\int\limits_0^{M_{b,S}} \left(\left\|\widehat{sp_1p_2}\right\| - \|\triangle p_1sp_2\|\right)dxdy,\\
=& \frac{S^2}{lb}\int\limits_0^l\int\limits_0^{M_{b,S}} \cos^{-1}\left(\frac{x}{S}\right)dxdy - \int\limits_0^l\int\limits_0^{M_{b,S}} \frac{x\sqrt{S^2-x^2}}{lb}dxdy,\\
=& \frac{S^2}{b}\int\limits_0^{M_{b,S}} \cos^{-1}\left(\frac{x}{S}\right)dx - \frac{1}{b}\int\limits_0^{M_{b,S}} x\sqrt{S^2-x^2}dx,\\
=& \frac{S^2M_{b,S}}{b}\cos^{-1}\left(\frac{M_{b,S}}{S}\right) + \frac{(S^2-M_{b,S}^2)^{1.5}}{3b} + \frac{2S^3}{3b} - \frac{S^2\sqrt{S^2-M_{b,S}^2}}{b}.
\end{aligned} \tag{4.2}$$

Case 2) $S > d$: This case, illustrated in Fig. 4.3(b), occurs when the sensing range of the sensor is larger than the width of the region Ψ. It can be seen that the sensing disc intersects the region Ψ at points p_1, p_2, q_1, and q_2. From Fig. 4.3(d), it may be observed that the effective sensing region of a sensor at s can be expressed as

$$F^{(x,y)} = \left\|\widehat{sp_1p_2}\right\| - \|\triangle p_1sp_2\| - \left\|\widehat{sq_1q_2}\right\| + \|\triangle q_1sq_2\|\,. \tag{4.3}$$

The expected value of the effective sensing area for $s \in \Omega$ can be obtained by simply integrating Eq. 4.3 over Ω. Thus, $E[\|\Phi\|]$ can be expressed as

$$
\begin{aligned}
&= \frac{2}{\|\Omega\|} \iint\limits_{(x,y)\in\Omega} F^{(x,y)}\, d\Omega, \\
&= \frac{2}{\|\Omega\|} \iint\limits_{(x,y)\in\Omega} \left\|\widehat{sp_1p_2}\right\| - \|\triangle p_1 s p_2\| - \left\|\widehat{sq_1q_2}\right\| + \|\triangle q_1 s q_2\|\, d\Omega, \\
&= \frac{S^2}{b} \int_0^{M_{b,S}} \cos^{-1}\left(\frac{x}{S}\right) dx - \frac{1}{b} \int_0^{M_{b,S}} x\sqrt{S^2 - x^2}\, dx - \frac{S^2}{b} \int_d^{M_{b+d,S}} \cos^{-1}\left(\frac{x}{S}\right) dx \\
&\quad + \frac{1}{b} \int_d^{M_{b+d,S}} x\sqrt{S^2 - x^2}\, dx, \\
&= \frac{S^2 M_{b,S}}{b} \cos^{-1}\left(\frac{M_{b,S}}{S}\right) + \frac{(S^2 - M_{b,S}^2)^{1.5}}{3b} - \frac{S^2\sqrt{S^2 - d^2}}{b} \\
&\quad - \frac{S^2\sqrt{S^2 - M_{b,S}^2}}{b} - \frac{(S^2 - M_{b+d,S}^2)^{1.5}}{3b} + \frac{(S^2 - d^2)^{1.5}}{3b} \\
&\quad - \frac{S^2 M_{b+d,S}}{b} \cos^{-1}\left(\frac{M_{b+d,S}^2}{S}\right) + \frac{S^2 d}{b} \cos^{-1}\left(\frac{d}{S}\right) + \frac{S^2\sqrt{S^2 - M_{b+d,S}^2}}{b}.
\end{aligned} \tag{4.4}
$$

Next, let $A(x)$ denote the event that a point $x \in \Psi$ falls within the sensing region of a sensor. Under the assumption that the sensors are deployed uniformly at random in Ω, the probability of this event can be expressed as

$$
\mathbf{P}(A(x)) = \frac{E[\|\Phi\|]}{\|\Psi\|} = \frac{E[\|\Phi\|]}{l \times d}. \tag{4.5}
$$

Let $B_i(x)$ denote the event that a point $x \in \Psi$ is covered by exactly i sensors, the probability of which can be expressed as, $\mathbf{P}(B_i(x)) = \binom{n}{i} (\mathbf{P}(A(x)))^i (1 - \mathbf{P}(A(x)))^{n-i}$.

By the definition of k-coverage of a point, a point in Ψ is said to be k-covered if it falls within the sensing region of at least k sensors. Let $E^k(x)$ denote the event that the point x is k-covered, whose probability is given by

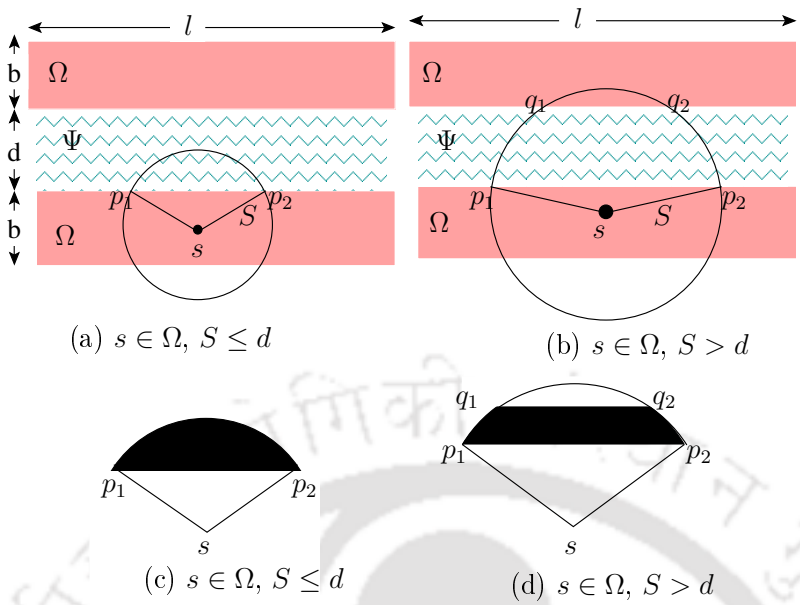

Figure 4.3 Illustration of the effective sensing region of a sensor located at $s \in \Omega$.

$$\begin{aligned}\mathbf{P}(E^k(x)) =& 1 - \sum_{i=0}^{k-1} \mathbf{P}(B_i(x)), \\ =& 1 - \sum_{i=0}^{k-1} \binom{n}{i} (\mathbf{P}(A(x)))^i (1 - \mathbf{P}(A(x)))^{n-i}. \end{aligned} \tag{4.6}$$

The expected fraction of the area of the FoI Ψ covered by at least k sensors, denoted by $E[\eta_k]$, can be obtained by integrating $\mathbf{P}(E^k(x))$ over Ψ. Therefore,

$$E[\eta_k] = \frac{1}{\|\Psi\|} \iint_{\Psi} \mathbf{P}(E^k(x)) d\Psi. \tag{4.7}$$

By substituting $\mathbf{P}(E^k(x))$ from Eq. 4.6, $E[\eta_k]$ can be written as

$$E[\eta_k] = \frac{1}{\|\Psi\|} \iint_{\Psi} \left(1 - \sum_{i=0}^{k-1} \binom{n}{i} \left(\mathbf{P}(A(x))\right)^i \left(1 - \mathbf{P}(A(x))\right)^{n-i}\right) d\Psi,$$

$$= 1 - \sum_{i=0}^{k-1} \binom{n}{i} \left(\mathbf{P}(A(x))\right)^i \left(1 - \mathbf{P}(A(x))\right)^{n-i},$$

$$\text{where } \mathbf{P}(A(x)) = \frac{E[\|\Phi\|]}{l \times d} \text{ and } E[\|\Phi\|] = \begin{cases} Eq.\ 4.2 & \textbf{if}(S \leq d) \\ Eq.\ 4.4 & \textbf{otherwise}. \end{cases} \tag{4.8}$$

The expected area of the FoI that is k-covered can be interpreted as follows: If $E[\eta_2] = 0.80$, when we pick several points from the FoI randomly, 80% of them are covered by at least two sensors.

Example 1: Consider a FoI, similar to the one illustrated in Fig. 4.2, in which sensors with a sensing range of $60m$ are uniformly deployed at random. Let the values of l, d, and b be $500m$, $60m$, and $60m$, respectively. We want to compute the minimum number of sensors to be deployed in Ω such that Ψ is almost surely 2-covered. Substituting $E[\eta_2]$, S, l, d, and b in Eq. 4.8, we get n=112. That means, if we deploy 56 sensors across each side of the FoI following a uniform distribution, we can be sure that Ψ is almost surely 2-covered.

4.4 Analysis of Connectivity with Boundary Deployment

In this section, we compute the expected value of the effective communication area of a sensor picked at random, which is the area useful for a connected WSN. We define the effective communication region of a sensor, denoted by Υ, as the region of intersection between its communication disc and the boundary region Ω, *i.e.*, $\Upsilon = A(s, C) \cap \Omega$. Given the location of the sensor $s \in \Omega$, the width b of the region Ω, and the communication range C, the effective communication region Υ is determined. We evaluate the expected value of effective communication area of a sensor for the two

cases given below:

Case 1) $b \geq 2C$: When the width of the boundary region Ω is greater than or equal to twice the communication range of a sensor, it can be seen in Fig. 4.4(a), that the communication disc intersects the boundary region Ω at points p_1 and p_2. Fig. 4.4(c) shows the effective communication region (dark shaded region) for $b \geq 2C$ (with the sensor at $s = (x, y)$) whose area can be expressed as

$$F^{(x,y)} = \begin{cases} \pi C^2 - \big(\|\widehat{sp_1p_2}\| - \|\triangle p_1 s p_2\| \big), & \textbf{if}(0 \leq x < C) \\ \pi C^2, & \textbf{if}(C \leq x \leq b - C) \\ \pi C^2 - \big(\|\widehat{sp_1p_2}\| - \|\triangle p_1 s p_2\| \big), & \textbf{if}(b - C < x \leq b) \end{cases} \tag{4.9}$$

The above equation gives the effective communication area of a sensor at $s = (x, y)$, but we need to consider all the possible locations for a sensor in the boundary region Ω formally defined by $\{(x,\ y) \mid 0 \leq x \leq b,\ 0 \leq y \leq l\}$.

The expected value of the effective communication area when a sensor lies in the boundary region Ω can be obtained by simply integrating Eq. 4.9 over Ω, *i.e.*,

$$\begin{aligned} E[\|\Upsilon\|] =& \frac{2}{\|\Omega\|} \iint\limits_{(x,y)\in\Omega} F^{(x,y)}\, d\Omega = \frac{1}{lb} \int\limits_0^l \int\limits_0^b F^{(x,y)}\, dxdy, \\ =& \frac{1}{b} \int\limits_0^b \pi C^2 dx - \frac{2}{b} \int\limits_0^C \Big(\|\widehat{sp_1p_2}\| - \|\triangle p_1 s p_2\| \Big) dx. \end{aligned} \tag{4.10}$$

Case 2) $b < 2C$: As illustrated in Fig. 4.4(b),when the width of the boundary region Ω is smaller than twice the communication range of a sensor, the communication disc intersects the boundary region Ω at points p_1, p_2 , q_1, and q_2. From Fig. 4.4(d), it may be observed that the effective communication region when the sensor is at $s = (x, y)$

can be expressed as

$$F^{(x,y)} = \begin{cases} \pi C^2 - \left(\left\| \widehat{sp_1p_2} \right\| - \| \triangle p_1 s p_2 \| \right), & \textbf{if}(0 \leq x < b - C) \\ \pi C^2 - \left(\left\| \widehat{sp_1p_2} \right\| - \| \triangle p_1 s p_2 \| \right) - \left(\left\| \widehat{sq_1q_2} \right\| - \| \triangle q_1 s q_2 \| \right), & \textbf{if}(b - C \leq x \leq C) \\ \pi C^2 - \left(\left\| \widehat{sq_1q_2} \right\| - \| \triangle q_1 s q_2 \| \right), & \textbf{if}(C < x \leq b) \end{cases} \tag{4.11}$$

The expected value of the effective communication area in this case is obtained by integrating Eq. 4.11 over Ω, *i.e.*,

$$E[\|\Upsilon\|] = \frac{2}{\|\Omega\|} \iint\limits_{(x,y)\in\Omega} F^{(x,y)}\, d\Omega = \frac{1}{lb} \int\limits_0^l \int\limits_0^b F^{(x,y)}\, dxdy,$$

$$= \frac{1}{b} \int\limits_0^b \pi C^2 dx - \frac{1}{b} \int\limits_0^C \left(\left\| \widehat{sp_1p_2} \right\| - \| \triangle p_1 s p_2 \| \right) dx - \frac{1}{b} \int\limits_{b-C}^b \left(\left\| \widehat{sq_1q_2} \right\| - \| \triangle q_1 s q_2 \| \right) dx,$$

After changing the variables and limits of the integration

$$= \frac{1}{b} \int\limits_0^b \pi C^2 dx - \frac{2}{b} \int\limits_0^C \left(\left\| \widehat{sp_1p_2} \right\| - \| \triangle p_1 s p_2 \| \right) dx. \tag{4.12}$$

It can be observed from Fig. 4.4 that, the difference between $\left\| \widehat{sp_1p_2} \right\|$ and $\| \triangle p_1 s p_2 \|$ depends on the values of b and C, *i.e.*,

$$\left\| \widehat{sp_1p_2} \right\| - \| \triangle p_1 s p_2 \| = \begin{cases} > 0, & \textbf{if}(0 \leq x \leq b \,\textbf{and}\, b \leq C) \\ > 0, & \textbf{if}(0 \leq x \leq C \,\textbf{and}\, C \leq b) \\ 0, & else. \end{cases}$$

$$= \begin{cases} > 0, & \textbf{if}(0 \leq x < M_{b,C}) \\ 0, & else. \end{cases} \tag{4.13}$$

Using Eq. 4.13 in Eqs. 4.10 and 4.12, $E[\|\Upsilon\|]$ can be written as

$$\begin{aligned} E[\|\Upsilon\|] =& \frac{1}{b}\int_0^b \pi C^2 dx - \frac{2}{b}\int_0^{M_{b,C}} \Big(\|\widehat{sp_1p_2}\| - \|\triangle p_1 s p_2\| \Big) dx, \\ =& \pi C^2 - \frac{2}{b}\int_0^{M_{b,C}} (C^2 \cos^{-1}\left(\frac{x}{C}\right) - x\sqrt{C^2 - x^2}) dx, \\ =& \pi C^2 - \frac{2\sqrt[3]{C^2 - M_{b,C}^2}}{3b} + \frac{2C^2\sqrt{C^2 - M_{b,C}^2}}{b} - \frac{4C^3}{3b} - \frac{2C^2 M_{b,C}}{b}\cos^{-1}\left(\frac{M_{b,C}}{C}\right). \end{aligned} \tag{4.14}$$

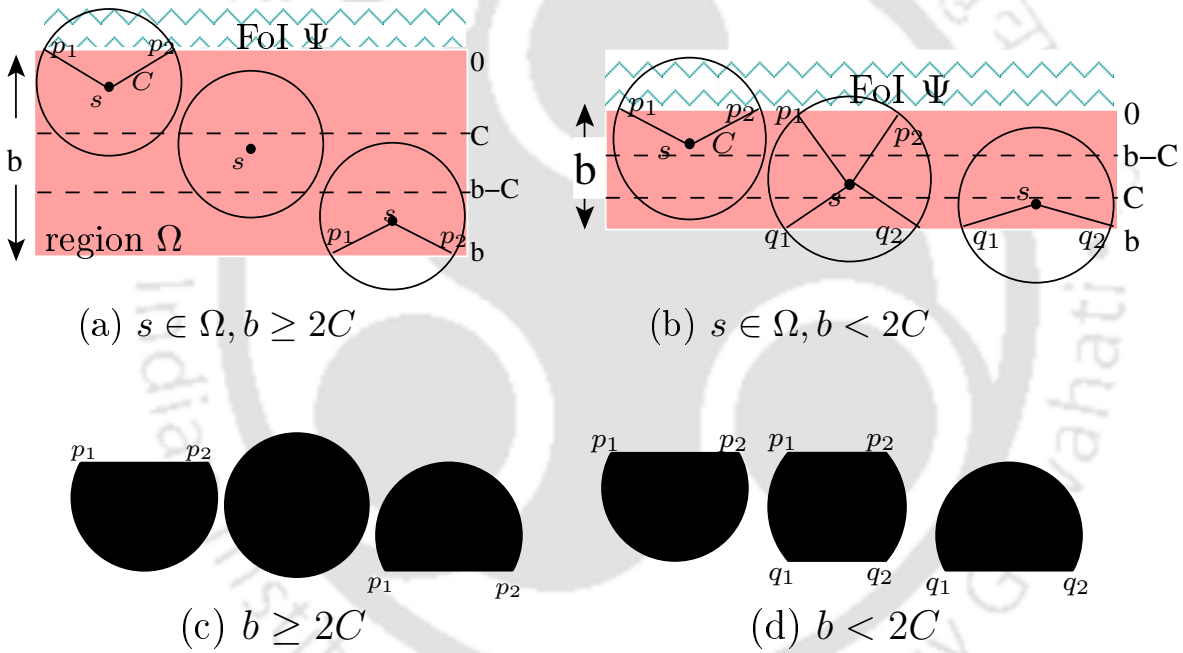

Figure 4.4 Illustration of the effective communication region of a sensor located at $s \in \Omega$.

Next, let G be the communication graph defined on $n/2$ sensors with the expected value of effective communication area being $E[\|\Upsilon\|]$. Let $A(s)$ be the event that there is at least one sensor inside the communication disc of an arbitrary sensor $s \in G$ whose probability is given by

$$\mathbf{P}(A(s)) = 1 - \left(1 - \frac{2E[\|\Upsilon\|]}{\|\Omega\|}\right)^{\frac{n}{2}}. \tag{4.15}$$

By the definition of the minimum sensor degree, $d(G) \geq 1 \Leftrightarrow \min_{\forall s \in V} d(s) \geq 1$. Because the sensors are distributed independently, the probability of the event that G has the minimum sensor degree $d(G)$ is

$$\mathbf{P}(d(G) \geq 1) = \left(\mathbf{P}(A(s))\right)^{\frac{n}{2}} = \left(1 - \left(1 - \frac{2E[\|\Upsilon\|]}{\|\Omega\|}\right)^{\frac{n}{2}}\right)^{\frac{n}{2}}. \tag{4.16}$$

We use a property of geometric random graphs proved in [55] which states that, for a large value of $n/2$, if we start with an empty graph and include the links formed by increasing the communication range, then the resulting graph is connected at the moment when the minimum sensor degree is unity. Therefore,

$$\mathbf{P}(G \text{ is connected}) = \mathbf{P}(d(G) \geq 1). \tag{4.17}$$

From Eqs. 4.16 and 4.17, the expected connectivity probability of the graph G, denoted by $E[\gamma]$, is given by

$$E[\gamma] = \mathbf{P}(G \text{ is connected}) = \left(1 - \left(1 - \frac{2E[\|\Upsilon\|]}{\|\Omega\|}\right)^{\frac{n}{2}}\right)^{\frac{n}{2}},$$
$$\text{where } \|\Omega\| = 2bl \text{ and } E[\|\Upsilon\|] \text{ is given by } Eq.\ 4.14. \tag{4.18}$$

The expected connectivity probability can be interpreted as follows: If $E[\gamma]$ is equal to unity with probability one, when we select several sensors from a given boundary region randomly, all of them form a almost surely connected WSN.

Example 2: Consider a boundary region Ω, similar to the one illustrated in Fig. 4.2, in which sensors with a communication range of $60m$ are uniformly deployed at random. Let the values of l, d, and b be $500m$, $60m$, and $60m$, respectively. We want to compute the minimum number of sensors to be deployed on each side of the FoI such that 99% of the sensors selected at random are almost surely connected. The expected value of the effective communication area is $E[\|\Upsilon\|] = 6.493 \times 10^3 m^2$. Substituting $E[\|\Upsilon\|]$ and $E[\gamma]$ in Eq. 4.18, we get $n/2$=44. That means, if we deploy 44

sensors with a uniform distribution across each side of the FoI, we can be sure that the sensors on each side of the FoI are almost surely connected.

4.5 Minimum Number of Sensors

In this section, we demonstrate the utility of the expressions derived in the previous sections to compute the minimum number of sensors required to ensure the desired level of coverage and connectivity.

Lemma 4.1 *Assume that n sensors are independently and uniformly distributed at random along the boundary region Ω. The FoI Ψ is almost surely k-covered by a single-hop connected WSN if $E[\eta_k]$ is equal to the unity with probability one and $C \geq \sqrt{b^2 + l^2}$.*

Proof: Eq. 4.8 shows that the region Ψ is almost surely k-covered if $E[\eta_k]$ is equal to the unity with probability one. The maximum distance between any two sensors located on either side of the boundary is $\sqrt{b^2 + l^2}$, as illustrated in Fig. 4.5. Therefore, any two sensors on a given strip of the boundary region can directly communicate if $C \geq \sqrt{b^2 + l^2}$, where C is the communication range of the sensors. Hence the lemma is proved. □

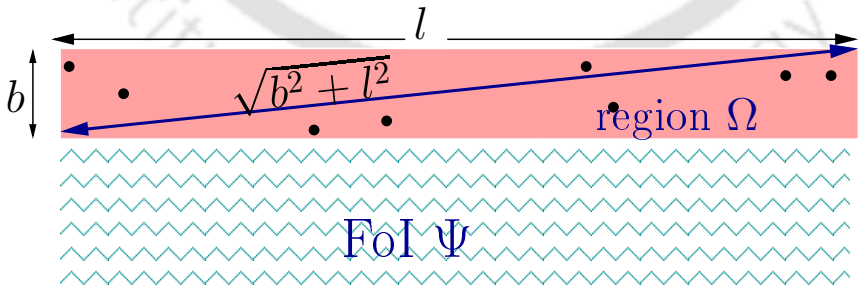

Figure 4.5 Illustration of a connected WSN.

Lemma 4.2 *Assume that n sensors are independently and uniformly distributed at random along the boundary region Ω. The FoI Ψ is almost surely k-covered by a*

multi-hop connected WSN if $E[\eta_k]$ and $E[\gamma]$ are equal to the unity with probability one.

Proof: Eq. 4.8 shows that the region Ψ is almost surely k-covered if $E[\eta_k]$ is equal to the unity with probability one. Eq. 4.18 shows that a WSN on either side of the FoI is almost surely connected if $E[\gamma]$ is equal to the unity with probability one. Hence the lemma is proved. □

Example 3: Consider a boundary region Ω, similar to the one illustrated in Fig. 4.5 in which sensors are uniformly deployed at random in the boundary region. Let l, d, b, k, S, and C be $21m$, $10m$, $2m$, 1, $7m$, and $30m$, respectively. We want to compute the minimum number of sensors to be deployed on each side of the FoI such that FoI Ψ is almost surely 1-covered and connected. Substituting the values of l, d, b, k, S, and C in Lemma 4.1, we get $n/2$=10. That means, if we deploy 10 sensors on each side of the FoI uniformly, we can ensure that the FoI Ψ is almost surely 1-covered with a single-hop connected WSN.

Example 4: Consider a boundary region Ω, similar to the one illustrated in Fig. 4.2 in which sensors are uniformly deployed at random outside the FoI near the boundary. Let l, d, b, k, S, and C be $500m$, $60m$, $60m$, 1, $60m$, and $60m$, respectively. We want to compute the minimum number of sensors to be deployed on each side of the FoI such that FoI Ψ is almost surely 1-covered and connected. Substituting l, d, b, k, S, and C in Lemma 4.2, we get $n/2$=44. That means, if we deploy 44 sensors with a uniform distribution across each side of the FoI, we can be sure that the FoI Ψ is almost surely 1-covered by a multi-hop connected WSN.

• **Validation of Lemma 4.1:** To verify Lemma 4.1, we evaluate it numerically for the scenario described in Example 3, and compare with the results obtained from a Monte Carlo simulation. The methodology used in Monte Carlo simulation is already discussed in Chapter 3, Section 3.4. Fig. 4.6 shows the number of sensors required for a desired coverage level of the FoI and single-hop connectivity. We observed that the

results with numerical evaluation match with those from simulation. The simulation results are with 95% confidence level though the error bars are not visible in the plots.

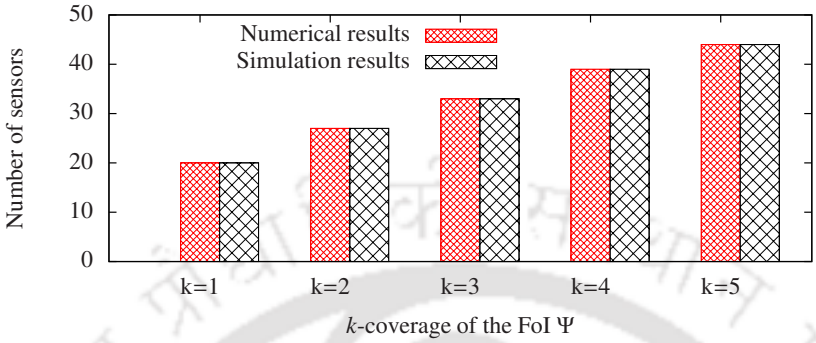

Figure 4.6 Number of sensors required for k-coverage and single-hop connectivity.

• **Validation of Lemma 4.2:** To verify Lemma 4.2, we evaluate it numerically for the scenario described in Example 4, and compare with the results obtained from a Monte Carlo simulation as described in the previous case. Fig. 4.7 shows that the number of sensors for k-coverage and multi-hop connectivity obtained with numerical evaluation matches with that from simulation. The simulation results are with 95% confidence level though the error bars are not visible in the plots.

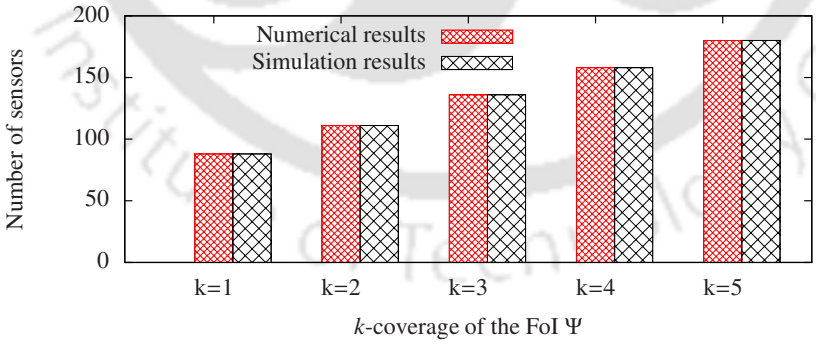

Figure 4.7 Number of sensors required for k-coverage and multi-hop connectivity.

4.5.1 Numerical Results

In this section, we apply Lemma 4.1 and Lemma 4.2 to study the effect of area of the regions Ψ and Ω on the number of sensors required for coverage and connectivity.

• **Impact of the area of the boundary region:** First, we compute the number of sensors required for k-coverage and connectivity as the area of Ω is varied. We consider the scenarios described in Example 3 and Example 4. Results in Fig. 4.8 show that the required number of sensors increases with the area of the boundary region is increased, for k-coverage of Ψ, $k = 1, \ldots, 5$. The value of b increases from $2m$ to $6m$ and $20m$ to $40m$ in part (a) and part (b) of Fig. 4.8, respectively. As the area of the boundary region increases, larger number of sensors are required to maintain the desired level of the coverage and connectivity. This is because the effective sensing area decreases with an increase in the boundary area. It may be observed that for a smaller k value, the difference between the number of sensors for $(k+1)$-coverage and k-coverage is prominent. It shows that higher value of k increases the utility of the sensors because of reduced wastage in the sensing area.

• **Impact of the area of the FoI:** We studied the effect of the area of the FoI on the number of sensors for the desired level of coverage and connectivity. We consider the scenarios described in Example 3 and Example 4 to evaluate Lemma 4.1 and Lemma 4.2, respectively. Fig. 4.9 shows that the number of sensors required to maintain a given level of coverage and connectivity, increases with the area of the FoI. The value of d increases from $8m$ to $12m$ and $20m$ to $40m$ in part (a) and part (b) of Fig. 4.9, respectively. Similar to the results in the previous case, as the area of Ψ (or width of Ψ at fixed l) increases, the effective sensing region of the sensors decreases, which leads to an increase in the number of sensors.

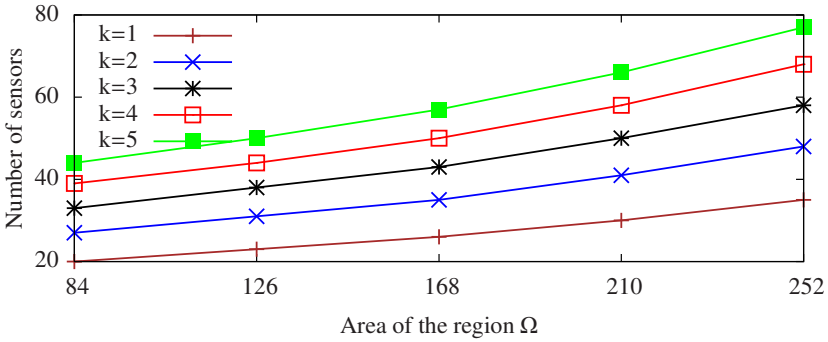

(a) Evaluation of Lemma 4.1.

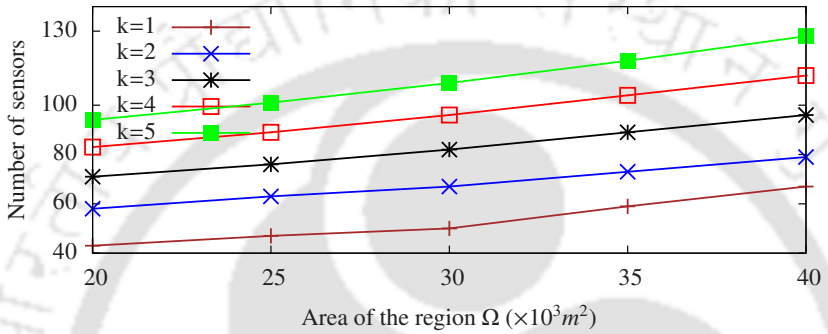

(b) Evaluation of Lemma 4.2.

Figure 4.8 Impact of the area of boundary region on the number of sensors for k-coverage and connectivity, $k = 1, \ldots, 5$.

4.5.2 Effect of irregular sensing and communication model

In our analysis, we assumed that the sensors have circular sensing and communication regions. However, in practice, the sensing and communication regions are irregular. Gang *et al.* in [56] investigated the impact of radio irregularity on the communication performance in wireless sensor networks. Radio irregularity arises due to factors such as, variance in the RF transmission power and different loss rate based on the direction of propagation. If the value of degree of irregularity (DoI) is equal to zero, the sensors have circular sensing and communication regions and an increasing DoI indicates an increasing degree of radio irregularity. The work in [46] shows that if the DoI is set to 0.1, the actual radio range in each direction is randomly selected using the Weibull distribution from 90 percent to 110 percent of the radio range.

With this model, instead of using the radius of an ideal disc in the analysis, $1 - h$

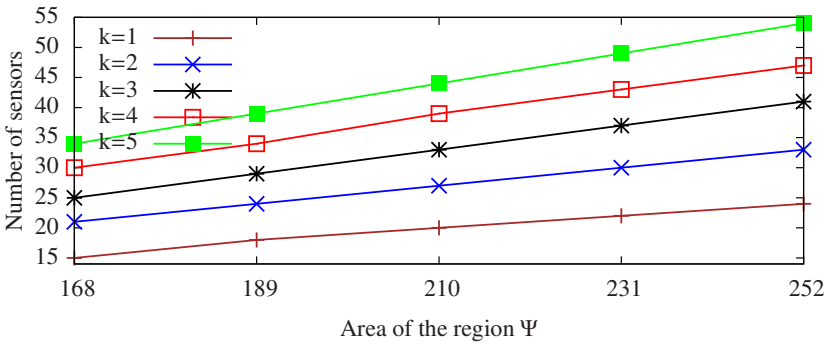

(a) Evaluation of Lemma 4.1.

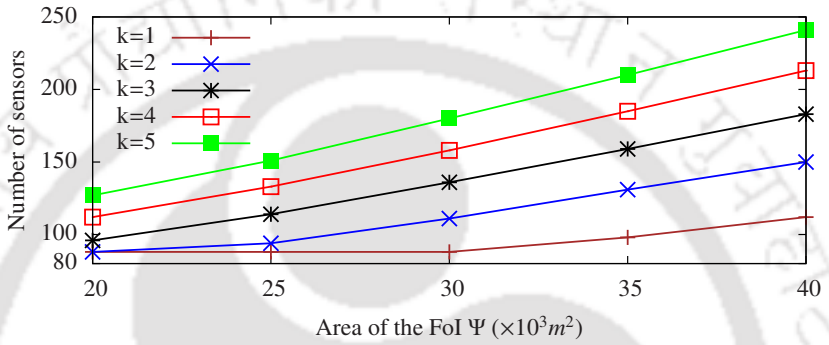

(b) Evaluation of Lemma 4.2.

Figure 4.9 Impact of the area of the FoI on the number of sensors required for k-coverage and connectivity, $k = 1, \ldots, 5$.

times the sensing and communication radii can be used in the analysis with h value of DoI, $0 \leq h < 1$. With this approximation, a sensor at point s can sense perfectly within the disc sensing region of radius $(1 - h) \times S$ centred at s. Similarly, a sensor at point s can communicate with other sensors within the communication disc of radius $(1 - h) \times C$ centred at s. Lemma 4.1 and Lemma 4.2 can be also used with irregular sensing and communication regions by replacing S and C with $(1 - h) \times S$ and $(1 - h) \times C$, respectively, where h is the value of the DoI.

We apply the DoI model and numerically evaluate Lemma 4.1 and Lemma 4.2 under the irregular sensing and communication (ISC) model. We consider the scenarios described in Example 3 and Example 4. Part (a) and part (b) of Fig. 4.10 illustrate that the number of sensors required for 1-coverage and connectivity, with ISC model is higher than that when the disc sensing and communication (DSC) model is used.

This is because, the ISC models lead to a reduction in the effective coverage and communication regions.

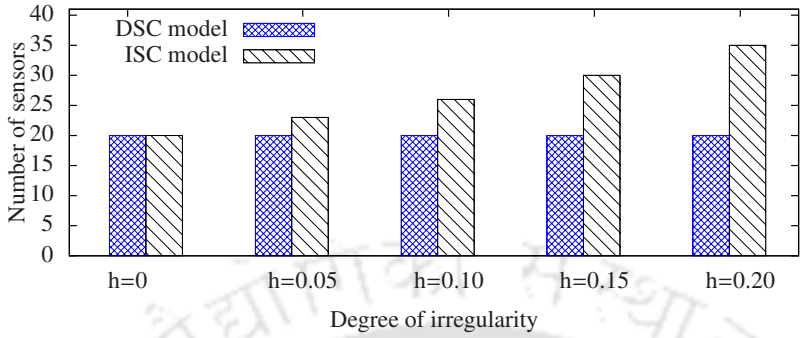

(a) Evaluation of Lemma 4.1.

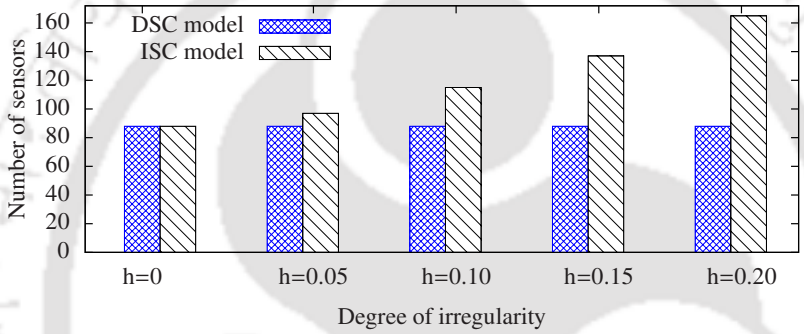

(b) Evaluation of Lemma 4.2.

Figure 4.10 Impact of the irregularity in sensing and communication regions on the number of sensors required for 1-coverage and connectivity.

4.6 Application of the Analysis

In this section, we demonstrate how the estimation of the minimum number of sensors required for coverage and connectivity can be used to deploy TINet. In our experiment, we used TINet to count the number of vehicles, detect the direction of the vehicles, and classify the vehicles that pass through the road, using sensors deployed along the boundaries of the road. We demonstrate that by deploying the minimum number of sensors estimated with our analysis we are able to effectively build a traffic monitoring system, without the sensors being directly deployed on the road.

4.6.1 Overview of TINet

TINet uses two types of nodes: sensor motes and data collection nodes. Fig. 4.11 shows the configuration of TINet with the sensor motes, data collection nodes, and base station using 802.15.4/Zigbee compliant and Wi-Fi (802.11.b) protocols to form a connected WSN. The number of sensors required to completely cover the road and to form a connected WSN is determined using our analysis.

Fig. 4.11 illustrates that the area of the effective sensing region of a sensor (indicated by checkered region), that is useful for coverage of a segment of the road, is less than the sensing area of the sensor.

The sensor node has a MICAz mote with a MDA100CA light sensor (indicated by blue rectangle in the figure), both from Crossbow technologies [57]. The MICAz mote is equipped with an 8 MHz Atmel microcontroller and a Chipcon CC2420 radio transceiver. The MDA100CA light sensor has a CdSe photocell. The resistance of a CdSe photocell varies inversely with the intensity of the light falling on it. With a sufficient intensity of light, the resistance of the MDA100CA light sensor drops and produces an electrical signal. The output of the sensor is connected to the analog-to-digital converter on the MICAz mote. The digital output is henceforth referred to as *sensory data* [58], which lies in the range of 0 to 1000 representing complete darkness and very bright light conditions [57].

Due to the limited communication range of the sensors, data collection nodes serve as the gateway nodes to interconnect the sensor motes and the base station as shown in Fig 4.11. A data collection node has a MICAz mote with MIB520 USB gateway and a computer. The MICAz mote with MIB520 USB gateway receives and transfers the sensory data from sensor motes to the computer. The data collection node then sends the sensory data to the base station using Wi-Fi (802.11.b) protocol as shown in Fig 4.11. At the base station, the sensory data from data collection nodes are merged and useful sensory data is communicated to the client via the WSN.

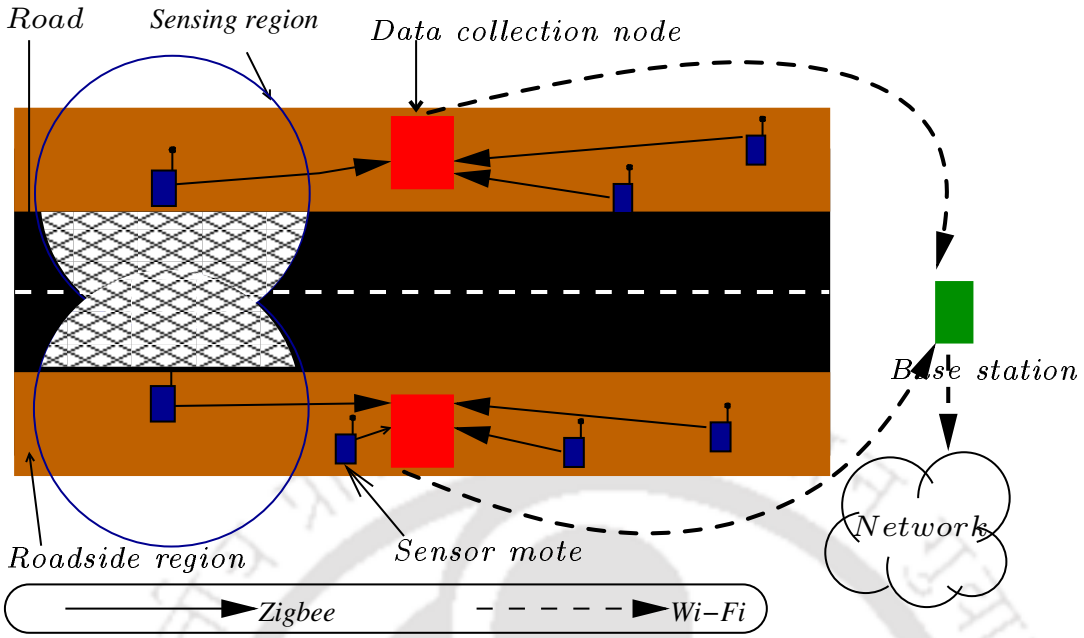

Figure 4.11 Illustration of TINet.

4.6.2 On-Road Experiment

We deployed TINet on a stretch of road in our campus, a snapshot of which is showed in Fig. 4.12. The experiments were carried out on a bidirectional two-lane road. A MICAz mote with a MDA100CA light sensor and a MICAz mote connected to a laptop served as the sensor node and data collection node in the experiment. Since we choose MDA100CA light sensor to detect the vehicles, we conducted the experiments at night. In our experiment, l, b, d, S and C are $21m$, $2m$, $10m$, $7m$ and $30m$, respectively. The area of the road and each road-side region are therefore $\|\Psi\|$=$210m^2$ and $\|\Omega\|$ /2=$42m^2$, respectively. Substituting l, b, d, S and C in Lemma 4.1, we get $n = 20$. Hence, we deployed 20 sensors and two data collection nodes along the boundaries of the road (left-side and right-side), to ensure that the road is almost surely covered and the WSN is connected. To validate the vehicle data collected by the WSN, we used a video camera to record the vehicle movement and the accuracy was computed by comparing the data from these two sources.

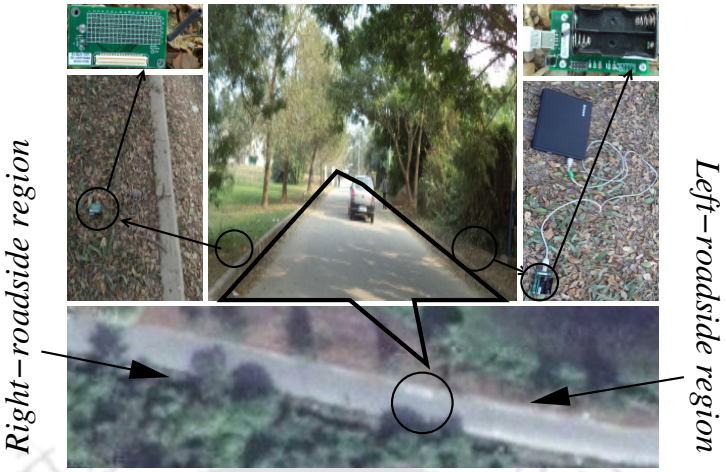

Figure 4.12 On-road experiment at Indian Institute of Technology Guwahati.

4.6.3 Experimental Results

• **Vehicle count:** Fig. 4.13(a) shows a scenario where 20 sensor motes and two data collection nodes are deployed along the boundaries and a vehicle passed through the road. A sensor mote collects a high value of the sensory data when a vehicle on the road is closer to it and light from the headlamps falls on the sensor. Let $L_{t,i}$ and $R_{t,j}$ indicate the sensory data of a left-side sensor i and a right-side sensor j at time instant t, respectively, where $1 \leq i \leq n/2$, $1 \leq j \leq n/2$, $0 \leq L_{t,i} \leq 1000$, and $0 \leq R_{t,j} \leq 1000$ for MICAz motes [57]. The sensory data of the left-side and the right-side sensor motes at time t is represented as $L_t = \{L_{t,1}, L_{t,2} \cdots, L_{t,n/2}\}$ and $R_t = \{R_{t,1}, R_{t,2} \cdots, R_{t,n/2}\}$, respectively. Fig. 4.13(a) indicates a case where $L_t = \{20, 700, 25, 0, \ldots, 0\}$ and $R_t = \{0, 0, 0, 0, \ldots, 0\}$ at time t. Since the sensory data of the left-side sensor are high, we can infer that a vehicle passed very close by the left-side of the road at time t. Fig. 4.13(b) indicates the sensory data of $L_t = \{20, 700, 25, 0, 0, 0, 10, 710, 10, 0\}$ and $R_t = \{0, 0, 0, 0, \ldots, 0\}$ at time t which signifies that two vehicles passed by the left-side of the road at time t.

Once a sensor produces a high value of sensory data, it sends a message to the data collection node which counts a vehicle and sends `a vehicle appeared` message to

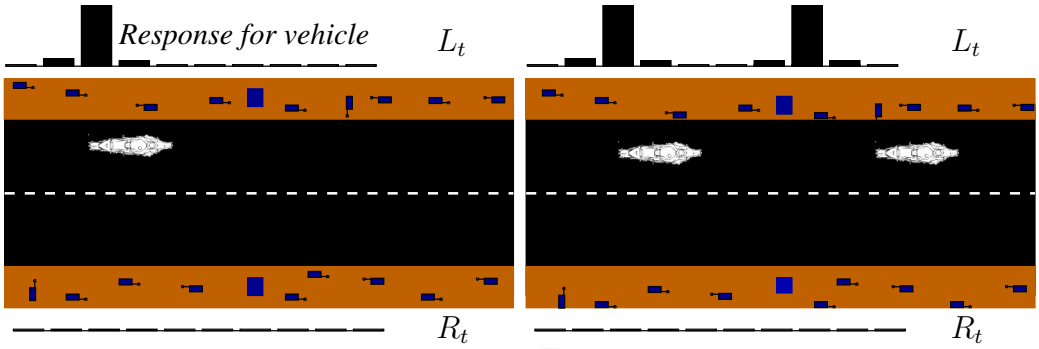

(a) One vehicle (b) Two vehicles

Figure 4.13 Scenarios for vehicle count result.

the base station. Using this procedure, we counted the number of vehicles passing on either lane of the road in several experiments. In all, we conducted ten experiments each lasting sixty minutes. Table 4.1 compares the number of vehicles counted by the sensors and the number of vehicles observed in the video recording in each of the 10 experiments. It can be observed that the overall accuracy with which the vehicles were detected is above 92%. In most of the experiments, it can be observed from Table 4.1 that not all the vehicles were detected by TINet. This is because the light from the headlamps did not fall on the sensor perfectly, which led to low values of sensory data.

Table 4.1 Results of vehicles counting experiments.

Expt. No.	Counted by camera	Counted by TINet
1	15	14
2	12	11
3	9	9
4	17	15
5	15	14
6	10	9
7	12	11
8	15	14
9	10	10
10	11	10
Total	**126**	**117**
Accuracy	**117/126=0.928**	

• **Vehicle direction detection:** It is sometimes observed that vehicles are driven on the wrong side of the road. On a highway, driving in the opposite side is a serious issue due to high speed of the vehicles. In this experiment, we use TINet to detect vehicles which change the lane or drive in the wrong direction. Fig. 4.14 shows the scenarios where 20 sensor motes and two data collection nodes are deployed along the boundaries and a vehicle passes through the road. Fig. 4.14(a) shows $L_t = \{10, 700, 15, 0, \ldots, 0\}$ and $R_t = \{0, 0, 0, 0, \ldots, 0\}$ at time t, indicating that a vehicle passed by the left-side of the road. Similarly, L_{t+3} and R_{t+3} in Fig. 4.14(d) illustrate that a vehicle passed by the left-side of the road at time $t+3$. The sensory data of a right-side sensor is high at time $t+1$ and $t+2$ as shown in Fig. 4.14(b) and Fig. 4.14(c), respectively. It indicates that a vehicle passed by the right-side of the road at $t+1$ and $t+2$. Based on the above sensory data, we can conclude that a vehicle has changed the direction in the road, since no other vehicle was detected by the sensors.

Since, we recorded the traffic with video camera, we could verify the events of wrong-lane driving detected by the TINet. The results of the direction detection experiments are presented in Table 4.2. In all, ten experiments of sixty minutes each were conducted. The overall accuracy of detecting vehicles changing the lanes is above 87.5%. We noticed that TINet detected fewer vehicles than those observed in video recording when the vehicle changed the lane for a very short duration or the light from the headlamps did not fall on the sensors.

• **Vehicle identification:** The ability to identify the vehicles (two-wheeler or four-wheeler) is desirable in building a good TIS. As mentioned in the previous section, the sensory data varies inversely with the strength of light that falls on the sensor motes. Since a two-wheeler has one headlight (showed in Fig 4.15(a)), either a left-side or a right-side sensor mote will register a high value of the sensory data when a two-wheeler passes by it. It can be seen from Fig. 4.15(c) that $L_t = \{10, 700, 15, 0, \ldots, 0\}$

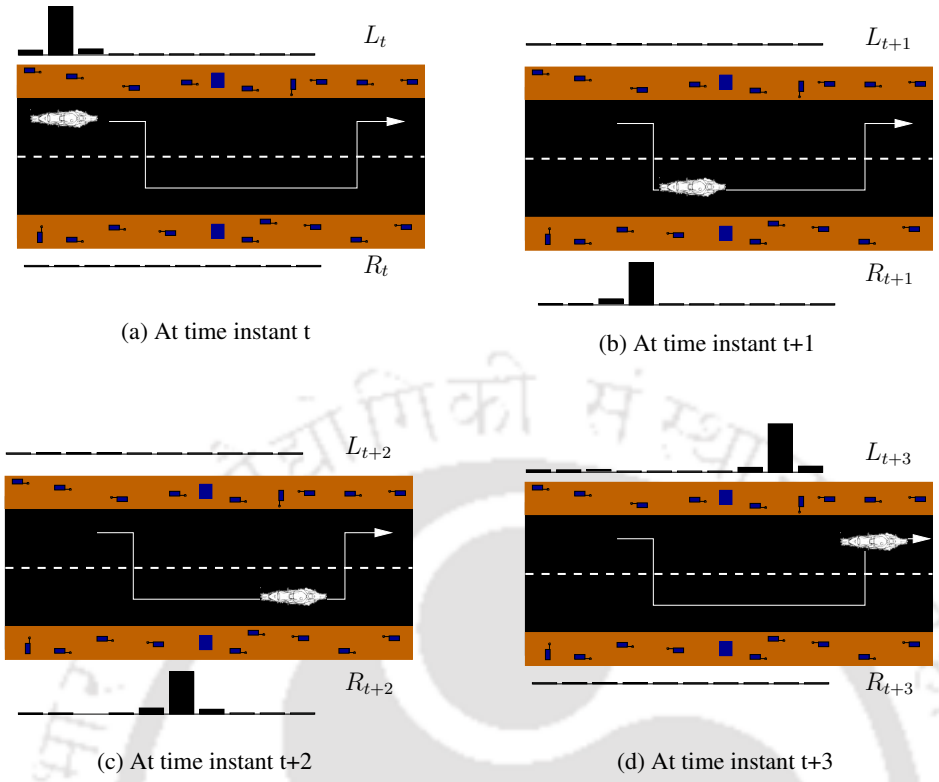

(a) At time instant t

(b) At time instant t+1

(c) At time instant t+2

(d) At time instant t+3

Figure 4.14 Scenarios for vehicle detection.

and $R_t = \{0, 0, 0, 0, \ldots, 0\}$ at time t. This indicates that a two-wheeler passed by the left-side of the road at time t. On the other hand, a four-wheeler has two headlights (shown in Fig 4.15(b)) so that the sensors on both sides of the road register high values of the sensory data when a four-wheeler passes through the road. Note that our campus roads are just two lane roads due to which the light from four wheeler is detected by sensors on each side. Fig. 4.15(d) shows that the sensory data of a left-side sensor mote and a right-side sensor mote are high at time instants t from which it can be concluded that a four-wheeler passed by the road. It can also be observed from Fig. 4.15(d) that, the sensory data of a left-side sensor mote is higher than a right-side sensor mote at time t. This is because the vehicle passed through the left-side and hence, the light intensity on the right-side sensor mote is less.

Ten experiments of sixty minutes each were conducted to identify two-wheelers and four-wheelers passing on the road. In the set of experiments, the total number

Table 4.2 Results of vehicle direction detection experiments

Expt. No.	Detected by Camera	Detected by TINet
1	4	3
2	3	3
3	1	1
4	4	3
5	3	3
6	4	3
7	4	4
8	5	5
9	0	0
10	4	3
Total	**31**	**28**
Accuracy	**28/31=0.875**	

of vehicles detected was 126, of which 103 were two-wheelers and the rest were four-wheelers. The overall vehicle detection accuracy for two-wheeler and four-wheeler was above 95% and 83%, respectively. The four-wheeler vehicle detection requires the light to be detected by the sensors on both the sides of the road. Since the light from the headlamps may not be sufficiently intense on the opposite side of the road, we found that the detection accuracy of four-wheelers was lower.

Table 4.3 Results of vehicle identification experiments

Experiment	Identified by camera		Identified by TINet	
	2-W	4-W	2-W	4-W
1	12	3	12	2
2	10	2	8	2
3	7	2	7	2
4	14	3	13	2
5	13	2	13	1
6	10	0	9	0
7	9	3	8	3
8	12	3	12	3
9	8	2	8	1
10	8	3	8	3
Total	**103**	**23**	**98**	**19**
Accuracy	**98/103=0.951**	**19/23=0.826**		

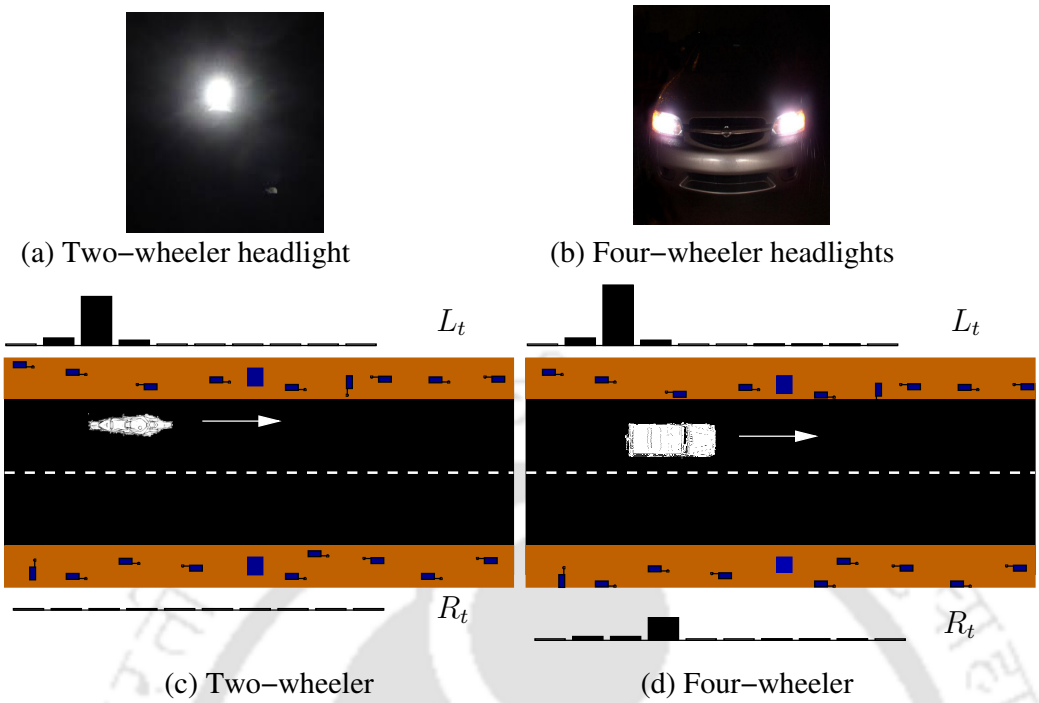

Figure 4.15 Scenarios for vehicle identification result.

• **Impact of number of sensors on experiment results:** We also studied the impact of the number of sensors on the accuracy of all the three sets of experiments. This is to verify, if the number of sensors required for coverage as computed from our analysis is correct. We consider the same scenario used in previous results. Fig. 4.16 shows the variation in the accuracy of the results as the number of sensors in TINet is increased. This result shows that 20 sensors are necessary for sufficient accuracy of on-road experiment results. It may be observed that a large number of sensors are desirable for the accurate detection of four-wheelers because, this experiment requires the sensory data of sensors on both the sides at a given time instance.

4.7 Conclusion

In this chapter, we analyzed k-coverage of the FoI and connectivity of the WSN when the sensors are deployed uniformly at random outside the FoI near the boundary. This problem is relevant for many real-world applications where the sensors cannot

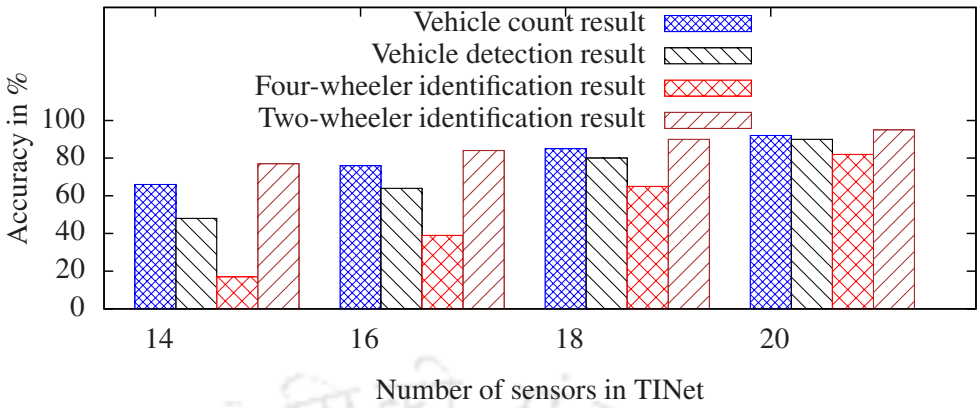

Figure 4.16 Impact of the number of sensors on vehicle count, detection, and identification results.

be deployed directly on the surface of the FoI. We determined the effective sensing area and effective communication area of a sensor located outside the FoI. The expected values of these were used in the estimation of the minimum number of sensors required for a desired level of coverage and connectivity. The analysis was validated with the simulations.

We demonstrated an application of the analysis to develop a TIS based on WSNs called TINet. TINet was deployed along the road-side to gather traffic data. TINet does not require excavation of the road surface. We demonstrated that our analysis can be used in planning and design of large scale WSNs with stochastic deployment of sensors outside the FoI.

Chapter 5

Analysis of k-Coverage and m-Connectivity in 3D Heterogeneous Directional WSNs

5.1 Introduction

WSNs monitoring a 3D FoI are commonly found in applications such as monitoring of wildlife habitats, where the sensors are deployed on trees in a forest at different heights [47], structural health monitoring of multi-storied buildings [59], underwater surveillance for oceanographic, marine life or coral reef monitoring [60], intelligent computer vision systems, constructing aerial defense systems, and building aerosphere pollution monitoring systems [45]. Most of the literature on 3D WSNs assumed the omni-directional sensing model [6, 31, 47, 32, 45] where a sensor can perfectly sense within the sphere of a given radius centred at the location of the sensor. However, there are many sensors in which the sensing region of the sensors is limited to a fixed direction and a specific angle. Examples of such sensors are camera sensors, infrared sensors, ultrasonic sensors, lidar sensors, and radar sensors. A 3D WSN with such a type of sensors is called 3D *directional WSN* in the literature [61].

The literature on 3D WSNs assumed either that the probability of a sensor being alive is unity [47, 6] or is constant for all the sensors [62, 63, 64]. In a large scale random deployment of sensors, this assumption is difficult to make. In a practical scenario, all the sensors may not have the same sensing and communication ranges, and may not have the same probability of being alive. The sensing range of the sensors might be different due to different hardware and imperfect sensing conditions. Such 3D WSNs are often called 3D *heterogeneous WSNs* (HWSNs) in the literature. The sensors in a 3D HWSN may be categorised into different types based on their sensing range, communication range, and/or the probability of being alive.

In this chapter, we address the problem:*when a large number of heterogeneous directional sensors are deployed uniformly at random in a 3D FoI, what is the expected value of the FoI that is k-covered and the expected value of m-connectivity of the WSN?* We assume that sensors of different types have different sensing range, communication range, or the probability of being alive.

Major Contributions: To the best of our knowledge, this is the first work to address the problem of determining k-coverage and m-connectivity in 3D WSNs with a stochastic deployment of sensors with heterogeneous and directional sensing capabilities. We derive an expression to evaluate the expected value of the k-coverage ratio of the 3D FoI. Specifically, we estimate the probability of a point in the 3D FoI, being covered by at least k heterogeneous sensors. Next, we estimate the expected value of m-connectivity in a 3D HWSN which can determine the communication range and the liveness fraction required to create an m-connected WSN. Finally, we demonstrate an application of the analysis to compute the number of sensors of each type required to ensure the desired k-coverage ratio and m-connectivity probability while optimizing the network cost.

The rest of this chapter is organised as follows. In the next section, we briefly discuss the literature on the analysis of coverage and connectivity in 3D WSNs. In

Sections 5.3, we state the assumptions, define the sensing and communication models, the terms and notation used in this chapter. In Sections 5.4 and 5.5, we derive the expressions for the expected value of k-coverage ratio and m-connectivity, respectively. The implication of irregular sensing model on the proposed work is discussed in Section 5.6. Section 5.7 presents an application of our analysis to design heterogeneous WSNs and conclude the chapter in Section 5.8.

5.2 Related work

Most of the literature on the coverage and connectivity in WSNs considers only deployment in a 2D FoI. A recent study in [6] reveals that the issues in 3D WSNs are significantly different from those in a 2D WSN, and the analysis for 2D WSNs cannot be applied to 3D WSNs directly. In this section, we review some work from the literature on the analysis of coverage and connectivity for 3D WSNs using stochastic deployment. However, our work is the first one to analyse coverage and connectivity in a stochastic deployment scenario with directional and heterogeneous sensors.

The authors in [31] estimated critical transmitting and sensing ranges for desired coverage and connectivity in 3D homogeneous WSNs. They computed the required sensing range to guarantee a certain degree of coverage of a region, the minimum and maximum network degrees for a given communication range as well as the hop-diameter of the network. Ammari and Das in [6] proposed the Reuleaux tetrahedron model to characterize k-coverage of a 3D FoI and investigated the minimum sensor density required when the sensors are deployed following a uniform distribution. It was proved that a FoI is guaranteed to be k-covered if any Reuleaux tetrahedron region of the field contains at least k sensors. The authors also computed the connectivity of homogeneous and heterogeneous 3D k-covered WSNs based on the size of the connected component that includes the sink. It was concluded that the connectivity of 3D k-covered WSNs is much higher than the degree of k-coverage. The same

authors in [47] addressed the coverage and connectivity problem in 3D WSNs using percolation theory. The authors modeled the coverage and connectivity problem as an integrated continuum percolation problem. They proposed an integrated-concentric-sphere model to analyse both coverage and connectivity in an integrated way. Critical density above which coverage and connectivity percolation will almost surely occur was derived. Recently the work in [32] studied the fundamental properties of 3D MANETs: link probability, node degree, and network coverage. The authors estimated the link probability, node degree, and coverage of 3D MANETs assuming random uniform distribution.

5.3 Preliminaries

In this section, we state the assumptions made about the network and define the terms used in this work.

Assumptions: The sensors are assumed to be deployed in a 3D FoI, denoted by Ψ, uniformly at random independent of each other. In a 3D HWSN, the sensors are categorised into t different types based on their sensing range, communication range, and/or probability of being alive. Let n_i be the number of type i sensors such that $\sum_{i=1}^{t} n_i = n$, where n is the total number of sensors in the network. All the sensors of a given type are assumed to have identical sensing and communication ranges and equal probability of being alive.

In this chapter, we assume the *binary directional sensing model* in which any type i sensor ($1 \leq i \leq t$), say s_i, has a sensing range S_i, a cone-of-view angle θ_i, and an orientation vector $\overrightarrow{w}$, which together define the 3D sector sensing region, denoted by ϕ_i. For any two points x and y, let $|xy|$ denote the Euclidean distance between them. For any two vectors $\overrightarrow{v_1}$ and $\overrightarrow{v_2}$, let $\alpha(\overrightarrow{v_1}, \overrightarrow{v_2})$ denote the angle between them. A point x is covered by a type i sensor if $|s_i x| \leq S_i$ and $\alpha(\overrightarrow{w}, \overrightarrow{s_i x}) \leq \theta_i/2$. The volume covered by s_i is nothing but the volume of the 3D sector region denoted

by $\|\phi_i\| = \frac{2}{3}\pi {S_i}^3(1 - \cos(\theta_i/2))$. The communication region of a sensor is modelled by the *binary spherical communication model*. The communication sphere is the region over which the sensor s_i can communicate with other sensors. The volume of communication region of s_i is nothing but the volume of the communication sphere given by $\|\zeta_i\| = \frac{4}{3}\pi {C_i}^3$, where C_i is the communication range.

Definition 1: *Liveness fraction* for a type i sensors, denoted by p_i, is the fraction of the type i sensors that are alive among the total number of them initially deployed.

Definition 2: In a HWSN, for any two sensors s_i and s_j, $\ni 1 \leq i, j \leq t$, $\forall\{i \neq j\}$, $S_i \neq S_j$, $\theta_i \neq \theta_j$, $C_i \neq C_j$, and/or $p_i \neq p_j$.

Definition 3: The *k-coverage ratio* of the FoI, denoted by η_k is defined as the fraction of the volume of the FoI in which each point is k-covered.

Definition 4: If two sensors s_i and s_j are such that the distance between them is less than $\min(C_i, C_j)$, then they are said to be *neighbours*.

Definition 5: A network can be modelled by a graph G=(V, E), where $V = \{v_1, ..., v_n\}$ and $E = \{e_1, \ldots, e_m\}$ are the set of n sensors and the bi-directional wireless links between them, respectively. The number of neighbours of a sensor of any type, say s, is called the *sensor degree*, denoted by $d(s)$. The *minimum sensor degree* in a communication graph G is given by $d(G)$=$\min_{s \in V} d(s)$.

Definition 6: A network is said to be *m-node-connected* or simply *m-connected* if for each pair of sensors in the communication graph G, there are at least m mutually independent communication paths connecting them [54]. The *m-connectivity probability*, denoted by γ_m is defined as the fraction of the sensors deployed in which every sensor is m-connected to the network.

5.4 Analysis of the k-coverage of the FoI

Let $A_{i,w}(x)$ denote the event that a point x in the 3D FoI Ψ is covered by exactly w number of type i sensors, $1 \leq i \leq t$. The probability of the event $A_{i,w}(x)$ depends

on the event that r of the n sensors at random are of the type i (denoted by $Q_{r,n}$), the event that m of those r type i sensors are alive (denoted by $C_{m,r}$), and the event that the point x is covered by exactly w of those m type i alive sensors (denoted by $D_{w,m}(x)$), where $w \leq m \leq r \leq n$. Assuming that the sensors are deployed independent of each other, the probability of the event $A_{i,w}(x)$ can be written as

$$\mathbf{P}(A_{i,w}(x)) = \sum_{m=w}^{n} \left(\sum_{r=m}^{n} \mathbf{P}(Q_{r,n}) \times \mathbf{P}(C_{m,r}) \right) \times \mathbf{P}(D_{w,m}(x)). \tag{5.1}$$

Since sensors are deployed uniformly at random in the FoI, we can write

$$\mathbf{P}(Q_{r,n}) = \binom{n}{r} \left(\frac{n_i}{n}\right)^r \left(1 - \frac{n_i}{n}\right)^{n-r}. \tag{5.2}$$

Similarly, the probability of the event $C_{m,r}$ is given by

$$\mathbf{P}(C_{m,r}) = \binom{r}{m} (p_i)^m (1 - p_i)^{r-m}, \tag{5.3}$$

where p_i is the fraction of type i sensors that are alive, and the probability of the event $D_{w,m}(x)$ is given by

$$\mathbf{P}(D_{w,m}(x)) = \binom{m}{w} \left(\frac{\|\phi_i\|}{\|\Psi\|}\right)^w \left(1 - \frac{\|\phi_i\|}{\|\Psi\|}\right)^{m-w}, \tag{5.4}$$

where $\|\phi_i\|/\|\Psi\|$ is the probability that the point $x \in \Psi$ is covered by a type i sensor. By substituting Eqs. 5.2, 5.3, and 5.4 into Eq. 5.1, we get

$$\mathbf{P}(A_{i,w}(x)) = \sum_{m=w}^{n} \left(\sum_{r=m}^{n} \binom{n}{r} \left(\frac{n_i}{n}\right)^r \left(1 - \frac{n_i}{n}\right)^{n-r} \times \binom{r}{m} (p_i)^m (1 - p_i)^{r-m} \right) \times \binom{m}{w} \left(\frac{\|\phi_i\|}{\|\Psi\|}\right)^w \left(1 - \frac{\|\phi_i\|}{\|\Psi\|}\right)^{m-w}.$$

Set $r = m + l$, so that

$$\mathbf{P}(A_{i,w}(x)) = \sum_{m=w}^{n} \left(\sum_{l=0}^{n-m} \binom{n}{m+l} \left(\frac{n_i}{n}\right)^{m+l} \left(1 - \frac{n_i}{n}\right)^{n-m-l} \times \binom{m+l}{m} (p_i)^m (1-p_i)^l \right) \times \binom{m}{w} \left(\frac{\|\phi_i\|}{\|\Psi\|}\right)^w \left(1 - \frac{\|\phi_i\|}{\|\Psi\|}\right)^{m-w},$$

$$= \sum_{m=w}^{n} \left(\sum_{l=0}^{n-m} \binom{n}{m} \left(\frac{n_i p_i}{n}\right)^m \binom{n-m}{l} \times \left(1 - \frac{n_i}{n}\right)^{n-m-l} \left(\frac{n_i}{n} - \frac{n_i p_i}{n}\right)^l \right) \times \binom{m}{w} \left(\frac{\|\phi_i\|}{\|\Psi\|}\right)^w \left(1 - \frac{\|\phi_i\|}{\|\Psi\|}\right)^{m-w}.$$

Using $(a+b)^n = \sum_{i=0}^{n} \binom{n}{i} a^{n-i} b^i$, we get

$$\mathbf{P}(A_{i,w}(x)) = \sum_{m=w}^{n} \binom{n}{m} \left(\frac{n_i p_i}{n}\right)^m \left(1 - \frac{n_i p_i}{n}\right)^{n-m} \times \binom{m}{w} \left(\frac{\|\phi_i\|}{\|\Psi\|}\right)^w \left(1 - \frac{\|\phi_i\|}{\|\Psi\|}\right)^{m-w}.$$

Set $m = w + q$, so that

$$\mathbf{P}(A_{i,w}(x)) = \sum_{q=0}^{n-w} \binom{n}{w+q} \left(\frac{n_i p_i}{n}\right)^{w+q} \left(1 - \frac{n_i p_i}{n}\right)^{n-w-q} \times \binom{w+q}{w} \left(\frac{\|\phi_i\|}{\|\Psi\|}\right)^w \left(1 - \frac{\|\phi_i\|}{\|\Psi\|}\right)^q,$$

$$= \sum_{q=0}^{n-w} \binom{n}{w} \left(\frac{n_i p_i \|\phi_i\|}{n \|\Psi\|}\right)^w \binom{n-w}{q} \times \left(1 - \frac{n_i p_i}{n}\right)^{n-w-q} \left(\frac{n_i p_i}{n} - \frac{n_i p_i \|\phi_i\|}{n \|\Psi\|}\right)^q.$$

Using $(a+b)^n = \sum_{i=0}^{n} \binom{n}{i} a^{n-i} b^i$, we get

$$\mathbf{P}(A_{i,w}(x)) = \binom{n}{w} \left(\frac{n_i p_i \|\phi_i\|}{n \|\Psi\|}\right)^w \left(1 - \frac{n_i p_i \|\phi_i\|}{n \|\Psi\|}\right)^{n-w}. \quad (5.5)$$

Next, let $C_k(x)$ denote the event that a point x in the 3D FoI Ψ is covered by at

least k sensors. The probability of the event $C_k(x)$ can be written as

$$\begin{aligned}
\mathbf{P}(C_k(x)) = 1 &- \mathbf{P}(x \text{ is not covered by any sensor}) \\
&- \mathbf{P}(x \text{ is covered by exactly one sensor}) \\
&- \mathbf{P}(x \text{ is covered by exactly two sensors}) \\
&\vdots \\
&- \mathbf{P}(x \text{ is covered by exactly } k-1 \text{ sensors}), \\
= 1 &- \sum_{l_1+l_2+\cdots+l_t=0} \prod_{j=1}^{t} \mathbf{P}(A_{j,l_j}(x)) \\
&- \sum_{l_1+l_2+\cdots+l_t=1} \prod_{j=1}^{t} \mathbf{P}(A_{j,l_j}(x)) \\
&- \sum_{l_1+l_2+\cdots+l_t=2} \prod_{j=1}^{t} \mathbf{P}(A_{j,l_j}(x)) \\
&\vdots \\
&- \sum_{l_1+l_2+\cdots+l_t=k-1} \prod_{j=1}^{t} \mathbf{P}(A_{j,l_j}(x)), \\
= 1 &- \sum_{\substack{l_1,l_2,\cdots,l_t\in[0,k-1] \\ 0\le l_1+l_2+\cdots+l_t\le k-1}} \prod_{j=1}^{t} \mathbf{P}(A_{j,l_j}(x)).
\end{aligned} \tag{5.6}$$

By substituting $\mathbf{P}(A_{j,l_j}(x))$ from Eq. 5.5, with i and w replaced by j and l_j, respectively, we get

$$\mathbf{P}(C_k(x)) = 1 - \sum_{\substack{l_1,l_2,\cdots,l_t\in[0,k-1] \\ 0\le l_1+l_2+\cdots+l_t\le k-1}} \prod_{j=1}^{t} \binom{n}{l_j} \left(\frac{n_i p_i}{n} \frac{\|\phi_i\|}{\|\Psi\|}\right)^{l_j} \times \left(1 - \frac{n_i p_i}{n} \frac{\|\phi_i\|}{\|\Psi\|}\right)^{n-l_j}.$$

The expected value of the FoI Ψ that is covered by at least k sensors can be obtained by simply integrating $\mathbf{P}(C_k(x))$ over Ψ. The expected value of the k-coverage ratio, denoted by $E[\eta_k]$, is the ratio of the expected volume of FoI Ψ covered by at least k

sensors to the volume of Ψ. Therefore,

$$E[\eta_k] = \frac{1}{\|\Psi\|} \iiint_{\Psi} \mathbf{P}(C_k(x)) d\Psi,$$

$$= 1 - \sum_{\substack{l_1,l_2,\cdots,l_t \in [0,k-1] \\ 0 \le l_1+l_2+\cdots+l_t \le k-1}} \prod_{j=1}^{t} \binom{n}{l_j} \times \left(\frac{n_i p_i}{n} \frac{\|\phi_i\|}{\|\Psi\|}\right)^{l_j} \left(1 - \frac{n_i p_i}{n} \frac{\|\phi_i\|}{\|\Psi\|}\right)^{n-l_j},$$

$$\text{where } \|\phi_i\| = \frac{2}{3}\pi {S_i}^3 (1 - \cos(\theta_i/2)). \tag{5.7}$$

The expected k-coverage ratio of the FoI can be interpreted as follows: If $E[\eta_3] = 0.80$, when we select several points from the FoI randomly, 80% of them are covered by at least three sensors.

Example 1: Consider a 3D FoI Ψ in which an equal number of two types of sensors are uniformly deployed at random. Let S_1, θ_1, p_1, S_2, θ_2, p_2, and the volume of Ψ be $100m$, $2\pi/3$, 0.80, $150m$, $2\pi/3$, 0.90, and $500^3 m^3$, respectively. We want to compute the minimal number of type 1 sensors and type 2 sensors to be deployed in Ψ such that 99% of the points selected at random are almost surely covered by at least two sensors. Substituting η_2=0.99, S_1, θ_1, S_2, θ_2, and $\|\Psi\|$ in Eq. 5.7, we get n_1=205 and n_2=205. That is, if we deploy 205 sensors of each type uniformly in Ψ, we can ensure that at least 99% of the volume is 2-covered.

5.4.1 Validation of the analysis

To verify the proposed analysis, we evaluate Eq. 5.7 numerically and compare the result with that obtained from a simulation. We use the toroidal distance metric to eliminate the border effects in the simulation [65]. In toroidal distance metric, the network is modelled in such a way that the sensors at an edge are assumed to cover the region near the opposite edge since the field is assumed to wrap around like a torus. Due to this, all the sensors have the same sensing and communication volumes. For the simulation results a Monte Carlo simulation is conducted as described in

Chapter 3, Section 3.4. The simulation results are with 95% confidence level though the error bars are not visible in the plots.

Fig. 5.1 shows the expected k-coverage ratio obtained with both simulation and numerical evaluation, for different densities of the sensors deployed. It can be observed that the expected k-coverage ratio evaluated using Eq. 5.7 matches with that from the simulation. We assume a cubical-shaped FoI of $500^3 m^3$ volume. By comparing Fig. 5.1(a) with parts (b), (c), and (d) of Fig. 5.1 it may be observed that for the same level of coverage of the FoI, the number of sensors required is smaller when only type 2 sensors are used (*i.e.*, case of $n_1 : n_2$=0 : 1) compared to the other three cases. This is because type 2 sensors have larger radii for sensing and therefore have higher utility for coverage. However, often the cost of such sensors may be higher prohibiting the use of only sensors with larger ranges. If we assume type 2 sensors to be costlier than type 1 sensors, then instead of deploying the sensors in the ratio of 1 : 3, deploying them in the ratio of 1 : 1 gives the desired level of coverage with a slightly larger number of sensors as seen from Figs. 5.1(b) and 5.1(c).

5.4.2 Numerical Results

Next, we evaluate Eq. 5.7 numerically to study the relationship between the volume of the FoI, the sensing range, the liveness fraction of the sensors, the number of sensors of different types, and the k-coverage ratio of the FoI. We consider the scenario described in Example 1 for all the results.

• **Impact of the volume of the FoI:** We study the relationship between k-coverage ratio, number of sensors of different types, and the volume of the FoI. Consider a 3D FoI Ψ in which two types of sensors are uniformly deployed at random. Fig. 5.2 shows the variation in the number of sensors of different types as the volume of Ψ is increased, for k-coverage ratio of 0.8 and 0.9, where k=1, 2. Obviously as the volume of FoI increases, a larger number of sensors are required to maintain the desired level

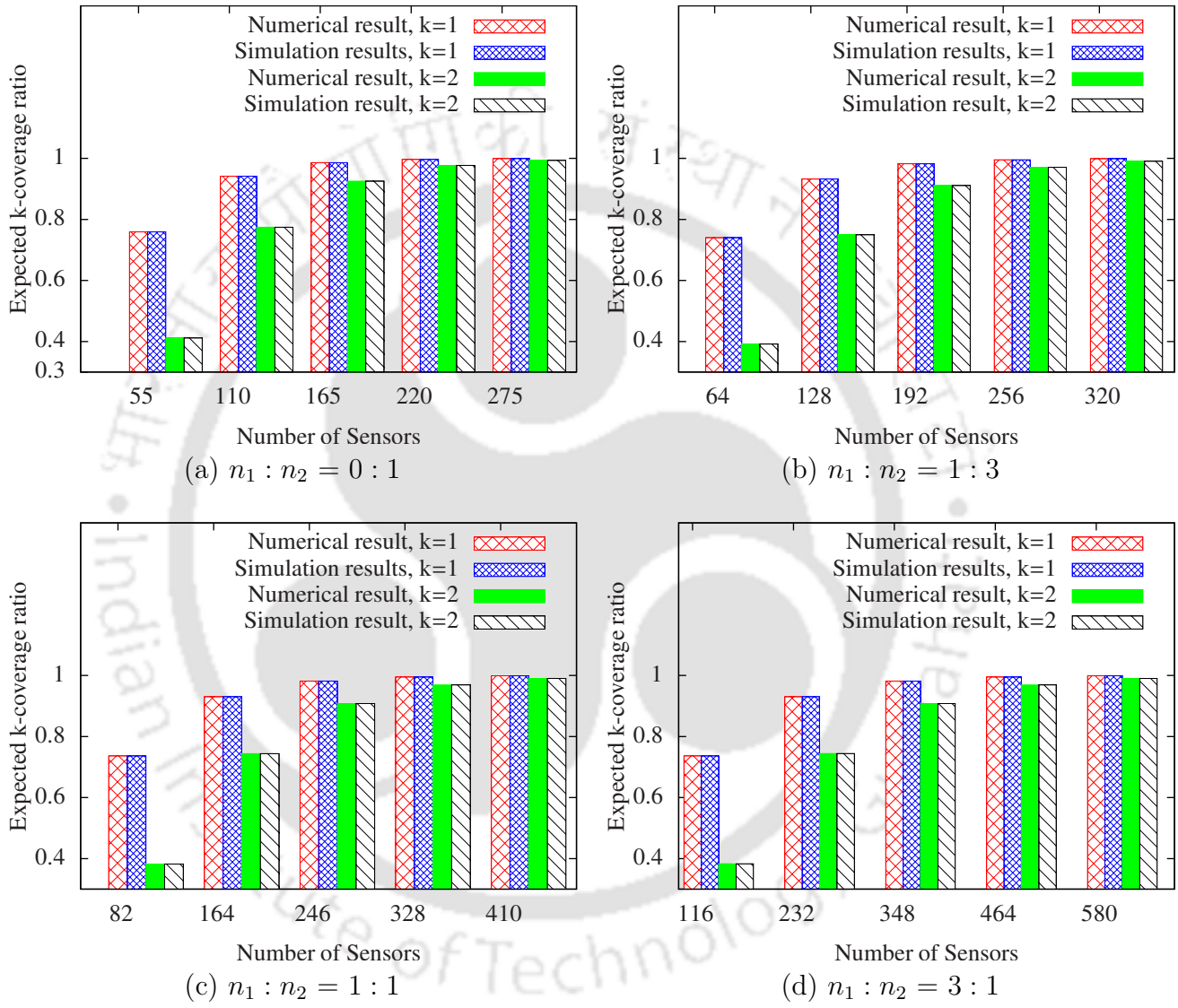

Figure 5.1 Variation in the expected k-coverage ratio of the FoI with number of sensors, k=1, 2.

of coverage ratio. Interestingly, the difference in the number of sensors required for a desired k-coverage ratio of 0.8 and 0.9 is smaller when only type 2 sensors are used (*i.e.*, $n_1 : n_2$=0 : 1) compared to the other three cases. This is because, as we have seen earlier, type 2 sensors have a larger sensing range and liveness fraction.

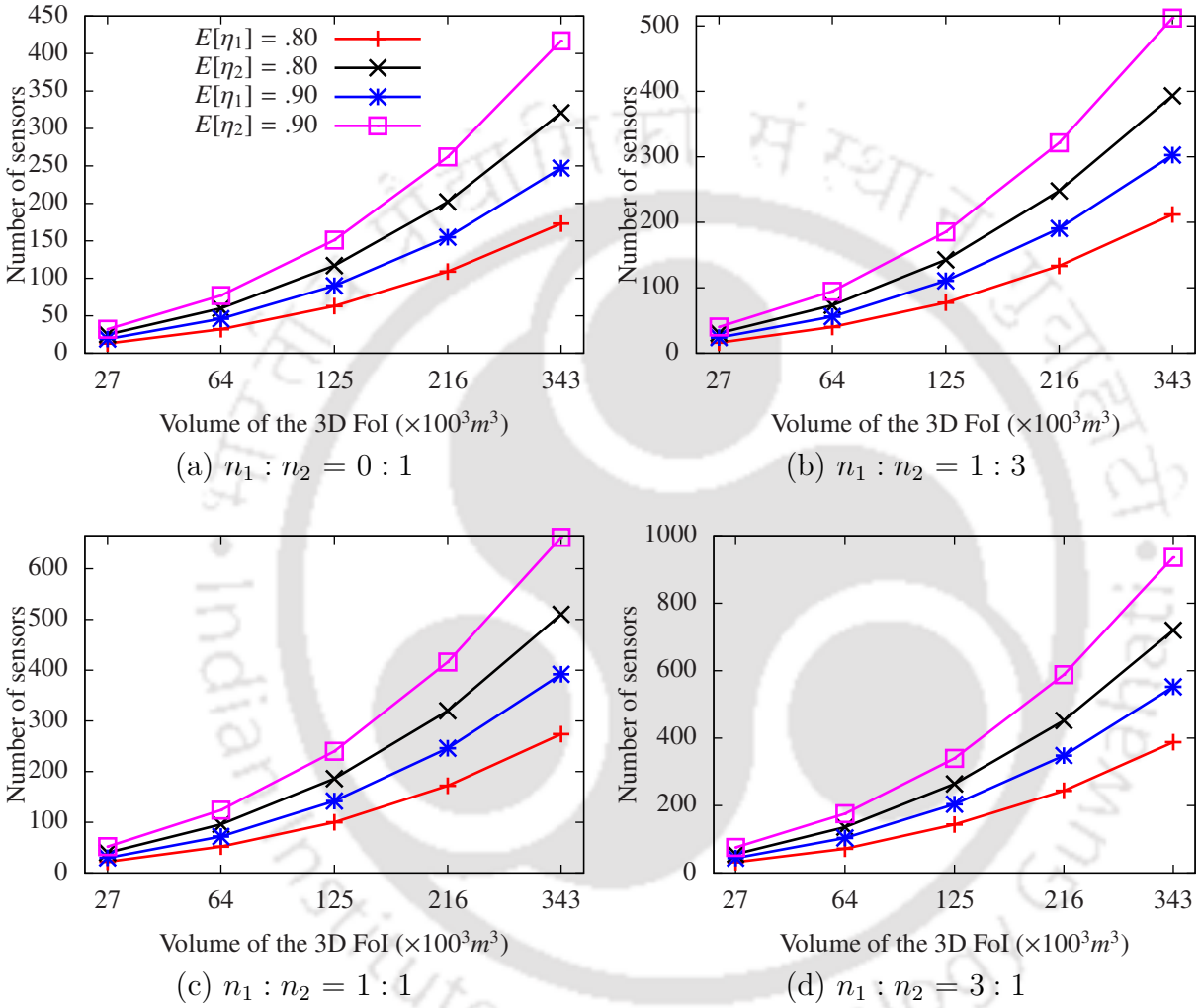

Figure 5.2 Relationship between the number of sensors and the volume of the 3D FoI.

• **Impact of liveness fraction:** Next, we study the impact of the liveness fraction of different types of sensors on the 2-coverage ratio of the 3D FoI. Parts (a)-(d) of Fig. 5.3 shows that for a fixed liveness fraction of type 1 and type 2 sensors, the number of sensors required for a 2-coverage ratio of 0.9 is smaller when only type 2 sensors are used (*i.e.*, $n_1 : n_2$=0 : 1) compared to the other three cases. This is

because type 2 sensors have larger sensing range. Fig. 5.3 also shows that for a fixed ratio of the type 1 and type 2 sensors, the number of sensors required for a desired 2-coverage ratio of 0.9 is smaller when the liveness fraction of type 2 sensors is high. It indicates that the high liveness fraction and large sensing range of type 2 sensors increase their utility for coverage.

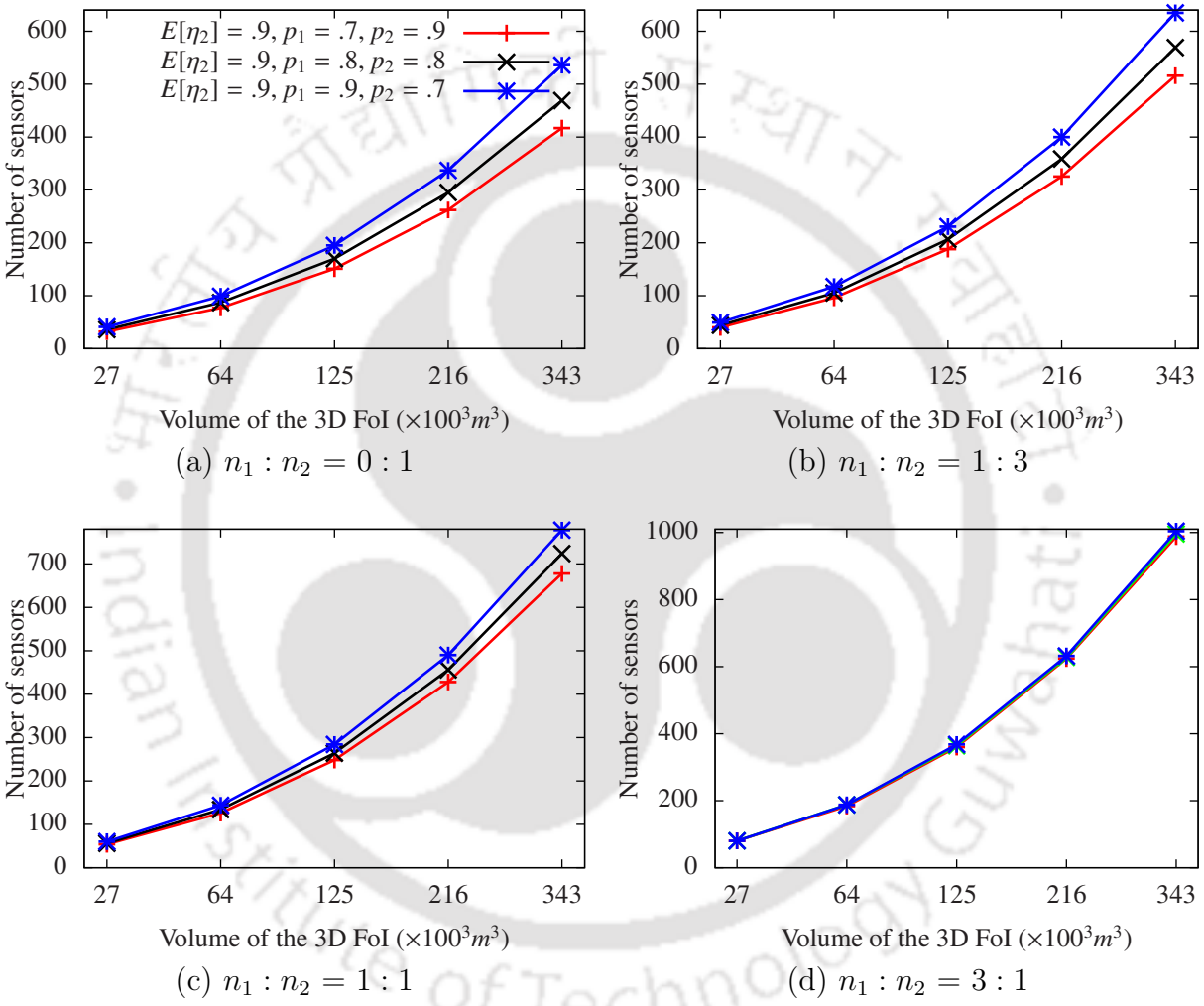

Figure 5.3 Relationship between the number of sensors and the volume of the 3D FoI for $E[\eta_2] = 0.90$.

5.5 Analysis of m-connectivity of the 3D HWSN

Let $G(\zeta_{min})$ be a communication graph formed by n sensors whose effective communication region is ζ_{min}, where $\|\zeta_{min}\|=\min(\|\zeta_1\|, \|\zeta_2\|, \cdots, \|\zeta_t\|)$, $\|\zeta_i\|=\frac{4}{3}\pi C_i^3$, and

$1 \leq i \leq t$. Let $A_{i,w}(s)$ denote the event that a sensor s, $s \in G(\zeta_{min})$ has exactly w number of type i neighbours. The probability of the event $A_{i,w}(s)$ depends on the probability that r of n sensors at random are of the type i, the event that m of those r type i sensors are alive, and the event that the sensor s has exactly w of those m as the neighbours, where $w \leq m \leq r \leq n$. The probability of the event $A_{i,w}(s)$ can be expressed as

$$\begin{aligned}\mathbf{P}(A_{i,w}(s)) = &\sum_{m=w}^{n}\left(\sum_{r=m}^{n}\binom{n}{r}\left(\frac{n_i}{n}\right)^r\left(1-\frac{n_i}{n}\right)^{n-r}\times\binom{r}{m}(p_i)^m(1-p_i)^{r-m}\right)\times\\ &\binom{m}{w}\left(\frac{\|\zeta_{min}\|}{\|\Psi\|}\right)^w\left(1-\frac{\|\zeta_{min}\|}{\|\Psi\|}\right)^{m-w},\\ =&\binom{n}{w}\left(\frac{n_i p_i\,\|\zeta_{min}\|}{n\,\|\Psi\|}\right)^w\left(1-\frac{n_i p_i\,\|\zeta_{min}\|}{n\,\|\Psi\|}\right)^{n-w}. \end{aligned} \tag{5.8}$$

Next, let $C_m(s)$ denote the event that a sensor s, $s \in G(\zeta_{min})$ has at least m neighbours. The probability of the event $C_m(s)$ can be written as

$$\begin{aligned}\mathbf{P}(C_m(s)) &= 1-\mathbf{P}(s\text{ is an isolated sensor})-\mathbf{P}(s\text{ has one neighbor})\\ &\quad\vdots\\ &\quad-\mathbf{P}(s\text{ has }(m-1)\text{ neighbors}),\\ &= 1-\sum_{l_1+l_2+\cdots+l_t=0}\prod_{j=1}^{t}\mathbf{P}(A_{j,l_j}(s))\\ &\quad-\sum_{l_1+l_2+\cdots+l_t=1}\prod_{j=1}^{t}\mathbf{P}(A_{j,l_j}(s))\\ &\quad\vdots\\ &\quad-\sum_{l_1+l_2+\cdots+l_t=m-1}\prod_{j=1}^{t}\mathbf{P}(A_{j,l_j}(s)),\\ &= 1-\sum_{\substack{l_1,l_2,\cdots,l_t\in[0,m-1]\\ 0\leq l_1+l_2+\cdots+l_t\leq m-1}}\prod_{j=1}^{t}\mathbf{P}(A_{j,l_j}(s)). \end{aligned} \tag{5.9}$$

By substituting $\mathbf{P}(A_{i,w}(s))$ from Eq. 5.8, with i and w replaced by j and l_j, respectively, we get

$$\mathbf{P}(C_m(s)) = 1 - \sum_{\substack{l_1,l_2,\cdots,l_t\in[0,m-1] \\ 0\le l_1+l_2+\cdots+l_t\le m-1}} \prod_{j=1}^{t} \binom{n}{l_j} \left(\frac{n_i p_i}{n}\frac{\|\zeta_{min}\|}{\|\Psi\|}\right)^{l_j} \times \left(1 - \frac{n_i p_i}{n}\frac{\|\zeta_{min}\|}{\|\Psi\|}\right)^{n-l_j}. \tag{5.10}$$

By definition of the minimum sensor degree, $d(G(\zeta_{min})) \ge m \Leftrightarrow \min_{\forall s\in V} d(s) \ge m$. Because the sensors are distributed independently, the probability of the event that $G(\zeta_{min})$ has the minimum sensor degree is

$$\mathbf{P}(d(G(\zeta_{min})) \ge m) = \binom{n}{n} \big(\mathbf{P}(C_m(s))\big)^n \big(1 - \mathbf{P}(C_m(s))\big)^0 = \big(\mathbf{P}(C_m(s))\big)^n. \tag{5.11}$$

Now, we use a property of geometric random graph proved in [55]. For a very large value of n, when we start with an empty graph and include the links formed by increasing the communication range, then the resulting graph is almost surely connected at a moment when the minimum sensor degree is unity with probability one. Therefore,

$$\mathbf{P}(G(\zeta_{min}) \text{ is } m\text{-connected}) = \mathbf{P}(d(G(\zeta_{min})) \ge m). \tag{5.12}$$

Since the event of $G(\zeta_{min})$ being m-connected is a necessary condition for a directed communication graph G as defined in Definition 5, the probability of the event that the graph G is m-connected is given by

$$\mathbf{P}(G \text{ is } m\text{-connected})) \ge \mathbf{P}(G(\zeta_{min}) \text{ is } m\text{-connected}).$$

By using both Eq. 5.11 and Eq. 5.12 for $\mathbf{P}(G(\zeta_{min})$ is m-connected), we get

$$\begin{aligned} \mathbf{P}(G \text{ is } m\text{-connected})) &\ge \mathbf{P}(G(\zeta_{min}) \text{ is } m\text{-connected}), \\ &\ge \big(\mathbf{P}(C_m(s))\big)^n. \end{aligned} \tag{5.13}$$

From Eqs. 5.13 and 5.10, the expected m-connectivity probability of the graph G, denoted by $E[\gamma_m]$, is given by

$$E[\gamma_m] = \mathbf{P}(G \text{ is } m\text{-connected})),$$
$$\geq \left(1 - \sum_{\substack{l_1,l_2,\cdots,l_t \in [0,m-1] \\ 0 \leq l_1+l_2+\cdots+l_t \leq m-1}} \prod_{j=1}^{t} \binom{n}{l_j} \left(\frac{n_i p_i}{n} \frac{\|\zeta_{min}\|}{\|\Psi\|}\right)^{l_j} \times \left(1 - \frac{n_i p_i}{n} \frac{\|\zeta_{min}\|}{\|\Psi\|}\right)^{n-l_j}\right)^n. \tag{5.14}$$

The expected m-connectivity can be interpreted as follows: If $E[\gamma_2] = 0.99$, when we select several sensors from the network randomly, 99% of them are almost surely 2-connected.

Example 2: Consider a 3D FoI Ψ in which two types of sensors (same number of each type) are uniformly deployed at random. Let C_1, p_1, C_2, p_2, and the volume of Ψ be $100m$, 0.80, $150m$, 0.90, and $500^3 m^3$, respectively. We want to compute the minimum number of sensors of each type to be deployed in the FoI such that 99% of the sensors selected at random are almost surely 2-connected. The volumes of the communication regions of either type are $\|\zeta_1\| = 4.19 \times 10^6 m^3$ and $\|\zeta_2\| = 14.13 \times 10^6 m^3$. The effective communication volume $\|\zeta_{min}\| = \min(\|\zeta_1\|, \|\zeta_2\|) = 4.19 \times 10^6 m^3$. Substituting $\|\zeta_{min}\|$ and $E[\gamma_2]$ in Eq. 5.14, we get $n_1 = n_2 = 233$. That is, if we deploy 233 sensors of each type uniformly in the FoI, we can ensure that 99% of the sensors selected at random are almost surely 2-connected.

5.5.1 Validation of the analysis

To verify the proposed analysis, we evaluate Eq. 5.14 numerically for the scenario described in Example 2, and compare the result with that obtained in a simulation. For the simulation results a Monte Carlo simulation is conducted as described in Chapter 3, Section 3.4. Fig. 5.4 shows the expected m-connectivity probability obtained from simulation and numerical evaluation, for different communication ranges of the

sensors. The volume of the FoI Ψ is $10^9 m^3$ and $E[\gamma_m] \geq 0.99$. It can be observed that the expected m-connectivity probability evaluated using Eq. 5.14 matches with that obtained in the simulation. The simulation results are with 95% confidence level though the error bars are not visible in the plots.

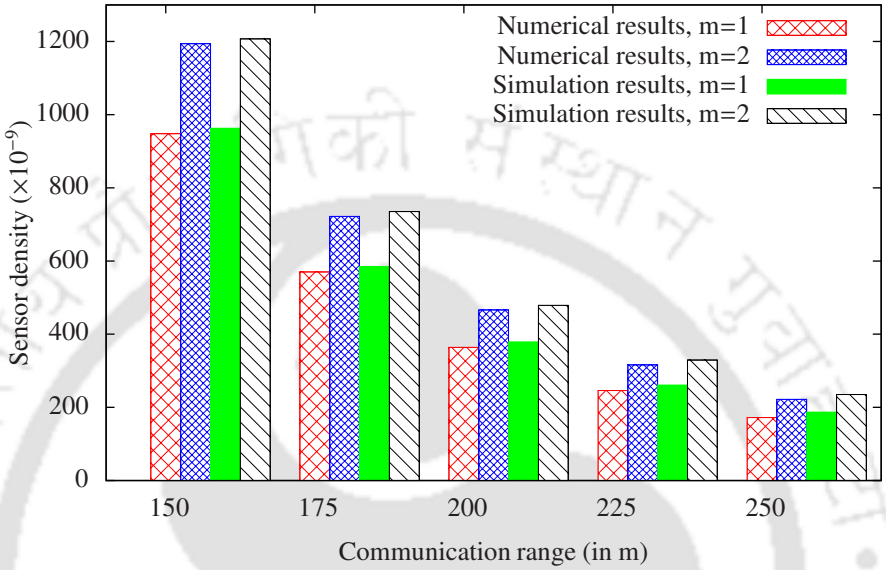

Figure 5.4 Relationship between the sensor density and the communication range of the sensors.

5.5.2 Numerical Results

In this section, we present results based on the numerical evaluation of Eq. 5.14 that demonstrate the relationship between the volume of the FoI, the communication range of the sensors, the liveness fraction of the sensors, the number of sensors of different types, and the 2-connectivity. We consider the same scenario described in Example 2. Fig. 5.5 shows the variation in the number of sensors of different types as the volume of Ψ is increased, for 2-connectivity probability of at least 0.99. Obviously as the volume of Ψ increases, a larger number of sensors are required to maintain the desired degree of connectivity. Interestingly, parts (a) and (b) of Fig. 5.5 show that for a fixed ratio of the type 1 and type 2 sensors, the number of sensors required for a desired level of connectivity is smaller when the liveness fraction of the sensors is

high. This indicates that a greater liveness fraction of the sensors increases the utility of sensors for connectivity.

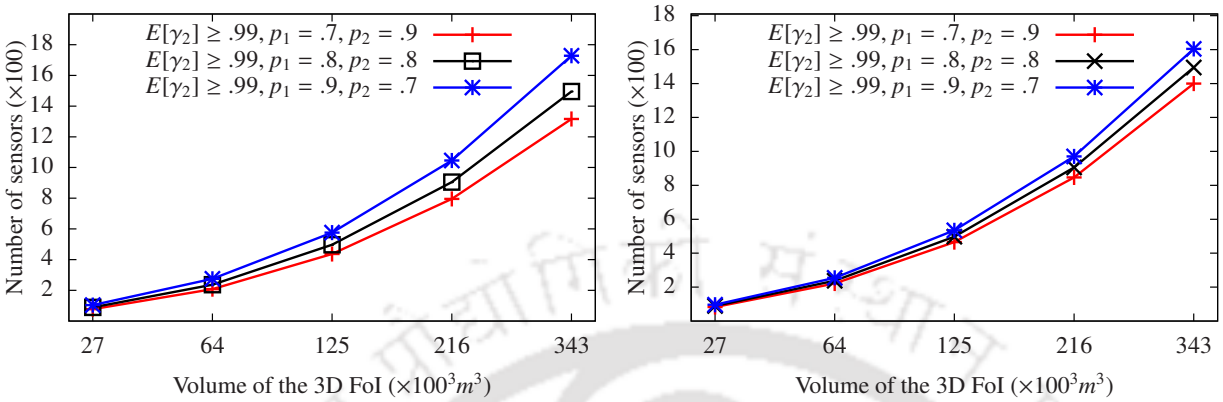

(a) $n_1 : n_2 = 0 : 1$ (b) $n_1 : n_2 = 1 : 3$

Figure 5.5 Relationship between the number of sensors and the volume of the 3D FoI for $E[\gamma_2 \geq .99]$.

5.6 Irregular directional sensing and spherical communication models

In our analysis so far, we assumed that the sensors have directional sensing and spherical communication regions. Similar to Chapter 4, in a practical scenario, the directional sensing and spherical communication regions are irregular. The degree of irregularity (DoI) model, as described in Chapter 4, Section 4.5.2 is also assumed for this work. With this model, instead of using the radius of an ideal 3D sector or sphere in the analysis, $1 - h$ times the sensing and communication radii can be used in the analysis with h value of DoI, $0 \leq h < 1$. With this approximation a sensor s_i can sense perfectly within the directional sensing region of radius $(1 - h) \times S_i$ centred at the location of s_i. Similarly, a sensor s_i can communicate with other sensors within the communication sphere of radius $(1 - h) \times C_i$ centred at the location of s_i. Eq. 5.7 for expected k-coverage ratio and Eq. 5.14 for expected m-connectivity probability can be also used with irregular sensing and communication regions by replacing S_i

and C_i with $(1-h) \times S_i$ and $(1-h) \times C_i$, respectively, where h is the value of the DoI.

We apply the DoI model and present the results based on numerical evaluation of Eqs. 5.7 and 5.14 under the irregular sensing and communication (ISC) models. We consider the same scenario described in Example 1 and Example 2 for this evaluation. We varied the ratio of the number of sensors of each type deployed in the 3D FoI (shown as $n_1 : n_2$ in the plot). For each simulation, we conducted ten runs with different seeds and average the results. We studied the relationship between 2-coverage and 2-connectivity on the number of sensors in the FoI with the spherical sensing and communication (SSC) model and ISC model using 0.05 value of DoI. Results in parts (a) and (b) of Fig. 5.6 show that the number of sensors required for 2-coverage and 2-connectivity with the ISC model using h=0.05 is greater than that required when the SSC model is used. This is because, the ISC model reduces the effective region covered by the sensors or effective communication range while, the SSC model ignores this irregularity.

5.7 Application of the Analysis

In this section, we show an application of the analysis to compute the minimum number of sensors of each type required for the desired level of coverage and connectivity thereby minimising the network cost. Eqs. 5.7 and 5.14 show that the expected k-coverage ratio and m-connectivity probability, respectively depend on the number of different types of sensors, their sensing and communication regions, and the liveness fraction of the sensors. In a 3D HWSN any combination of the number of sensors (of different types) that maintains the k-coverage and m-connectivity above the threshold value is valid. In Table. 5.1 we show several such valid combinations for the number of sensors to achieve $E[\eta_2] \geq 0.99$ and $E[\gamma_2] \geq 0.99$. Since the network cost is not same for all valid combinations, we devise an algorithm to compute the number of different

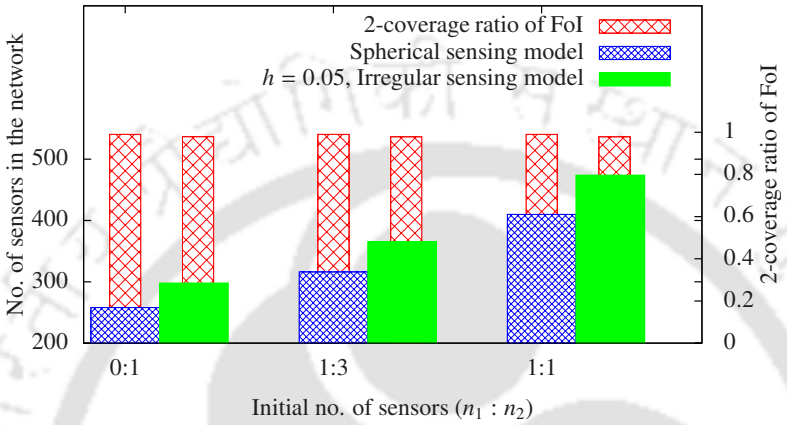

(a)Variation in the $E[\eta_2]$ with SSC and ISC models.

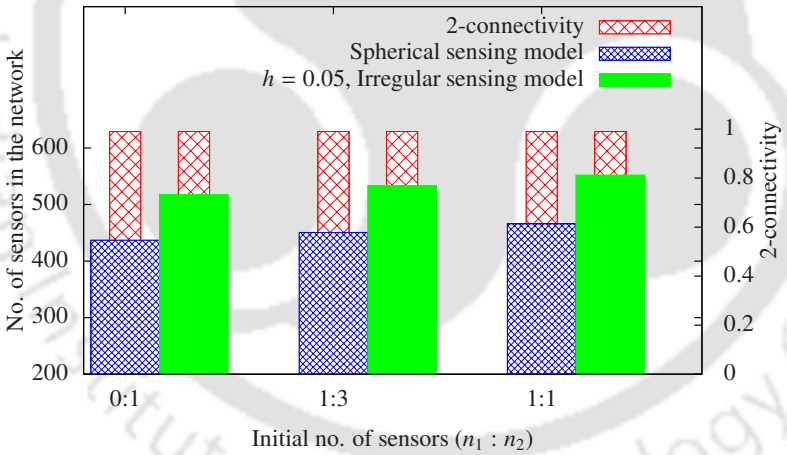

(b)Variation in the $E[\gamma_2]$ with SSC and ISC models.

Figure 5.6 Impact of the irregularity in sensing and communication regions on the number of sensors required for 2-coverage and 2-connectivity.

types of sensors required to maintain the desired k-coverage ratio and m-connectivity probability and then select the combination that minimises the network cost. The problem can be expressed by the following mathematical formulation:

$$\begin{aligned} \min \quad & \sum_{i=1}^{t} Cost_i \times n_i \\ \text{subject to} \quad & E[\eta_k] \geq \eta_{th}, \\ & E[\gamma_m] \geq \gamma_{th}. \end{aligned} \tag{5.15}$$

where $Cost_i$ is the cost of a type i sensor, η_{th} and γ_{th} are the threshold values of the desired k-coverage and m-connectivity, respectively.

Algorithm: Algorithm 1 computes the requirements for a minimum-cost 3D HWSN to achieve the desired k-coverage and m-connectivity. We start by fixing the maximum number of sensors of each type *i.e.*, n_i to say n_{max} for $1 \leq i \leq t$. Algorithm 1 takes S_i, θ_i, C_i, $Cost_i$, k, m, η_{th}, γ_{th}, and n_{max} as input. It then computes $E[\eta_k]$ and $E[\gamma_m]$ iteratively for all combinations of sensors using the function *covered* and *connected*, respectively. If $E[\eta_k]$ and $E[\gamma_m]$ satisfy the thresholds *i.e.*, $E[\eta_k] \geq \eta_{th}$ and $E[\gamma_k] \geq \gamma_{th}$, then that combination of sensors is considered to be valid. For each valid combination, the algorithm computes the network cost. The algorithm finally returns the number of sensors of each type required to minimise the network cost and to satisfy the desired k-coverage ratio and m-connectivity.

Time Complexity: There are t **for** loops in the functions *covered* and *connected*, resulting in a time complexity of $O(n_{max}^t \times (r + m + c))$, where r, m, and c are the time complexities of the functions *covered*, *connected*, and the function to compute minimum-cost of the network, respectively. Thus, the time complexity of the algorithm is $O(n_{max}^t \times (r + m + c))$=$O(n_{max}^t)$ which is in polynomial time.

Algorithm 1: DESIGN OF A MINIMUM COST HWSN.

Input: S_i, θ_i, C_i, $Cost_i$, k, m, η_{th}, γ_{th}, n_{max}, t
Output: $n_1, ..., n_t$, $Cost$
Initialization: $Cost$=∞;
for *int* $q_1 \leftarrow 1$ ***to*** n_{max} **do**
  ⋮
  for *int* $q_t \leftarrow 1$ ***to*** n_{max} **do**
    if *(covered* $(k,q_1, ..., q_t) \geq \eta_{th}$ *and connected* $(m,q_1, ..., q_t) \geq \gamma_{th}$*) and* $\left(\sum_{i=1}^{t} Cost_i \times q_i \leq Cost\right)$ **then**
      $n_1 = q_1, \ldots, n_t = q_t$ and $Cost$=$\sum_{i=1}^{t} Cost_i \times q_i$;

Function *covered*$(k, q_1, ..., q_t)$
begin
  return the computation result ($E[\eta_k]$) of Eq. 5.7,
  where $n_i = q_i$ and $n = q_1 + q_2 + \cdots + q_t$, $1 \leq i \leq t$;
end

Function *connected*$(m, q_1, ..., q_t)$
begin
  return the computation result ($E[\gamma_m]$) of Eq. 5.14,
  where $n_i = q_i$ and $n = q_1 + q_2 + \cdots + q_t$, $1 \leq i \leq t$;
end

Example 3: Consider the scenario described in Example 1 and Example 2. Let the cost of type 1 and type 2 sensors be $Cost_1 = 105$ units and $Cost_2 = 122$ units, respectively. We want to compute a minimum-cost 3D HWSN such that $E[\eta_2] \geq 0.99$ and $E[\gamma_2] \geq 0.99$. Table 5.1 shows the result of executing Algorithm 1. Columns 3 and 4 in Table 5.1 show the 2-coverage and 2-connectivity, respectively for a given number of sensors of each type (shown in the first two columns). Cost of the network for a given number of sensors of different types is shown in columns 5. It can be seen that the minimum network cost for the deployment is obtained with $n_1 = 283$ and $n_2 = 188$.

Table 5.1 The network cost computed with Algorithm 1.

n_1	n_2	$E[\eta_2]$	$E[\gamma_2]$	Cost
266	203	0.99	0.99	52696
267	202	0.99	0.99	52679
275	195	0.99	0.99	52665
283	**188**	**0.99**	**0.99**	**52651**
		⋮		
242	224	0.99	0.99	52738
250	217	0.99	0.99	52724
258	210	0.99	0.99	52710

5.8 Conclusion

In this chapter, we studied the k-coverage and m-connectivity problem in 3D WSNs that use stochastic deployment of sensors. We considered the directional sensing model and heterogeneity in the sensors to estimate the expected k-coverage ratio and m-connectivity probability. To the best of our knowledge this work is the first one to consider practical aspects in heterogeneous WSNs like directionality and probability of sensor being alive in the analysis of k-coverage and m-connectivity. We suggested a modification to the analysis in practical scenarios with irregular sensing and communication regions. We demonstrated an application of the analysis in the design of cost-effective 3D HWSN. We believe that this work can motivate further research in energy-efficient provisioning of k-coverage and m-connectivity in 3D HWSNs.

Till now, this thesis considered that the sensors are deployed uniformly at random in the FoI or outside the FoI near the boundary. We estimated the minimum number of sensors required for a desired level of coverage and connectivity in WSNs. A limited battery power and difficulty in recharging/replacing the batteries in a hostile environment require that the sensors be deployed with a high density to prolong the lifetime of the WSN. A popular technique used for energy-efficient coverage of the FoI is to identify if there are any redundant sensors and schedule them to sleep without compromising the desired level of coverage of the FoI. In the rest of the thesis,

we propose coverage-preserving scheduling protocols for the cases of k-coverage and partial coverage of the FoI.

Chapter 6

Sleep Scheduling for k-Coverage in 3D Heterogeneous WSNs

6.1 Introduction

In the previous chapters, we derived probabilistic expressions for the desired level of coverage and connectivity that are useful to optimise the cost of the stochastic deployment of WSNs. Minimising the energy consumed while ensuring the desired level of coverage of a FoI is another important issue to be addressed in WSNs, because the batteries powering the sensors may not be accessible for recharging often. A popular technique used for energy-efficient coverage of the FoI is to identify if there are redundant sensors and schedule them to sleep without decreasing the desired coverage of the FoI [66, 67, 68].

In this chapter, we estimate the probability of a sensor in a 3D heterogeneous WSN being redundant for k-coverage and propose a protocol for duty cycling the sensors while ensuring the desired level of coverage. We consider a sensor to be redundant for k-coverage of a FoI, if each point in its sensing sphere is also covered by at least k neighbouring sensors. While there is similar work in the literature on 3D homogeneous WSNs [2], there is no equivalent work for 3D heterogeneous WSNs

to the best of our knowledge.

Major Contributions: We derive an expression to quantify the redundancy in stochastic k-coverage of a point in a 3D FoI. We extend the analysis to derive an expression to determine the probability of a sensor, with a set of neighbours of different types, being redundant for k-coverage of the FoI. We propose a distributed scheduling protocol to put the redundant sensors to sleep yet maintaining the desired level of coverage in the FoI. This protocol does not require the sensor to have any information about its geographical location/relative position to discover its redundancy.

The rest of the chapter is organised as follows: In the next section, we briefly discuss the literature on the scheduling protocols for 3D WSNs which also addresses the coverage problem. In Section 6.3 we define the network model, the terms and the notation used. In Section 6.4 we derive the expressions for the probability of a point being redundantly covered and the condition for the redundancy of a sensor in a 3D heterogeneous WSN. We also validate the expressions with numerical evaluation and simulation results. Section 6.5 discusses the proposed simple scheduling protocol which can help a sensor determine if it is redundant based on the information about its neighbours and schedule its activity. Simulation results to demonstrate the benefit of sleep scheduling on the lifetime of a WSN are presented for different network scenarios. A few practical considerations for the proposed work are discussed in Section 6.6 and the chapter is concluded in Section 6.7.

6.2 Related work

In this section, we discuss only the literature related to coverage-preserving scheduling algorithms for 3D WSNs. Ammari and Das [2] analysed the coverage problem in 3D WSNs and showed that the results for 2D WSNs cannot be directly applied due to the inherent characteristics of the Reuleaux tetrahedron. The authors proposed a distributed k-coverage preserving protocol for 3D WSNs based on the closest shape

of the Reuleaux tetrahedron, where each point in a 3D FoI is k-covered. The basic approach is to divide the sensing region of a sensor into twelve equal-sized sectors and if each sector consists of another sensor then it is redundant. The proposed protocol guarantees that the sensing region of each sensor is k-covered. Huang *et al.* [3] formulated the coverage problem as a decision problem, where the goal is to determine whether each point in a FoI is covered by at least k sensors. The basic idea is to reduce the geometric problem from a 3D space to a 2D space by observing that the FoI is divided into number of regions by the sensing spheres and that the level of coverage of a region can be derived from the spherical segments comprising the same. Furthermore, each spherical segment must be bounded by a number of circular segments, and the level of coverage of a spherical segment can be derived from those circular segments that surround the spherical segment. This transforms the 2D problem into a one-dimensional (1D) problem which implies that it is sufficient to determine the coverage of the circular segment. The authors also proposed a distributed energy-conserving protocol that can reduce the number of sensors in active state and still maintain sufficient coverage eliminating the redundant sensors.

The authors in [29] derived a distributed algorithm to choose a subset of working sensors for full coverage. The authors proposed a backup scheme, where each sensor has a designated substitute set from the sleeping set of sensors. Xiao *et al.* in [28] proposed an immune-ant colony coverage control algorithm for energy efficient operation of a 3D WSN. An artificial immune algorithm is used to improve ant colony algorithm to avoid the possibility of a local optimal solution. A deployment strategy was also proposed for the placement of sensors in a 3D FoI. Xiaole *et al.* [69] studied the problem of constructing connected and full covered optimal 3D WSNs. The authors designed a set of regular patterns for k-connectivity and full coverage, where $k = 14, 6$.

Motivation: The work in this chapter is motivated by the following limitations observed in the literature. The work in [2] derives the necessary conditions to determine if a sensor is redundant but assumed that each sensor has location information. The use of technology for geolocation is not feasible for low cost and low power 3D WSNs. Without any geographical information, it is usually hard to check if a sensor is redundant. Similar limitations also apply to the work in [3, 28, 29] and to the best of our knowledge, none of the previous works can be applied if the sensors do not have their location information. The work in [28, 29] identified if there are redundant sensors only when the FoI is 1-covered and the results are not applicable for k-coverage. 1-coverage of the FoI is not sufficient in certain WSN applications such as military applications where a high degree of reliability is necessary. All the work in the literature so far assumed that the sensors are homogeneous. Though the work in [6] considered the heterogeneity of sensors for the connectivity problem, the results are approximate since, only the sensors with smallest range are considered for the analysis. The assumption of homogeneity is usually hard to maintain in large scale WSNs and there is no work that explicitly addresses the coverage problem in heterogeneous 3D WSNs.

In summary, there is no work in the literature on coverage-preserving scheduling protocols for 3D heterogeneous WSNs that can work with sensors without location information. Considering these limitations in the literature, we propose an approach to identify the sensors redundant for k-coverage of a FoI with the sensors deployed uniformly at random. We also propose a distributed scheduling protocol that does not require geographical information and schedule the redundant sensors to sleep without creating holes in the coverage.

6.3 Preliminaries

In this section, we state the assumptions made about the network and define a few terms used in this chapter.

Assumptions: The sensors are assumed to be deployed in a 3D FoI, denoted by Ψ, uniformly at random independent of each other. This is an assumption widely used in the literature on theoretical analysis of coverage problem [6] but, our analysis can be extended for any other distribution with a known density function. The shape of the 3D FoI Ψ is assumed to be a cuboid. In a 3D heterogeneous WSN, the sensors are categorised into t different types based on their sensing and/or communication ranges. Let N_i be the number of type i sensors such that $\sum_{i=1}^{t} N_i = N$, where N is the total number of sensors in the WSN. All the sensors of a given type are assumed to have equal sensing and communication radii. We assume the *binary 3D sensing model* in which the sensing region of a sensor is modelled with a sphere called sensing sphere. A type i sensor ($1 \leq i \leq t$), say s_i, can sense perfectly within the sensing sphere of radius S_i centred at the location of s_i, denoted by $R(s_i, S_i)$. The sensor s_i cannot sense any activity beyond $R(s_i, S_i)$. The volume covered by s_i is nothing but the volume of the sensing sphere denoted by $\|R(s_i, S_i)\| = \frac{4}{3}\pi S_i^3$. Similarly, we assume that the communication region of a sensor is also modelled by the *binary 3D communication model*. The communication sphere denoted by $R(s_i, C_i)$, is the region over which the sensor s_i can communicate with other sensors, where C_i is the communication range.

Definition 1: In a heterogeneous WSN, for any two sensors s_i and s_j, $1 \leq i, j \leq t$, if $i \neq j$ (*i.e.* not same type), then $S_i \neq S_j$ and/or $C_i \neq C_j$.

Definition 2: If s_i and s_j are located such that the distance between them is less than $S_i + S_j$, then s_j is called the *sensing neighbour* of s_i. On the other hand, if the distance between s_i and s_j is less than C_j, *i.e.*, the sensor s_j can communicate with

the sensor s_i directly, then s_j is called the *communication neighbour* of s_i. If s_j is both the sensing neighbour and the communication neighbour of s_i, then s_j is called the *sensing and communication neighbour* or simply the *neighbour* of s_i.

Definition 3: For two neighbouring sensors s_i and s_j, the effective range for coordination between them, denoted by δ is given by $\min(S_i + S_j, C_j)$. A sphere denoted by $R\big(s_i, \min(S_i + S_j, C_j)\big)$ is called the *effective coordination sphere* of s_i with its neighbour s_j.

Definition 4: The *k-coverage ratio* of the FoI, denoted by η_k is defined as the fraction of the volume of the FoI in which each point is k-covered. Under stochastic deployment of sensors, a FoI is said to be almost surely *k-covered* only if the expected value of η_k is equal to unity with probability one.

Intersection Volume: The volume of intersection between two spheres centred at p and q with radii r and s, respectively $\big(\, \|R(p,r) \cap R(q,s)\| \,\big)$ is given by

$$\frac{\pi(r+s-d)^2(d^2+2\,d\,r-3r^2+2\,d\,s+6\,r\,s-3s^2)}{12\,d}, \tag{6.1}$$

where d is the distance between p and q [70].

6.4 Analysis of the Redundancy of a Sensor for *k*-coverage

In this section we take a probabilistic approach to determine if a sensor is redundant for k-coverage. We first determine the probability that a point in the sensing sphere of a sensor is covered by at least k of its neighbours. Next, we extend the analysis to determine the probability of a sensor being redundant for k-coverage of the FoI.

6.4.1 Redundancy in Coverage of a Point

Consider the cross sections of the sensing and communication spheres of a type i and a type j sensor as shown in Fig. 6.1(a). Fig. 6.1(b) shows the cross section of the

region which is covered by both s_i and s_j (shaded region). Let Y denote the random variable representing the distance between the sensor s_i and a point q in its sensing region which takes the possible values $0 \leq d \leq S_i$. Let $A_j(q)$ denote the event that a point $q \in R(s_i, S_i)$ at a distance of d from s_i, is also covered by a type j neighbour. To estimate the probability of the event $A_j(q)$, it may be noted that the neighbouring sensor s_j should not be at a distance greater than S_j from the point q, and s_j should also be able to communicate with s_i. It can be seen from Fig. 6.1(b) that if s_j lies in the shaded region, then it covers the point q and it can also communicate with s_i. Note that by *Definition 3*, the shaded region is a part of the effective coordination region of s_i.

For a point $q \in R(s_i, S_i)$, the probability of the event $A_j(q)$ is equal to the ratio of the volume of intersection of the sensing sphere of neighbour s_j and the effective coordination sphere of s_i, to the volume of the effective coordination sphere of s_i. This estimation is valid under the assumption that sensors are deployed uniformly at random in the FoI. The probability of a point q in the sensing sphere of s_i, also being covered by its neighbour s_j is given by

$$\mathbf{P}(A_j(q)) = \frac{\|R(q, S_j) \cap R(s_i, \min(C_j, S_i + S_j)\|}{\|R(s_i, \min(C_j, S_i + S_j))\|}. \tag{6.2}$$

To interpret Eq. 6.2, if $\mathbf{P}(A_j(q))$ is unity and a point $q \in R(s_i, S_i)$ is also covered by a type j neighbour s_j, then s_j lies in the effective coordination region of s_i ($w.r.t$ s_j). Note that $\mathbf{P}(A_j(q))$ depends on the location of q, S_j, and $\min(C_j, S_i + S_j)$. For any pair of neighbouring sensors s_i and s_j, the effective coordination region denoted by $R\big(s_i, \min(C_j, S_i + S_j)\big)$ is fixed. Based on the values of S_i, S_j, and C_j there could be different cases in the evaluation of Eq. 6.2 which are considered below:

Case 1) $\boldsymbol{S_j < \min(C_j, S_i + S_j)}$ **and** $\boldsymbol{C_j < S_i + S_j}$: This case is illustrated in Figs. 6.2(a)

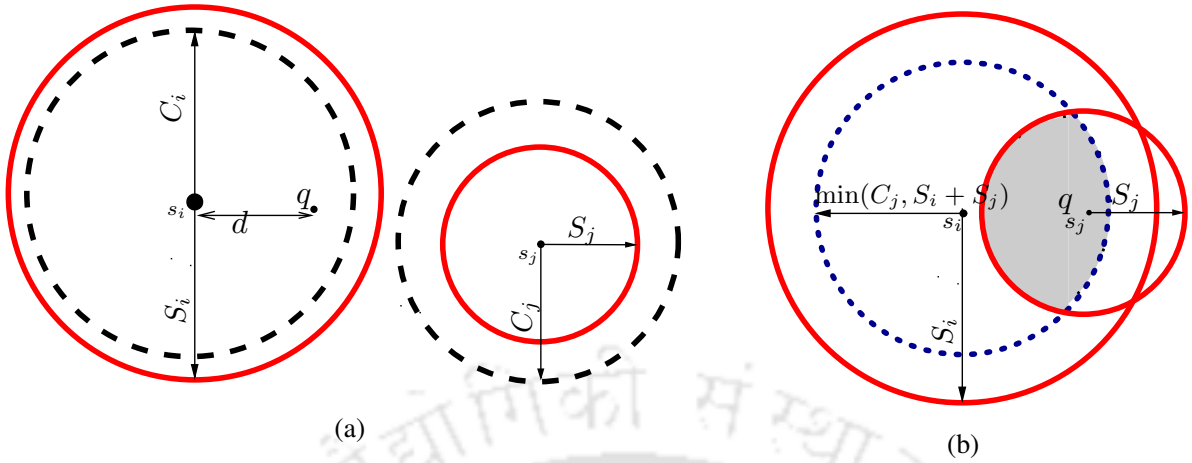

Figure 6.1 Illustration of a point q in the sensing region of a type i sensor also being covered by a type j neighbour.

and 6.2(b) when the sensing and communication ranges of s_i and s_j satisfy either of these conditions. As illustrated in Figs 6.2(a), the point q is at a distance of at most $C_j - S_j$ from the sensor s_i. Since the sensing sphere of s_j is smaller than the other spheres, the terms in the numerator and the denominator of Eq. 6.2 are equal to $\|R(q, S_j)\|$ and $\|R(s_i, C_j)\|$, respectively. Similarly, as shown in Fig. 6.2(b), the distance of point q from s_i is in the range of $\big(C_j - S_j, S_i\big]$. Thus, $\mathbf{P}(A_j(q))$ for this case is given by

$$\begin{cases} \frac{\|R(q,S_j)\|}{\|R(s_i,C_j)\|} & 0 \leq d \leq C_j - S_j \quad (a) \\ \frac{\|R(q,S_j) \cap R(s_i,C_j)\|}{\|R(s_i,C_j)\|} & C_j - S_j < d \leq S_i \quad (b) \end{cases} \tag{6.3}$$

where d is the distance of the point q from s_i.

Case 2) $\boldsymbol{S_j < \min(C_j, S_i + S_j)}$ **and** $\boldsymbol{S_i + S_j \leq C_j}$: As illustrated in Fig. 6.2(c), this case occurs when the point q is within the sensing sphere of s_i, *i.e.*, $0 \leq d \leq S_i$. Then the terms in the numerator and the denominator of Eq. 6.2 are equal to $\|R(q, S_j)\|$ and $\|R(s_i, S_i + S_j)\|$, respectively. Thus, $\mathbf{P}(A_j(q))$ for this case is given by

$$\frac{\|R(q,S_j)\|}{\|R(s_i,S_i+S_j)\|} \qquad 0 \le d \le S_i \qquad (6.3c)$$

Case 3) $\min(C_j, S_i+S_j) \le S_j$ and $C_j < S_i+S_j$: This case occurs when the neighbouring sensor s_j is at a distance of at most $S_j - C_j$ from s_i as illustrated in Fig. 6.2(d). Then the terms in the numerator and the denominator of Eq. 6.2 are equal to $\|R(s_i, C_j)\|$. This case could also occur, as illustrated in Fig. 6.2(e), when the distance of point q from s_i is in the range of $\left(S_j - C_j, S_i\right]$. Thus, $\mathbf{P}(A_j(q))$ for this case is given by

$$\begin{cases} \frac{\|R(s_i,C_j)\|}{\|R(s_i,C_j)\|} = 1 & 0 \le d \le S_j - C_j \qquad (6.3d) \\ \frac{\|R(q,S_j) \cap R(s_i,C_j)\|}{\|R(s_i,C_j)\|} & S_j - C_j < d \le S_i \qquad (6.3e) \end{cases}$$

Eq. 6.3 gives the probability of a point in the sensing sphere of a type i sensor also being covered by a neighbouring sensor of type j, for different values of their sensing and communication ranges. If the point is to be only 1-covered, then s_i can be considered redundant. However, for k-coverage of the point, we need to estimate the probability of a point in the sensing sphere of s_i also being covered by at least k neighbours.

Let $B_{j,w}(q)$ denote the event that a point q in the sensing sphere of s_i is also covered by exactly w number of type j neighbours, $1 \le j \le t$. Let n be the number of neighbours of s_i such that $\sum_{j=1}^{t} n_j = n$, where n_j is the number of type j neighbours. The probability of $B_{j,w}(q)$ depends on the probability that r of the n neighbours belong to type j and the probability that the point q is covered by exactly w of them, where $w \le r \le n$. Since it is assumed that the sensors are deployed uniformly at random in the 3D FoI, the probability that r out of n neighbours picked at random, are of type j is given by $\binom{n}{r}\left(\frac{n_j}{n}\right)^r\left(1-\frac{n_j}{n}\right)^{n-r}$, where n_j/n is the probability that a neighbour is of type j [71]. Similarly, the probability that a point q is covered by exactly

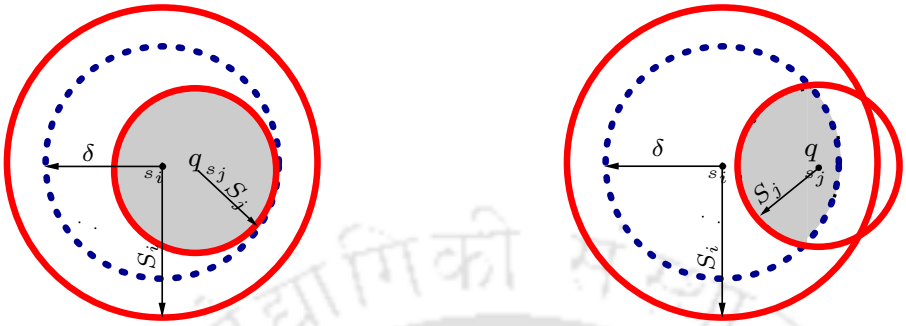

$S_j < \min(C_j, S_i + S_j), C_j < S_i + S_j,$ and $\delta = \min(C_j, S_i + S_j)$

(a) $0 \leq d \leq C_j - S_j$ (b) $C_j - S_j < d \leq S_i$

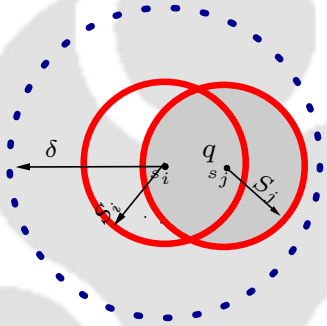

$S_j < \min(C_j, S_i + S_j), S_i + S_j \leq C_j,$ and $\delta = \min(C_j, S_i + S_j)$

(c) $0 \leq d \leq S_i$

$\min(C_j, S_i + S_j) \leq S_j, C_j < S_i + S_j,$ and $\delta = \min(C_j, S_i + S_j)$

(d) $0 \leq d \leq S_j - C_j$ (e) $S_j - C_j < d \leq S_i$

Figure 6.2 Illustration of the cases considered in deriving $\mathbf{P}(A_j(q))$.

w of its r type j neighbours can be written as $\binom{r}{w}\left(\mathbf{P}(A_j(q))\right)^w\left(1-\mathbf{P}(A_j(q))\right)^{r-w}$. Therefore, the probability of the event $B_{j,w}(q)$ can be expressed as

$$\mathbf{P}(B_{j,w}(q)) = \sum_{r=w}^{n}\binom{n}{r}\left(\frac{n_j}{n}\right)^r\left(1-\frac{n_j}{n}\right)^{n-r}\binom{r}{w}\left(\mathbf{P}(A_j(q))\right)^w\left(1-\mathbf{P}(A_j(q))\right)^{r-w},$$

set $r = w+m$.

$$\begin{aligned}
&= \sum_{m=0}^{n-w}\binom{n}{w+m}\left(\frac{n_j}{n}\right)^{w+m}\left(1-\frac{n_j}{n}\right)^{n-w-m}\times \\
&\quad \binom{w+m}{w}\left(\mathbf{P}(A_j(q))\right)^w\left(1-\mathbf{P}(A_j(q))\right)^m, \\
&= \sum_{m=0}^{n-w}\binom{n}{w}\left(\frac{n_j}{n}\mathbf{P}(A_j(q))\right)^w\binom{n-w}{m}\left(1-\frac{n_j}{n}\right)^{n-w-m}\left(\frac{n_j}{n}-\frac{n_j}{n}\mathbf{P}(A_j(q))\right)^m,
\end{aligned}$$

use $(a+b)^n = \sum_{i=0}^{n}\binom{n}{i}a^{n-i}b^i$.

$$= \binom{n}{w}\left(\frac{n_j}{n}\mathbf{P}(A_j(q))\right)^w\left(1-\frac{n_j}{n}\mathbf{P}(A_j(q))\right)^{n-w}. \tag{6.4}$$

Next, let $C^k(q)$ denote the event that a point q in the sensing region of a type i sensor is also covered by at least k of its neighbours of any type. For example, the probability of the event $C^2(q)$ can be interpreted as

$$\begin{aligned}
\mathbf{P}(C^2(q)) = 1 &- \mathbf{P}(q \text{ is not covered by any neighbour}) \\
&- \mathbf{P}(q \text{ is covered by exactly one neighbour}).
\end{aligned} \tag{6.5}$$

Since sensors are deployed independent of each other,

$$\mathbf{P}(q \text{ is not covered by any neighbour}) = \mathbf{P}(B_{1,0}(q))\mathbf{P}(B_{2,0}(q))\ldots\mathbf{P}(B_{t,0}(q)) \tag{6.6}$$

and

$$\begin{aligned}\mathbf{P}(q \text{ is covered by exactly one neighbour}) = \\ &\mathbf{P}(B_{1,1}(q))\mathbf{P}(B_{2,0}(q))\dots\mathbf{P}(B_{t,0}(q)) \\ +&\mathbf{P}(B_{1,0}(q))\mathbf{P}(B_{2,1}(q))\dots\mathbf{P}(B_{t,0}(q)) \\ &\vdots \\ +&\mathbf{P}(B_{1,0}(q))\mathbf{P}(B_{2,0}(q))\dots\mathbf{P}(B_{t,1}(q)) \end{aligned} \tag{6.7}$$

Substituting Eqs. 6.6 and 6.7 in Eq. 6.5 gives

$$\begin{aligned}\mathbf{P}(C^2(q)) =& 1 - \mathbf{P}(B_{1,0}(q))\mathbf{P}(B_{2,0}(q))\dots\mathbf{P}(B_{t,0}(q)) \\ &- \mathbf{P}(B_{1,1}(q))\mathbf{P}(B_{2,0}(q))\dots\mathbf{P}(B_{t,0}(q)) \\ &- \mathbf{P}(B_{1,0}(q))\mathbf{P}(B_{2,1}(q))\dots\mathbf{P}(B_{t,0}(q)) \\ &\vdots \\ &- \mathbf{P}(B_{1,0}(q))\mathbf{P}(B_{2,0}(q))\dots\mathbf{P}(B_{t,1}(q)) \\ =& 1 - \sum_{\substack{l_1,l_2,\cdots,l_t\in[0,2-1] \\ 0\le l_1+l_2+\cdots+l_t\le 2-1}} \prod_{j=1}^{t} \mathbf{P}(B_{j,l_j}(q)). \end{aligned} \tag{6.8}$$

In general, the probability of q in the sensing sphere of s_i being covered by at least k neighbours can be written as

$$\mathbf{P}(C^k(q)) = 1 - \sum_{\substack{l_1,l_2,\cdots,l_t\in[0,k-1] \\ 0\le l_1+l_2+\cdots+l_t\le k-1}} \prod_{j=1}^{t} \mathbf{P}(B_{j,l_j}(q)). \tag{6.9}$$

By substituting for $\mathbf{P}(B_{j,l_j}(q))$ from Eq. 6.4, with w replaced by l_j, we get

$$\mathbf{P}(C^k(q)) = 1 - \sum_{\substack{l_1,l_2,\cdots,l_t\in[0,k-1] \\ 0\le l_1+l_2+\cdots+l_t\le k-1}} \prod_{j=1}^{t} \binom{n}{l_j} \left(\frac{n_j}{n}\mathbf{P}(A_j(q))\right)^{l_j} \left(1 - \frac{n_j}{n}\mathbf{P}(A_j(q))\right)^{n-l_j}. \tag{6.10}$$

6.4.2 Redundancy of a Sensor for k-coverage

Eq. 6.10 gives the probability of a point q in the sensing sphere of a type i sensor also being covered by at least k neighbours. Next, the expected sensing volume of s_i that is covered by at least k neighbours, denoted by $E[\xi_i^k]$, can be obtained by simply integrating $\mathbf{P}(C^k(q))$ over its sensing sphere $R(s_i, S_i)$.

The expected sensing volume of s_i wherein each point $q \in R(s_i, S_i)$, is covered by at least k neighbours is given by

$$E[\xi_i^k] = \iiint_{R(s_i,S_i)} \mathbf{P}(C^k(q))dV \tag{6.11}$$

By substituting $\mathbf{P}(C^k(q))$ from Eq. 6.10 we get

$$\begin{aligned} E[\xi_i^k] &= \iiint_{R(s_i,S_i)} 1 - \sum_{\substack{l_1,l_2,\cdots,l_t\in[0,k-1] \\ 0\le l_1+l_2+\cdots+l_t\le k-1}} \prod_{j=1}^{t} \binom{n}{l_j} \left(\frac{n_j}{n}\mathbf{P}(A_j(q))\right)^{l_j} \left(1-\frac{n_j}{n}\mathbf{P}(A_j(q))\right)^{n-l_j} dV, \\ &= \frac{4\pi S_i^3}{3} - \iiint_{R(s_i,S_i)} \sum_{\substack{l_1,l_2,\cdots,l_t\in[0,k-1] \\ 0\le l_1+l_2+\cdots+l_t\le k-1}} \prod_{j=1}^{t} \binom{n}{l_j} \left(\frac{n_j}{n}\mathbf{P}(A_j(q))\right)^{l_j} \left(1-\frac{n_j}{n}\mathbf{P}(A_j(q))\right)^{n-l_j} dV. \end{aligned} \tag{6.12}$$

The above equation can be interpreted in the context of redundancy for k-coverage as follows: For a type i sensor, when $E[\xi_i^2]$ is equal to its sensing volume $\|R(s_i, S_i)\|$ with probability one, every point in its sensing sphere is almost surely covered by at least two neighbours.

To determine if a sensor can be considered to be redundant for k-coverage of a FoI, we define the following lemma that establishes the condition for redundancy of a sensor based on Eq. 6.12. In a densely deployed 3D heterogeneous WSN, the following lemma declares a sensor to be redundant for k-coverage if its entire sensing sphere is almost surely covered by at least k neighbours. This result is used by the distributed protocol proposed in Section 6.5 to schedule the redundant sensors to sleep.

Lemma 6.1 *Consider a 3D heterogeneous WSN with a large density of sensors deployed uniformly at random, independent of each other, and the FoI should be almost surely k-covered. If the expected sensing volume of s_i, $1 \leq i \leq t$, which is also covered by at least k neighbours, is equal to its sensing volume with probability one then, s_i is redundant for k-coverage.*

Proof: (Proof by Contradiction.) Let us assume that the lemma is not true. That is, even though $E[\xi_i^k] = \|R(s_i, S_i)\|$, s_i is not redundant. The term $E[\xi_i^k]$ gives the expected sensing volume of s_i which is also covered by k neighbours defined by Eq. 6.12. Let V^k be the volume of the FoI actually k-covered by the WSN. Thus, $V^k - (\|R(s_i, S_i)\| - E[\xi_i^k])$ is the volume of the FoI that is k-covered even without s_i. Further, if s_i is not redundant, then the following inequality should hold.

$$V^k - \big(\, \|R(s_i, S_i)\| - E[\xi_i^k]\big) < V' \tag{6.13}$$

Where V' is the volume of the FoI that is required to be k-covered by the WSN. Assume that the FoI, Ψ is densely deployed with sensors so that it is k-covered, *i.e.*, $V^k = \|\Psi\|$. Substituting $E[\xi_i^k] = \|R(s_i, S_i)\|$ and $V^k = \|\Psi\|$, in the above inequality and rearranging the terms, we get $\|\Psi\| < V'$. This is a contradiction because the volume of the FoI that is required to be k-covered by the WSN must be less than or equal to the volume of the FoI. Hence the lemma is proved. □

Next, we state the condition for a sensor to be redundant for k-coverage in a 3D heterogeneous WSN, in terms of the number of neighbours of different types.

Theorem 6.1 *Assume that sensors belonging to t different types are independently and uniformly distributed at random across the FoI. The sensor s_i is redundant for*

k-coverage if the following inequality holds:

$$\frac{4\pi S_i^3}{3} - \iiint\limits_{R(s_i,S_i)} \sum_{\substack{l_1,l_2,\cdots,l_t\in[0,k-1]\\ 0\le l_1+l_2+\cdots+l_t\le k-1}} \prod_{j=1}^{t} \binom{n}{l_j} \left(\frac{n_j}{n}\mathbf{P}(A_j(q))\right)^{l_j} \times \left(1-\frac{n_j}{n}\mathbf{P}(A_j(q))\right)^{n-l_j} dV \ge \|R(s_i,S_i)\|\,(1-\tau),$$

where $\tau = 0.01$ *and*

$$\mathbf{P}(A_j(q)) = \begin{cases} \textbf{if}\big(S_j < \min(C_j, S_i+S_j) \ \textit{and}\ C_j < S_i+S_j\big) \\ \qquad \frac{\|R(q,S_j)\|}{\|R(s_i,C_j)\|} \qquad 0 \le d \le C_j - S_j \\ \qquad \frac{\|R(q,S_j)\cap R(s_i,C_j)\|}{\|R(s_i,C_j)\|} \qquad C_j - S_j < d \le S_i \\ \textbf{elseif}\big(S_j < \min(C_j, S_i+S_j) \ \textit{and}\ S_i+S_j \le C_j\big) \\ \qquad \frac{\|R(q,S_j)\|}{\|R(s_i,S_i+S_j)\|} \qquad 0 \le d \le S_i \\ \textbf{elseif}\big(\min(C_j, S_i+S_j) \le S_j \ \textit{and}\ C_j < S_i+S_j\big) \\ \qquad \frac{\|R(s_i,C_j)\|}{\|R(s_i,C_j)\|} \qquad 0 \le d \le S_j - C_j \\ \qquad \frac{\|R(q,S_j)\cap R(s_i,C_j)\|}{\|R(s_i,C_j)\|} \qquad S_j - C_j < d \le S_i \\ \textbf{else} \\ \qquad 0 \end{cases} \tag{6.14}$$

Proof: Lemma 6.1 declares a sensor to be redundant with probability one if $E[\xi_i^k] = \|R(s_i,S_i)\|$. Alternately, we can declare a sensor to be redundant if $E[\xi_i^k] \ge \|R(s_i,S_i)\|\,(1-\tau)$ for a small value of τ, say $\tau = 0.01$. By substituting $E[\xi_i^k]$ from Eq. 6.12, we get

$$\frac{4\pi S_i^3}{3} - \iiint\limits_{R(s_i,S_i)} \sum_{\substack{l_1,l_2,\cdots,l_t\in[0,k-1]\\ 0\le l_1+l_2+\cdots+l_t\le k-1}} \prod_{j=1}^{t} \binom{n}{l_j} \left(\frac{n_j}{n}\mathbf{P}(A_j(q))\right)^{l_j} \times \left(1-\frac{n_j}{n}\mathbf{P}(A_j(q))\right)^{n-l_j} dV \ge \|R(s_i,S_i)\|\,(1-\tau). \tag{6.15}$$

Substituting Eqs. 6.3(a)- 6.3(e) for $\mathbf{P}(A_j(q))$ in Eq. 6.15 proves the theorem. □

6.4.3 Validation of the Analysis

To validate the proposed analysis, we evaluate Eq. 6.12 numerically and compare it with a simulation for the following scenario. A 3D FoI of volume $100^3 m^3$ is sprayed with heterogeneous sensors uniformly. There are two types of sensors with the sensing and communication ranges as: $S_1 = 15m$, $C_1 = 15m$, $S_2 = 18m$, and $C_2 = 20m$. These ranges are selected such that the estimation of volume of a sensor (of either type) redundantly covered considers the three cases used in the derivation of Eq. 6.3. We consider the redundancy of each type of sensor for k-coverage of the FoI, where $k = 1, 2$. For the numerical results, we evaluate Eq. 6.12 for the same scenarios considered in the simulation. For the simulation results a Monte Carlo simulation is conducted as described in Chapter 3, Section 3.4.

Fig. 6.3 shows the variation in the expected sensing volume of s_i that is redundantly covered $\left(\text{determined by } \frac{E[\xi_i^k]\times 100}{\|R(s_i,S_i)\|}\right)$, when there are different number of neighbours. Each plot shows $E[\xi_i^1]$ and $E[\xi_i^2]$ for a type i sensor, $i = 1, 2$, and for a different number of neighbours of each type (shown below x-axis in the form (n_1,n_2)), obtained with simulation and numerical evaluation. Note that the results for type 2 in Fig. 6.3(a) and type 1 in Fig. 6.3(b) correspond to homogeneous WSN scenarios while the rest are for heterogeneous WSN scenarios.

It can be observed from all the plots that the simulated value of expected sensing volume redundantly covered, matches with that obtained by evaluating Eq. 6.12 very closely. The results show that the expected redundant sensing volume increases with the number of neighbouring sensors making it a potential candidate for being redundant. However, on comparing Figs. 6.3(a) and 6.3(b), we can see that $E[\xi_i^1]$ and $E[\xi_i^2]$ for a type i sensor increase sharply with the number of type 2 neighbours because they have larger communication and sensing ranges. The higher utility of type 2 sensors for redundantly covering the volume can also be concluded from Fig. 6.3(d), where $E[\xi_1]$ and $E[\xi_2]$ increase sharply with the number of neighbours, because of greater

number of type 2 neighbours when compared to the case of Fig. 6.3(c), where most of the neighbours are of type 1. All the figures show that $E[\xi_i^1]$ for a type i sensor increases sharply with the number of neighbours, because $E[\xi_i^1]$ requires less number of neighbours when compared to $E[\xi_i^2]$, where $i = 1, 2$.

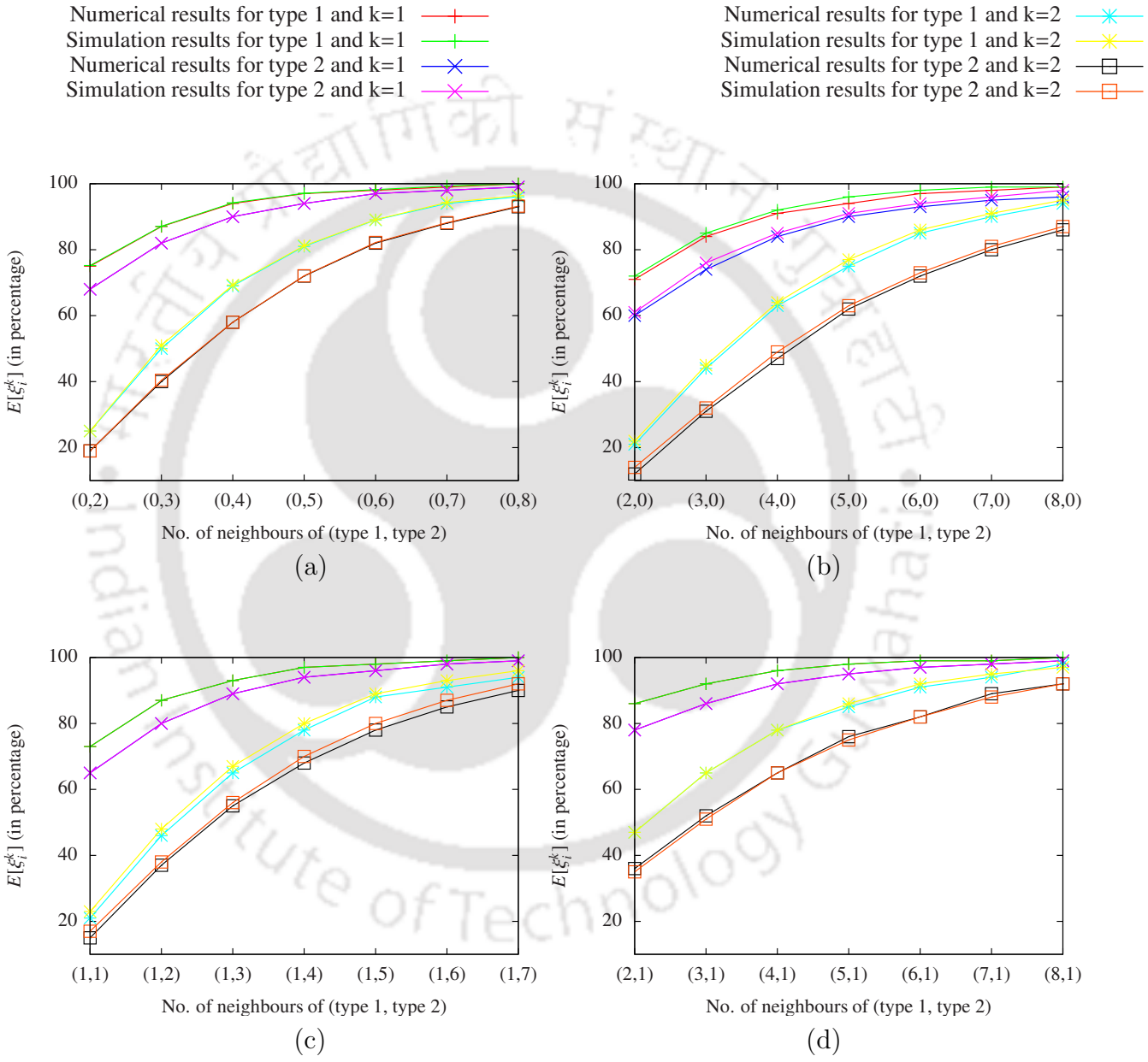

Figure 6.3 Variation in the expected sensing volume of a type i sensor redundantly covered for different number of neighbours.

6.5 Sleep Scheduling Protocol for k-coverage

In this section, we propose a protocol that helps each sensor to determine if it is redundant and go to sleep without compromising the k-coverage of the 3D FoI. The protocol is fully distributed and does not use any geographical information but, gathers information only about the number of neighbours and their type with periodic control messages.

6.5.1 Description of the scheduling protocol

Pre-processing phase: We assume that the sink or base station which is a powered node computes the expected sensing volume of a type i sensor that is redundantly covered for a desired k-coverage value, given the number of neighbours of each type, and their ranges for sensing and communication. All valid combinations for the number of neighbours that can make a sensor redundant for k-coverage are stored in a table called *Redundancy Table* (format shown in Table 6.1(b)). Computation of this table for a type i sensor, i=$1, 2, \ldots, t$ is facilitated by *Procedure 1*.

Let the maximum number of neighbours be n_{max}. *Procedure 1* takes i, k, t, S_i, C_i, and n_{max} as input. It then checks the redundancy of a type i sensor for various combinations of the number of neighbours of different types using Eq. 6.14. If the type i sensor is redundant, then that combination of the number of neighbours is considered *valid*. Each such valid combination is added to the *Redundancy Table* of a type i sensor. This table is stored in each sensor initially at the time of deployment. This is not an unreasonable assumption to make in the planning phase or pre-processing phase and is also used earlier in [72]. Once a sensor in the FoI determines the information about its neighbours, it can check if the number of neighbours of different types matches with any combination from this table, and thus determine if it is redundant for the desired coverage level.

Working phase: In the sleep scheduling protocol, the operation time is divided

Procedure 1: REDUNDANCY_TABLE CONSTRUCTION

```
/* Run the following at the base station initially at the time of deployment. */
Input: i, k, t, S_1, .., S_t, C_1, ..., C_t, n_max ;
Output: Redundancy Table for a type i sensor ;
for int n_1 ← 0 to n_max do
    for int n_2 ← 0 to n_max do
        ⋮
        for int n_t ← 0 to n_max do
            if (Eq. 6.14 is true) then   Add the combination (n_1, ..., n_t) into the
            Redundancy Table ;
```

into successive rounds. Each round consists of two phases: the decision phase and the sensing phase. In the decision phase, all sensors decide on their activity for the current round. During the sensing phase, all the active sensors continue sensing until the next round. After each round, all the sensors become active to participate in the decision phase of the next round. The duration of each round is chosen such that it is much longer than the decision phase but much shorter than the average lifetime of the WSN. At any given point in time, a sensor can be in one of these states: ACTIVE, WAIT, and SLEEP.

1. **ACTIVE state:** In ACTIVE state, a sensor is responsible to cover its sensing region and communicate with its neighbours. At the beginning of each round, all the sensors are in ACTIVE state and execute the scheduling protocol asynchronously.

2. **WAIT state:** A sensor goes into WAIT state if it determines itself to be redundant but is still in the process of informing its transition to SLEEP state to its neighbours.

3. **SLEEP state:** In SLEEP state, a sensor is put to sleep in order to conserve energy. All the sensors in this state are not required to cover the 3D FoI during the round.

The scheduling protocol uses two messages HELLO and SLEEP to communicate

with the neighbours. Each sensor turns active at the beginning of a round (*i.e.*, during the decision phase) and broadcasts a HELLO message to all its neighbours with its *id* and *type*. A sensor that receives the HELLO message stores information about its neighbours in the *Neighbour Table* in the format shown in Table 6.1(a). The table stores the unique id of each neighbour and its type. This information is updated with periodic HELLO messages between the sensors. The periodic HELLO messages also neglected the effect of the collisions of HELLO messages.

From the information in the *Neighbour Table*, each sensor knows the number of neighbours of each type. It then compares the number of different types of neighbours from the *Redundancy Table* (stored or hard-coded initially at the time of deployment of WSN) to check if any of the combinations is valid. Table 6.1(b) shows the format of the *Redundancy Table* for redundancy of a type 1 sensor for 1-coverage of the FoI. The columns in the table show the number of neighbours of each type. For example, if this sensor has seven type 2 and one type 1 sensors in the neighbourhood, the sensor is redundant. Since the *Redundancy Table* for each sensor can be computed and stored at the time of deployment, determining if a sensor with a given number of neighbours is redundant, is simplified to updating the *Neighbour Table* and looking up the *Redundancy Table*.

The redundancy determination is given by *Procedure 2*. If a sensor is potentially redundant, it switches to WAIT state. Otherwise it remains in the ACTIVE state. In WAIT state, the sensor starts a random back-off timer and keeps track of its neighbours with HELLO messages. The purpose of using back-off timer is to avoid a black hole when several sensors try to go to SLEEP state simultaneously. If the sensor has sufficient number of active neighbours at the end of back-off time, it broadcasts SLEEP message to the neighbours, and switches to SLEEP state until the next round. A SLEEP message carries the *id* of the sender. When a sensor receives the SLEEP message and if its *Neighbour table* has the *id* of the sender, then the sensor ignores the

sender and determines if it is still redundant. If the sensor is still redundant, it remains in the WAIT state. Otherwise it switches to ACTIVE state. *Algorithm* 2 shows the actions performed in the three possible states of a sensor during the scheduling protocol and the transitions between them.

Table 6.1 Data stored at a type 1 sensor for 1-coverage of the FoI.

ID	Type
1	type 1
2	type 2
3	type 2
4	type 1
5	type 1
6	type 2
7	type 1

(a) Neighbour Table.

n_1	n_2
4	4
1	7
1	8
8	1
5	5
6	6
7	7
8	8

(b) Redundancy Table

6.5.2 Complexity Analysis

Message complexity: Each sensor broadcasts a HELLO message at the beginning of each round. Each redundant sensor broadcasts a SLEEP message before the end of decision phase. Let N and N_r be the total number of sensors in the network and the expected number of redundant sensors at the end of decision phase of each round, respectively. Thus, in each round the total number of messages are $N + N_r$. Since $N_r < N$, the message complexity is $O(N)$ which is nearly optimal.

• **Space complexity:** In the sleep scheduling protocol, each sensor has a *Neighbour Table* and a *Redundancy Table*. The *Neighbour Table* stores the *id* and the *type* of each neighbour. The *Redundancy Table* stores different combinations of the number of neighbours of different types. Let n, t, and C be the expected number of neighbours of a sensor, types of sensors deployed in the network, and the maximum possible

combinations of the number of neighbours, respectively. Thus, each sensor requires $2 \times n + t \times C$ space. Since $n << N$ and $t \times C << N$, the space complexity is $O(N)$ which is also nearly optimal.

• **Computational complexity:** In the sleep scheduling protocol, each sensor receives HELLO messages and SLEEP messages from its neighbours. Let n and C be the expected number of neighbours of a sensor and the maximum possible combinations of the number of neighbours, respectively. Thus, each sensor requires $n \times O(1)$ and $n \times C \times O(1)$ operations for storing information about its neighbours in the *Neighbour Table* and comparing the number of different types of neighbours from the Redundancy Table, respectively. Since $n << N$ and $C << N$, the computational complexity is therefore $O(N)$ which is also nearly optimal.

Procedure 2: REDUNDANCY_CHECK

```
int l=1;                    /* First row of Redundancy Table*/
while l ≤ Length of Redundancy Table do
    if ∀_{i=1}^{t} (n_i in Neighbour Table ≥ n_i in the row l) then
        return true;        /*Sensor is a redundant sensor*/
        exit;
    else if l == Length of Redundancy Table then
        return false;       /*Sensor is not a redundant sensor*/
        exit;
    else
        l=l+1;              /* Switch to the next row*/
```

6.5.3 Performance Evaluation

In this subsection, we discuss the results from a simulation study of the proposed scheduling protocol using ns 2.34 simulator [73]. 3D environment is not directly supported in the ns 2.34 simulator. We used the Monarch Project wireless extension and modified the radio propagation model and trace file to enable these simulations.

Algorithm 2: SLEEP_SCHEDULING_PROTOCOL

```
/* To be performed by each sensor. */
Set self state as ACTIVE;
if state of the sensor is ACTIVE then
    if the sensor receives a HELLO message then
        append <ID, type> of sender in the Neighbour Table;
        if REDUNDANCY_CHECK then
            set self state as WAIT;
            set a timer with a random back-off time;
    if the sensor receives a SLEEP message then
        remove <ID, type> of sender from the Neighbour Table;
if state of the sensor is WAIT then
    if the sensor receives a HELLO message then
        append <ID, type> of sender in the Neighbour Table;
    if the sensor receives a SLEEP message then
        remove <ID, type> of sender from the Neighbour Table;
        if REDUNDANCY_CHECK then
            do nothing;
        else
            set self state ACTIVE;
if state of the sensor is SLEEP then
    set a timer with sleep time;
if back-off timer expires then
    broadcast a SLEEP message;
    set self state SLEEP;
if sleep timer expires then
    broadcast a HELLO message;
    set self state ACTIVE;
```

For all the simulations we consider the same scenario described in Section 6.4.3. The initial energy of a sensor is assumed to be 60J. The simulation is conducted by varying the ratio of the number of sensors of each type (shown as $N_1 : N_2$), volume of the FoI, and the number of sensors deployed. For each simulation, we conduct ten runs with different seeds, and average the results. All the results in this work are with 95% confidence level though the error bars are not visible in the plots.

• **Number of active sensors:** We first studied the impact of scheduling protocol on the number of active sensors used in the deployment. We determined the number of active sensors for k-coverage of the FoI, where $k = 1, 2$. For this simulation, 1800 sensors (of two types in different ratios) are deployed in 80^3m^3 volume of the FoI. Table 6.2 shows the number of active sensors required to provide 1-coverage and 2-coverage of the FoI. It can be observed that the number of active sensors required for coverage is smallest, when only type 2 sensors are used (*i.e.*, $N_1 : N_2$=0 : 1) compared to the other three cases. This is because type 2 sensors have larger sensing and communication ranges and thus have higher utility for k-coverage. Using a larger number of type 2 sensors in the FoI also causes a larger number of sensors to be redundant (see the results in Fig. 6.3), reducing the total number of active sensors. However, the cost of such sensors may be higher, prohibiting the use of only sensors with larger ranges. If we assume that the type 2 sensors are costlier than type 1 sensors then, instead of deploying the sensors in the ratio of 1 : 3, deploying them in the ratio of 1 : 1 gives the same level of coverage at a lower cost. Table 6.2 shows the number of active sensors required for the desired level of coverage in a fixed volume of 80^3m^3.

Next, we studied the impact of the volume of the FoI on the number of active sensors. We deploy 1800 sensors with different ratios of the two types of sensors and increase the volume of the FoI. Fig. 6.4 shows that the number of active sensors increases as the volume of the FoI is increased from 80^3m^3 to 100^3m^3 for k-coverage of

Table 6.2 Relationship between the number of active sensors and the initial number of sensors for k-coverage of the field, $k = 1, 2$.

k-coverage	**No. of active sensors** Initial number of sensors ($N_1 : N_2$)		
	0:1	1:3	1:1
1-coverage	175	204	234
2-coverage	259	296	332

the FoI, where $k = 1, 2$. Similar to the results in the previous simulation, the number of active sensors is smallest when all the sensors are of type 2.

• **Lifetime of the network:** Next, we studied the impact of the scheduling protocol on the lifetime of the 3D heterogeneous WSN. We measure the network lifetime in the number of simulation rounds till the FoI is k-covered. We deploy 1800 sensors uniformly at random independent of each other with different ratios of the two types of sensors and increase the volume of the FoI. We measured the number of rounds for which the FoI is k-covered, for $k = 1, 2$. Fig. 6.5 shows that the lifetime of the network (in units of simulation rounds) decreases as the volume of the FoI is increased from 80^3m^3 to 100^3m^3 for $k = 1, 2$. The results also show the network lifetime when no scheduling protocol is used. It can be observed from Fig. 6.5 that when the scheduling protocol is not used, all the sensors are active for a short duration and then their energy drains out rapidly.

Next, we studied if the network lifetime can be prolonged by increasing the number of deployed sensors. We increased the number of sensors deployed in 80^3m^3 volume and studied the lifetime of the network in units of simulation rounds. The results of this simulation are shown in Fig. 6.6. As expected, without the scheduling protocol the network lifetime is independent of the number of sensors deployed since all the sensors remain active. On the other hand, the lifetime increases when the scheduling protocol is used to put redundant sensors to sleep because, only some sensors remain active (as observed in Table 6.2 and Fig. 6.4). The active sensors take turns in

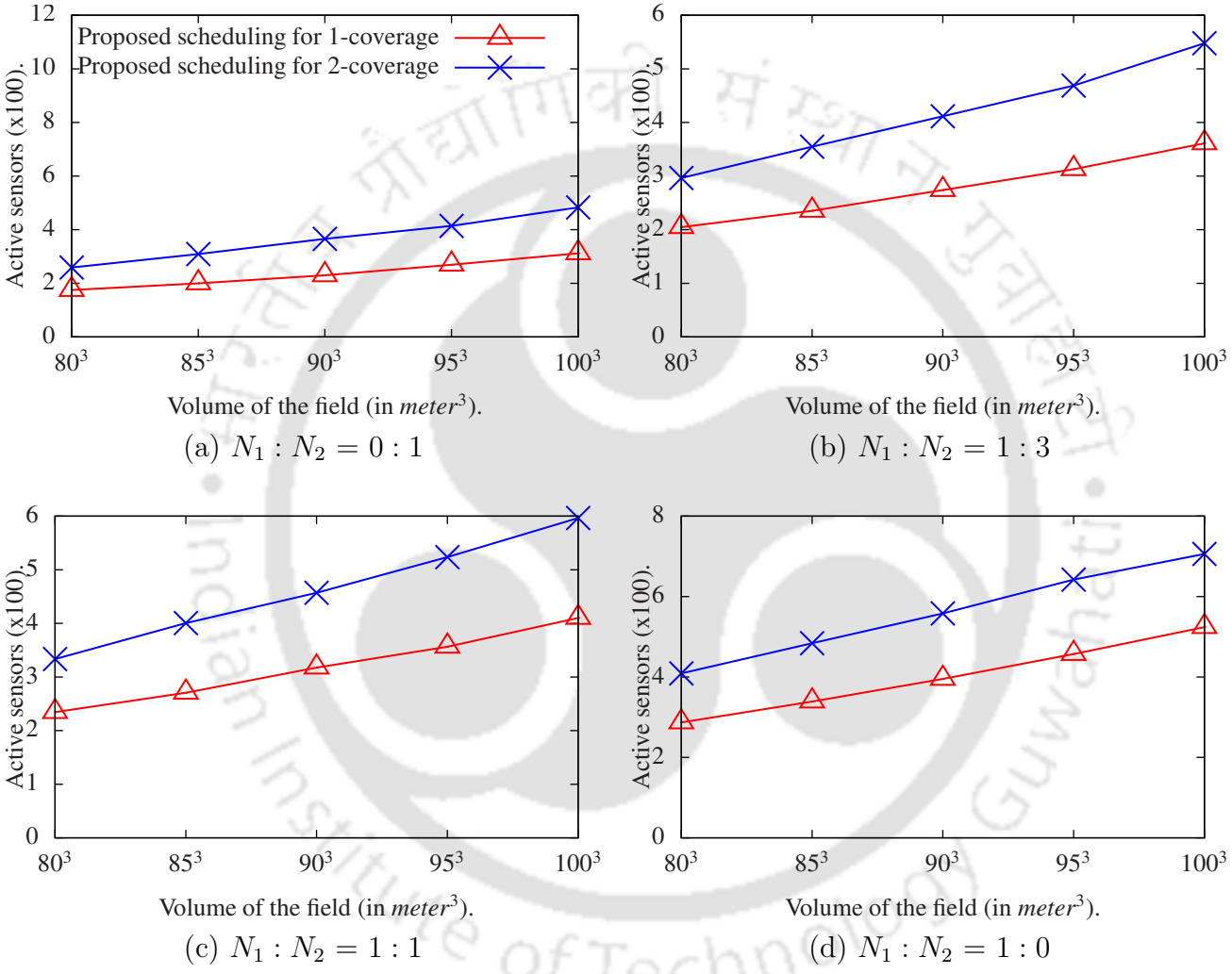

(a) $N_1 : N_2 = 0 : 1$ (b) $N_1 : N_2 = 1 : 3$

(c) $N_1 : N_2 = 1 : 1$ (d) $N_1 : N_2 = 1 : 0$

Figure 6.4 Relationship between the number of active sensors and the volume of the FoI for 1-coverage and 2-coverage.

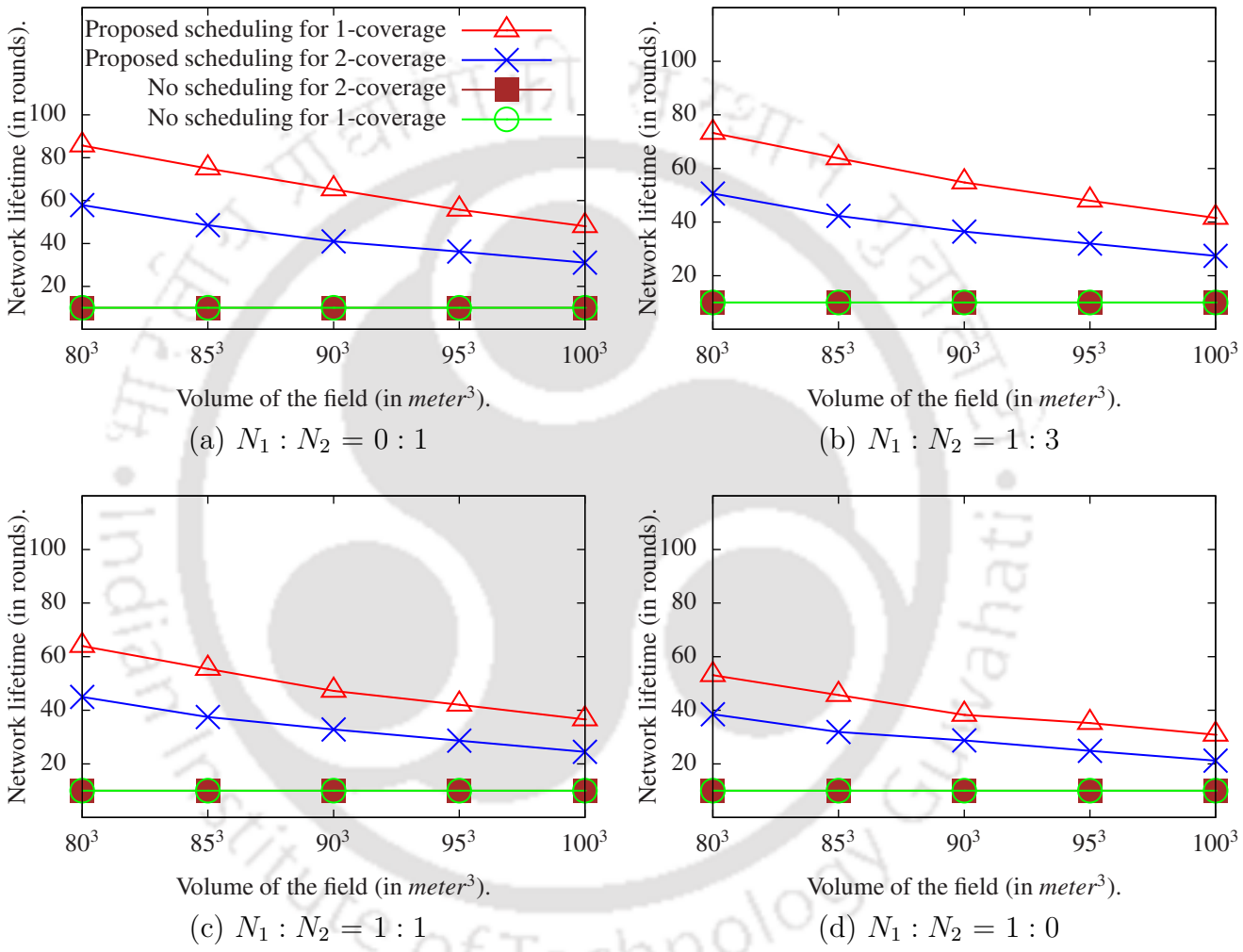

(a) $N_1 : N_2 = 0 : 1$ (b) $N_1 : N_2 = 1 : 3$

(c) $N_1 : N_2 = 1 : 1$ (d) $N_1 : N_2 = 1 : 0$

Figure 6.5 Demonstration of network lifetime in rounds for 1-coverage and 2-coverage.

ensuring the k-coverage of the FoI and hence the energy of the sensors is consumed evenly.

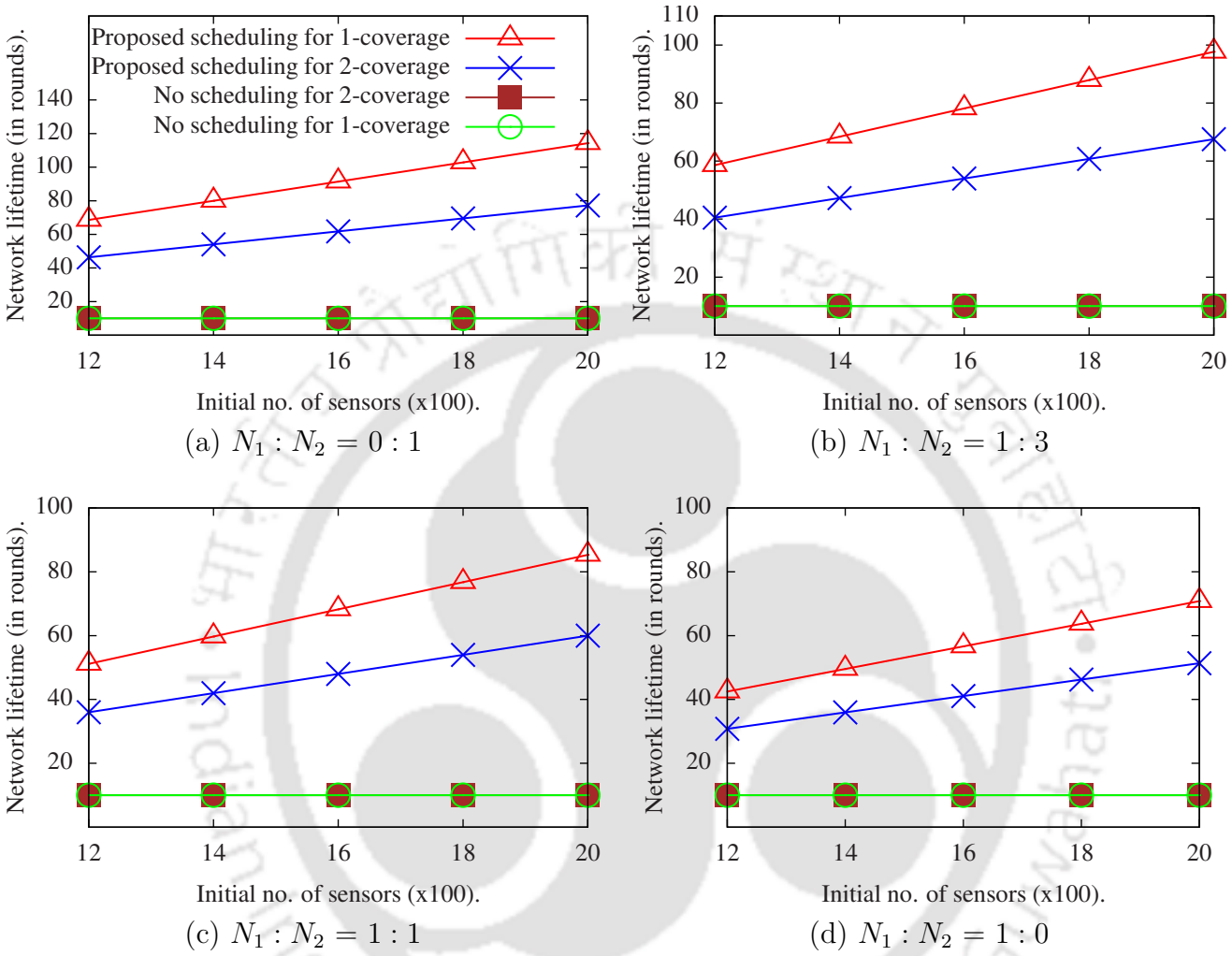

Figure 6.6 Relationship between network lifetime in rounds and k-coverage, $k = 1, 2$, with increasing number of sensors.

• **Comparison with protocol proposed in [2]:** Finally, we compared the proposed scheduling protocol with the protocol proposed in [2]. To the best of our knowledge, most of the existing sleep scheduling protocols rely on geographical information and work for homogeneous WSNs and $k = 1$. This makes a direct comparison between the proposed protocol and the existing ones unfair. To make the comparison fair, we only use homogeneous WSN scenarios in this simulation. For the simulation results in this section, we developed a high-level simulator in C++ to evaluate the

performance of the proposed scheduling protocol in practical scenarios for large scale WSNs. The high-level simulator in C++ supports much larger networks, which we need to rigorously evaluate the proposed scheduling protocol.

Fig. 6.7 shows that the number of active sensors increases with the volume of the FoI both in the case of proposed protocol and the protocol in [2]. However, we observed that the protocol proposed in this work requires fewer number of active sensors for a given volume and 3-coverage of the FoI. Thus, it can be concluded that the proposed protocol consumes lesser energy and prolongs the network lifetime when compared to the protocol in [2] even for a homogeneous WSN scenario.

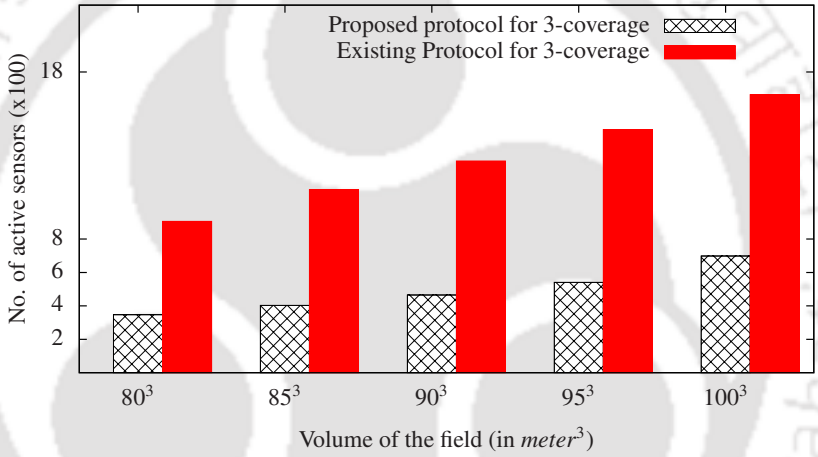

(a) $N_1 : N_2 = 0 : 1, N = 5000$

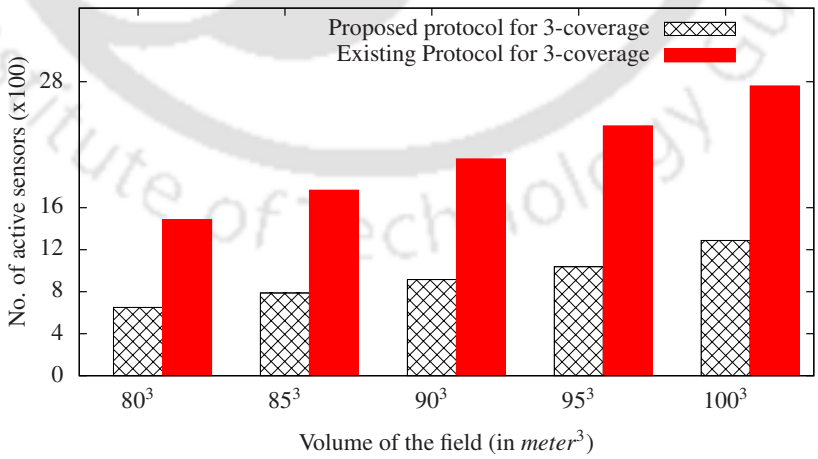

(b) $N_1 : N_2 = 1 : 0, N = 5000$

Figure 6.7 Comparison of the number of active sensors scheduled by the proposed protocol with that in [2].

6.6 Practical Considerations

In this work, we assumed that the sensors have spherical sensing and communication regions. However, in many practical scenarios, we may encounter border effects and irregular sensing and communication models. In this section, we discuss how to address these practical issues. Since such a study cannot be performed with the existing network simulator (ns 2.34), we used the modified simulator described in Section 6.5.3 to evaluate the performance of the proposed scheduling protocol in practical scenarios for large scale 3D heterogeneous WSNs. For the following simulations we consider the scenario described in Section 6.4.3.

6.6.1 Border effects

In reality, the sensors located near the edges of the FoI contribute to a smaller region of coverage than those deep inside the FoI. The reduction in the coverage area of sensors near the borders is called the *border effect* [9]. We use the toroidal distance metric to eliminate the border effects and simulate the scheduling protocol [65]. We consider the same scenario described in Section 6.4.3 for this simulation. We varied the ratio of the number of sensors of each type deployed in the FoI (shown as $N_1 : N_2$ in the plot). For each simulation, we conducted ten runs with different seeds and average the results. We studied the impact of scheduling protocol on the number of active sensors in the FoI both with and without the border effects. Fig. 6.8 illustrates that the number of active sensors for the k-coverage, $k = 1, 2$ with the toroidal distance is smaller than that when Euclidean distance is used. This is because, the Euclidean distance causes border effects which reduces the effective region covered by the sensors while, the toroidal distance ignores this effect. This result shows that the number of sensors to be deployed is under-estimated when the border effects are ignored since the sensing volume of every sensor is completely used in the coverage.

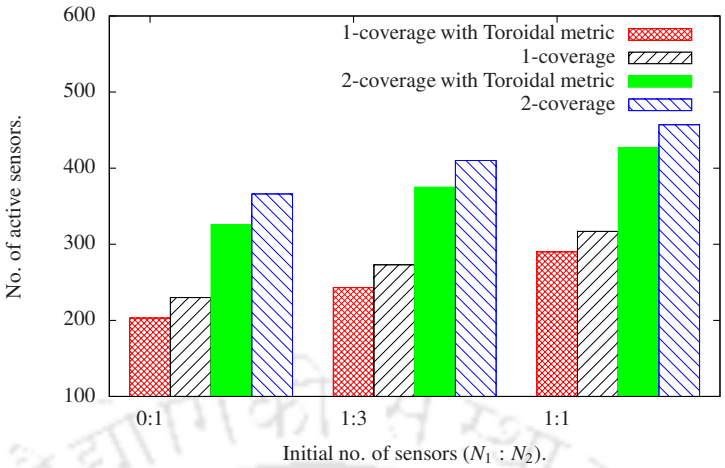

Figure 6.8 Impact of the border effects on the number of active sensors required for k-coverage of the FoI, $k = 1, 2$.

6.6.2 Irregular sensing and communication models

So far, we assumed that the sensors have spherical sensing and communication regions. Next, we studied the impact of radio irregularity using the degree of irregularity (DoI) model, as described in Chapter 4, Section 4.5.2.

With this model, instead of using the radius of an ideal sphere in the analysis, $1-h$ percent of the sensing and communication radii can be used in the analysis for h value of DoI, $0 \leq h < 1$. With this approximation a sensor s_i can sense perfectly within the sensing sphere of radius $(1-h) \times S_i$ centred at the location of s_i. Similarly, a sensor s_i can communicate with other sensors within the communication sphere of radius $(1-h) \times C_i$ centred at the location of s_i. Theorem 6.1 for redundancy of a type i sensor for k-coverage of the FoI is therefore also applicable for irregular sensing and communication models by replacing S_i and C_i with $(1-h) \times S_i$ and $(1-h) \times C_i$, where h is the value of the DoI.

We use the DoI model and simulate the scheduling protocol under the irregular sensing and communication (ISC) models. We consider the same scenario described in Section 6.4.3 for this simulation. We varied the ratio of the number of sensors of each type deployed in the FoI (shown as $N_1 : N_2$ in the plot). For each simulation,

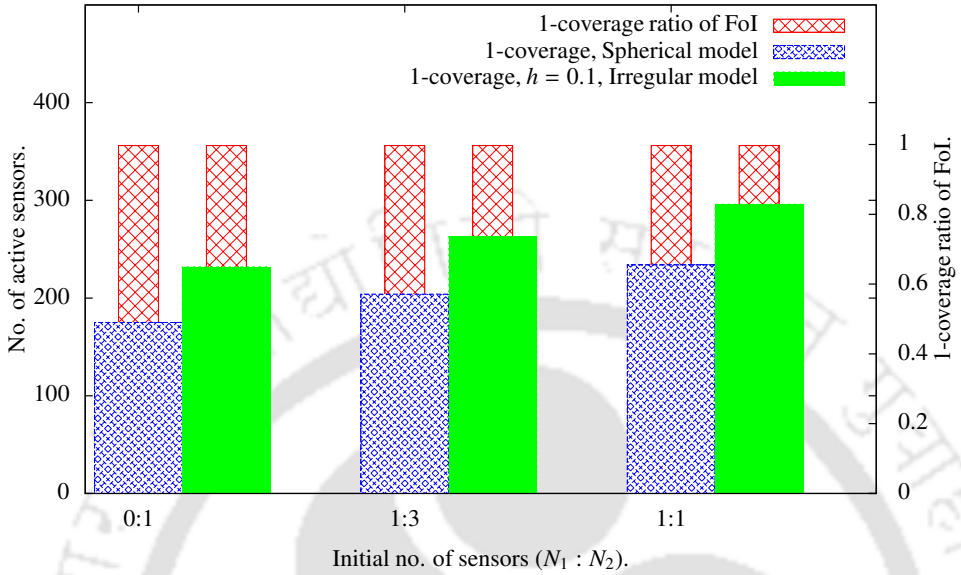

(a) 1-coverage of the FoI

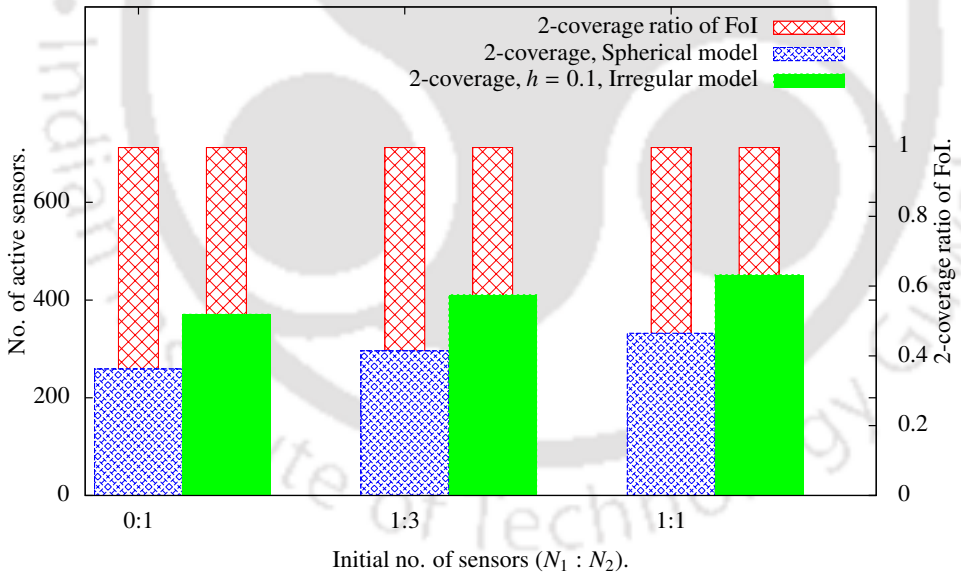

(b) 2-coverage of the FoI

Figure 6.9 Impact of the irregular sensing and communication models on the number of active sensors required for k-coverage of the FoI, $k = 1, 2$.

we conducted ten runs with different seeds and average the results. We studied the impact of scheduling protocol on the number of active sensors in the FoI and k-coverage ratio of the FoI with the spherical sensing and communication (SSC) model and ISC model using 0.1 value of DoI, where $k = 1, 2$. Parts (a) and (b) of Fig. 6.9 illustrate that the number of active sensors for the 1-coverage and 2-coverage, respectively with the ISC model using 0.1 DoI value is greater than that when the SSC model is used. This is because, the ISC model causes radio irregularity which reduces the effective region covered by the sensors while, the SSC model ignores this irregularity.

6.7 Conclusion

In this work, we proposed a probabilistic approach to determine if a sensor in a HWSN is redundant to meet the desired coverage requirements of a 3D FoI. We derived an expression to determine the probability of the region covered by a sensor of any type being redundantly covered by the neighbours. Then, we proved a result that identifies if the sensor is redundant based on the number of neighbours of different types and their state. We proposed a scheduling protocol to identify all the redundant sensors and schedule them to sleep without creating a coverage hole in the FoI. The proposed protocol is completely distributed, does not use any geographic information, and uses only the information gathered about the neighbours using a few control messages. We simulated the performance of the scheduling protocol for different network scenarios and demonstrated that the number of active sensors is reduced due to the scheduling protocol and hence the network lifetime is increased.

In this chapter, we addressed the problem of determining the probability of a sensor being redundant for k-coverage in 3D HWSNs. In the next chapter, we propose a scheduling protocol to identify the redundant sensors and schedule them to sleep while ensuring the partial coverage in 2D HWSNs.

Chapter 7

Sleep Scheduling for Partial Coverage in Heterogeneous WSNs

7.1 Introduction

Complete coverage usually means that the WSN can sense the whole FoI without any hole. Complete coverage indicates a high level of reliability yet is often difficult to be realized in practice. When sensors are deployed randomly, complete coverage may be difficult to achieve without a large number of sensors. In such cases the probability that the FoI is completely covered becomes an important measure of coverage.

In certain applications of WSNs like forest fire detection and weather forecasting, the requirement of complete coverage of the FoI, may be too expensive or unnecessary. In stochastic deployment of WSNs, the problem of partial coverage refers to a relaxation in the desired QoC that requires only a part of the FoI to be covered. In terms of the coverage ratio (defined in Section 3.1), the partial coverage problem requires that the coverage ratio be no less than a pre-defined threshold (smaller than unity). If the coverage ratio is desired to be unity then it degenerates to complete coverage problem.

In this chapter, we address the problem of identifying the redundant sensors in a

heterogeneous 2D WSN and schedule them to sleep while ensuring the desired coverage ratio of the FoI. This protocol does not require the sensor to have any information about its geographical location/relative position to discover its redundancy. To the best of our knowledge, this is the first work to address the redundancy for partial coverage in heterogeneous WSNs without any information about the geographical location or relative position.

Major Contributions: We argue that the analysis of the redundancy of a sensor for complete coverage as derived in previous chapter, is not suitable for partial coverage. We derive an expression to determine the probability of a sensor, with a set of neighbours of different types, being redundant for partial coverage of the FoI. We propose a distributed scheduling protocol to put the redundant sensors to sleep yet maintain the partial coverage of the FoI.

The rest of the chapter is organised as follows: In the next section, we briefly discuss previous work on coverage-preserving scheduling protocols in 2D WSNs. In Section 7.3, we define the network model, the terms and the notation used. In Section 7.4, we derive the expression for the redundancy degree of a sensor of any given type in a heterogeneous WSN and also show its use in identifying a redundant sensor. The analysis is numerically evaluated and validated with simulation. Section 7.5 presents the results of simulations conducted to evaluate the performance of the scheduling protocol in different network scenarios. We conclude the work in Section 7.6.

7.2 Related work

In this section, we review the literature on the scheduling protocols to achieve a desired coverage ratio of the 2D FoI. A variety of configuration protocols that use geometric information and maintain complete coverage in 2D WSNs are proposed in the literature with an objective to reduce the energy consumption.

Xing *et al.* in [30], proposed an integrated coverage and connectivity configuration

protocol (CCP) that guarantees both connectivity and coverage when the communication range of a sensor is at least twice its sensing range. CCP is a decentralized protocol that configures the network to provide complete coverage of the sensor field. In CCP, a sensor can be in one of three states: sleep, active, and listen. In the sleep state, the sensor turns off its sensing unit until the sleep timer expires, and then it enters the listen state. In the listen state, the sensor collects HELLO messages from its neighbors and executes the coverage eligibility algorithm. The coverage eligibility algorithm determines whether a sensor is eligible to switch states. If every location within a coverage region of the sensor is not covered by other active sensors, the sensor will be eligible to become active, else it goes back to sleep. In active state, the sensor periodically updates its sensing neighbor table and executes the coverage eligibility algorithm to determine if it has to remain active. A distributed and localised algorithm, based on k^{th}-order Voronoi diagram, to identify redundant sensors is proposed by Zhou *et al.* in [74]. It ensures fault tolerance in WSNs and extends the network lifetime, while maintaining complete coverage. Huang *et al.* in [75] proved that the whole sensor field is covered if and only if each sensor within the sensor field is perimeter-covered. A decentralised energy efficient algorithm is proposed to determine the level of coverage and connectivity, and schedule the redundant sensors into sleep mode. However, it is not applicable when two sensors are located at the same point. Identification of redundant sensors based on a geometric approach is considered in [76]. The sensing area of a sensor is divided into six equal-sized sectors and if each sector consists of a sensor then it is a redundant sensor.

Wu *et al.* in [77] proposed a method to discover the redundant sensing areas among neighbouring sensors and calculate the degree of redundancy without using any geographical information. The degree of redundancy is used to construct a distributed algorithm named lightweight deployment-aware scheduling (LDAS) algorithm that turns the redundant sensors off. However, this work only considers partial coverage

in homogeneous WSNs. Recently, another protocol to determine the coverage under both deterministic and probabilistic sensing models is proposed in [66]. This protocol called probabilistic coverage protocol (PCP), builds a triangular structure that determines if every point in a given deployment of WSN satisfies the desired coverage either definitely or with a probability. The PCP protocol computes the maximum possible distance between sensors to ensure that there are no holes in coverage. The authors also consider connectivity and energy efficiency while designing the protocol. The work in [78] proposed a centralised scheduling algorithm with location information and a distributed algorithm without location information to achieve the p-percent coverage ratio in a homogeneous WSN. Bulut and Korpeoglu in [72] proposed a distributed algorithm to extend the lifetime of a homogeneous WSN while maintaining the desired coverage and connectivity.

Motivation: Except the work in [68], no other work considers the partial coverage problem in heterogeneous WSNs. The work in [68] assumes that the sensing range follows a normal distribution, and use the mean value in the analysis. So it has limited scope in a typical heterogeneous WSN. Most of the earlier work on the partial coverage problem is applicable only for homogeneous WSNs and some of them use geographical information in identifying the redundant sensors [78, 77, 72]. Though the coverage problem is studied in the context of heterogeneous WSNs in [76, 30], only complete coverage is considered. Based on these observations, we study the partial coverage problem in heterogeneous WSNs, take a probabilistic approach to determine the redundancy degree of a sensor, and propose a distributed sleep scheduling algorithm that gathers only the characteristics of the sensors and does not use any geographical information.

7.3 Preliminaries

In this section, we state the assumptions made about the network and define the terms used in this work.

Assumptions: We assume that sensors are deployed in the FoI Ψ, uniformly at random independent of each other. The shape of the FoI is assumed to be a two-dimensional torus so that the border effects can be ignored [79]. In a heterogeneous WSN considered in this work, the sensors are categorised into t different types based on their sensing and/or communication ranges. Let n_i be the number of type i sensors such that $\sum_{i=1}^{t} n_i = n$, where n is the total number of sensors in the heterogeneous WSN. All the sensors of a given type are assumed to have equal sensing and communication radii. We assume the *binary disc sensing* model in which any sensor of type i denoted by s_i, $1 \leq i \leq t$, can sense perfectly within the disc of radius S_i centred at s_i, denoted by $A(s_i, S_i)$. s_i cannot sense any activity beyond $A(s_i, S_i)$. The area covered by the sensor s_i is nothing but the area of the sensing disc denoted by $\|A(s_i, S_i)\| = \pi S_i^2$. Thus, S_i denotes the sensing range of s_i. We assume that the communication of a sensor also follows the binary disc model and the disc $A(s_i, C_i)$ denotes the region over which s_i can communicate with other sensors, where C_i is the communication range. The QoC of the FoI is specified apriori as a desired coverage ratio denoted by η_{th}.

Definition 1: In a heterogeneous WSN, for any two sensors s_i and s_j, $\ni 1 \leq i, j \leq t$, $\forall\{i \neq j\}$, $S_i \neq S_j$ and/or $C_i \neq C_j$.

Definition 2: Two sensors s_i and s_j, $1 \leq i, j \leq t$ can communicate with each other directly only if the Euclidean distance between them is less than or equal to $\min(C_i, C_j)$ called the *effective communication range* between s_i and its neighbour s_j. We call the disc $A\big(s_i, \min(C_i, C_j, S_i + S_j)\big)$ as the *effective communication region* of s_i (with its neighbour s_j).

Definition 3: If two sensors s_i and s_j are such that the distance between them is

less than $S_i + S_j$, and if they can communicate with each other directly, then they are said to be *sensing and communication (SAC) neighbours* or simply *neighbours*.

Definition 4: A part of the sensing region of a sensor is said to be *redundantly covered* if each point therein is covered by at least one neighbour. The redundancy degree of a type i sensor, denoted by ξ_i is defined as the ratio of its sensing area redundantly covered by the neighbours to its entire sensing area. Note that this definition is similar to that in [68] except that we use a stronger definition for the neighbours, namely SAC neighbours using effective communication range, and estimate only the expected value of redundancy degree.

7.4 Analysis of the Redundancy of a Sensor for Partial Coverage

In the previous chapter, we have seen that a sensor is considered to be redundant for complete coverage if all the points in its sensing region are covered by at least one neighbour. It can be seen from part (a) of Fig. 7.1 that sensor s_j is redundant for complete coverage due to the sensor s_k and sensor s_i is redundant for complete coverage due to both s_j and s_k being present. Therefore, s_i and s_j both are redundant sensors for complete coverage. The problem of partial coverage refers to the relaxation in the QoC that requires only a part of the FoI to be covered by at least one sensor. Part (b) of Fig 7.1 illustrates that sensors s_i and s_j are redundant for partial coverage due to s_j and s_k, respectively. However, the sensing region of s_i is not redundantly covered by s_k. Therefore, if s_i is considered to be a redundant sensor, then s_j is not a redundant sensor for partial coverage. We refer to two sensors as *neighbours* for partial coverage if they can directly communicate with each other. To reflect the modified definition of neighbors, we replace $\min(C_j, S_i + S_j)$ with $\min(C_i, C_j, S_i + S_j)$ in Eq. 6.2. Therefore, the probability of an event that a point $X \in A(s_i, S_i)$ at a distance of x from s_i, is also covered by a type j neighbour for partial coverage is

given by

$$p_{ij}(x) = \frac{\|A(X, S_j) \cap A(s_i, \min(C_i, C_j, S_i + S_j))\|}{\|A\big(s_i, \min(C_i, C_j, S_i + S_j)\big)\|}. \tag{7.1}$$

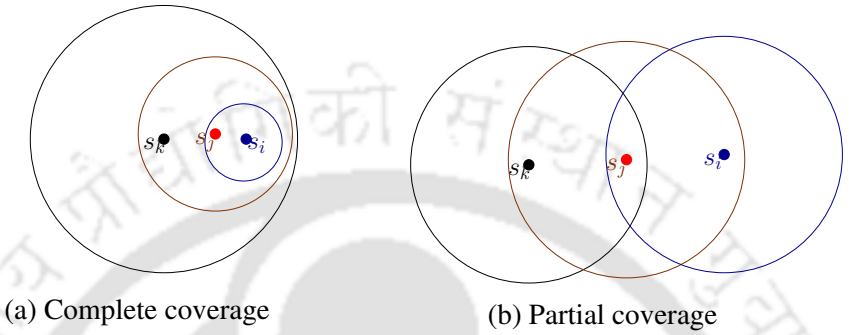

(a) Complete coverage (b) Partial coverage

Figure 7.1 Illustration of the redundancy of sensors for QoC.

To interpret Eq. 7.1, if $p_{ij}(x) = 0.80$ and a point X in the sensing region of s_i is also covered by a type j neighbour s_j, then s_j can only be present in 80% of the effective region of communication.

It is obvious that $p_{ij}(x)$ depends on the position of X, S_j, and $\min(C_i, C_j, S_i+S_j)$. For a given pair of neighbours, s_i and s_j, the effective communication region denoted by $A\big(s_i, \min(C_i, C_j, S_i+S_j)\big)$ is constant. For different values of S_j, we estimate $p_{ij}(x)$ for the two cases considered below:

• $\boldsymbol{S_j < \min(C_i, C_j, S_i + S_j)}$ **:** Fig. 7.2(a) and Fig. 7.2(b) illustrate two ways in which the sensing range of the type j neighbour is smaller than the effective communication range. In Fig. 7.2(a), the point X is at a distance of at most $\min(C_i, C_j, S_i + S_j) - S_j$ from s_i, *i.e.*, $0 \leq x \leq \min(C_i, C_j, S_i + S_j) - S_j$. Then the term in the numerator of Eq. 7.1 becomes equal to $\|A(X, S_j)\|$. In Fig. 7.2(b), the distance of point X from s_i is in the range of $\big(\min(C_i, C_j, S_i + S_j) - S_j, S_i\big]$, *i.e.*, $\min(C_i, C_j, S_i + S_j) - S_j < x \leq S_i$. Thus, $p_{ij}(x)$ for this case is given by

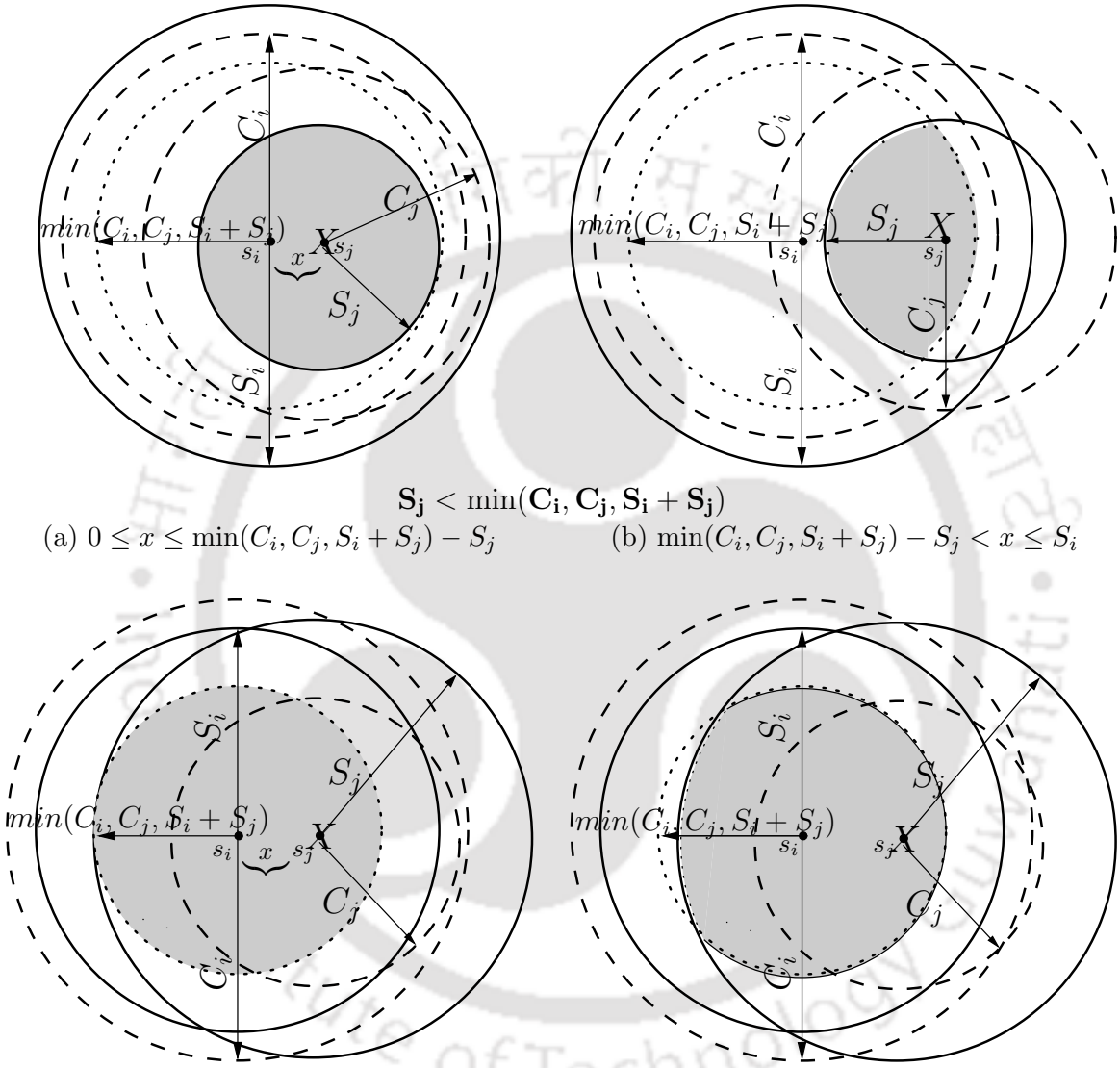

$\mathbf{S_j} < \min(\mathbf{C_i}, \mathbf{C_j}, \mathbf{S_i} + \mathbf{S_j})$

(a) $0 \leq x \leq \min(C_i, C_j, S_i + S_j) - S_j$ (b) $\min(C_i, C_j, S_i + S_j) - S_j < x \leq S_i$

$\min(\mathbf{C_i}, \mathbf{C_j}, \mathbf{S_i} + \mathbf{S_j}) \leq \mathbf{S_j}$

(c) $0 \leq x \leq S_j - \min(C_i, C_j, S_i + S_j)$ (d) $S_j - \min(C_i, C_j, S_i + S_j) < x \leq S_i$

Figure 7.2 Illustration of the cases considered in deriving $p_{ij}(x)$.

$$\begin{cases} \frac{\|A(X,S_j)\|}{\left\|A\left(s_i,\min(C_i,C_j,S_i+S_j)\right)\right\|} & 0 \le x \le \min(C_i,C_j,S_i+S_j) - S_j \quad (a) \\ \frac{\left\|A(X,S_j)\cap A\left(s_i,\min(C_i,C_j,S_i+S_j)\right)\right\|}{\left\|A\left(s_i,\min(C_i,C_j,S_i+S_j)\right)\right\|} & \min(C_i,C_j,S_i+S_j) - S_j < x \le S_i \quad (b) \end{cases} \tag{7.2}$$

• **$\min(C_i, C_j, S_i + S_j) \le S_j$:** Fig. 7.2(c) and Fig. 7.2(d) illustrate two ways in which the sensing range of the type j neighbour is greater than or equal to the effective communication range. In Fig. 7.2(c), the point X is at a distance of at most $S_j - \min(C_i, C_j, S_i + S_j)$ from s_i, *i.e.*, $0 \le x \le S_j - \min(C_i, C_j, S_i + S_j)$. Then the term in the numerator of Eq. 7.1 becomes equal to $\left\|A\left(s_i, \min(C_i, C_j, S_i + S_j)\right)\right\|$. In Fig. 7.2(d), the distance of point X from s_i is in the range of $\left(S_j - \min(C_i, C_j, S_i + S_j), S_i\right]$, *i.e.*, $S_j - \min(C_i, C_j, S_i + S_j) < x \le S_i$.

Thus, $p_{ij}(x)$ for this case is given by

$$\begin{cases} \frac{\left\|A\left(s_i,\min(C_i,C_j,S_i+S_j)\right)\right\|}{\left\|A\left(s_i,\min(C_i,C_j,S_i+S_j)\right)\right\|} = 1 & 0 \le x \le S_j - \min(C_i,C_j,S_i+S_j) \quad (a) \\ \frac{\left\|A(X,S_j)\cap A\left(s_i,\min(C_i,C_j,S_i+S_j)\right)\right\|}{\left\|A\left(s_i,\min(C_i,C_j,S_i+S_j)\right)\right\|} & S_j - \min(C_i,C_j,S_i+S_j) < x \le S_i \quad (b) \end{cases} \tag{7.3}$$

Eqs. 7.2 and 7.3 estimate the probability of a point in the sensing region of a type i sensor also being covered by a type j SAC neighbour. Next we estimate the probability that a part of the sensing region of a type i sensor is redundantly covered by a set of neighbours of different types.

7.4.1 Redundancy Degree of a Sensor

Let $C_j^i(X)$ denote the event that a point X in the sensing region of a type i sensor is also covered by at least one of the type j neighbours. The probability of this event is

$$\mathbf{P}(C_j^i(X)) = 1 - (1 - p_{ij}(x))^{n_{ij}}\,, \tag{7.4}$$

where n_{ij} is the number of type j neighbours of a type i sensor.

Similarly, let $D^i(X)$ denote the event that a point X in the sensing region of a type i sensor is covered by at least one neighbour of any type when there are n_{ij} neighbours of type j, for $1 \leq j \leq t$. The probability of this event is

$$\mathbf{P}(D^i(X)) = 1 - (1 - p_{i1}(x))^{n_{i1}} \ldots (1 - p_{it}(x))^{n_{it}} = 1 - \prod_{1 \leq j \leq t} (1 - p_{ij}(x))^{n_{ij}}. \tag{7.5}$$

The expected value of the sensing area of s_i that is redundantly covered by at least another neighbour can be obtained by simply integrating Eq. 7.5 over its sensing region *i.e.*,

$$\iint_{A(s_i,S_i)} \mathbf{P}(D^i(X))dA. \tag{7.6}$$

By the definition of redundancy degree of a sensor, the expected value of redundancy degree of a type i sensor is the fraction of the expected sensing area redundantly covered in the total sensing area. The expected redundancy degree of s_i is therefore given by

$$E[\xi_i] = \frac{1}{\|A(s_i, S_i)\|} \iint_{A(s_i,S_i)} \mathbf{P}(D^i(X))dA = \frac{2\pi}{\pi S_i^2} \int_0^{S_i} \mathbf{P}(D^i(X))xdx. \tag{7.7}$$

By substituting $\mathbf{P}(D^i(X))$ from Eq. 7.5 we get

$$E[\xi_i] = \frac{2}{S_i^2} \int_0^{S_i} \left(1 - \prod_{1 \leq j \leq t} (1 - p_{ij}(x))^{n_{ij}}\right) xdx = 1 - \frac{2}{S_i^2} \int_0^{S_i} \left(\prod_{1 \leq j \leq t} (1 - p_{ij}(x))^{n_{ij}}\right) xdx. \tag{7.8}$$

The expected redundancy degree can be interpreted as follows: if $E[\xi_1] = 0.80$, when we randomly pick several points from the sensing area of a type 1 sensor, 80% of them are redundantly covered its neighbours of different types.

Now that we can determine the expected value of the sensing area of any sensor that is redundantly covered with Eq. 7.8, we need to determine how to declare a

sensor as redundant. To do this, we define the following lemma that establishes the condition for redundancy of a sensor based on its expected redundancy degree. Assuming a dense WSN for which the desired coverage ratio of the FoI is specified, the lemma declares a sensor to be redundant if its expected redundancy degree is greater than or equal to the desired coverage ratio. This result is used by the distributed protocol proposed in Section 7.5 to schedule the redundant sensors to sleep.

Lemma 7.1 *In a densely deployed heterogeneous WSN, if the expected redundancy degree of a type i sensor s_i, $1 \leq i \leq t$ is greater than or equal to the desired coverage ratio of the FoI i.e., if $\eta_{th} \leq E[\xi_i]$, then the sensor is redundant, where $0 \leq \eta_{th} \leq 1$ indicates the QoC of the FoI.*

Proof: (Proof by Contradiction.) Let us assume that the lemma is not true. That is, even though $\eta_{th} \leq E[\xi_i]$, s_i is not redundant. The term $E[\xi_i] \, \|A(s_i, S_i)\|$ indicates the expected value of the sensing area of s_i that is redundantly covered by the neighbours as defined by the expression 7.6, while the term $\eta \, \|\Psi\|$ indicates the area of the FoI actually covered by the WSN, where η is the actual coverage ratio of the FoI. Thus, $\eta \, \|\Psi\| - (1 - E[\xi_i]) \, \|A(s_i, S_i)\|$ is the area of the FoI covered even without the type i sensor. Further, if s_i is not redundant, then the following inequality should hold.

$$\eta \, \|\Psi\| - \big(1 - E[\xi_i]\big) \, \|A(s_i, S_i)\| < \eta_{th} \, \|\Psi\| \tag{7.9}$$

Assume that the FoI is densely deployed with sensors so that it is completely covered *i.e.*, $\eta = 1$. Substituting $\eta_{th} \leq E[\xi_i]$ and $\eta = 1$, in the above inequality and rearranging the terms, we get $\|\Psi\| < \|A(s_i, S_i)\|$. This is a contradiction because the area of the FoI is much larger than the sensing area of any type i sensor. Hence the lemma is proved. □

Given a heterogeneous WSN and a desired coverage ratio of the FoI, the following

corollary determines the condition for redundancy of a sensor in terms of the number of neighbours of each type it has and their sensing and communication ranges.

Corollary 1 *Assume that sensors belonging to t different types are independently and uniformly distributed at random across the FoI. Let the desired coverage ratio of the FoI be η_{th}. For any type i sensor, if the number of neighbours of a given type j is say n_{ij}, $1 \leq i, j \leq t$, then the sensor is redundant if the following inequality holds:*

$$\eta_{th} \leq 1 - \frac{2}{S_i^2} \int_0^{S_i} \left(\prod_{1 \leq j \leq t} (1 - p_{ij}(x))^{n_{ij}} \right) x dx, \tag{7.10}$$

where $p_{ij}(x)$ is defined in Eqs. 7.2 and 7.3

Proof: Substitute $E[\xi_i]$ from Eq. 7.8 in Lemma 7.1. □

7.4.2 Validation of the Analysis

To validate the proposed analysis, we evaluate the expected redundancy degree from Eq. 7.8 numerically and compare it with that obtained with a simulation for the following scenario of deployment. A rectangular FoI of $10,000m^2$ is sprayed with 200 sensors randomly with a uniform distribution. There are two types of sensors (100 sensors of each type) with the sensing and communication ranges as: $S_1 = 15m$, $C_1 = 15m$, $S_2 = 18m$, and $C_2 = 20m$. For the numerical results, we evaluate Eq. 7.8 for different scenarios considered in the simulations. For the simulation results a Monte Carlo simulation is conducted as described in Chapter 3, Section 3.4.

Fig. 7.3 shows the variation in the expected redundancy degree for a sensor of each type (*i.e.*, $E[\xi_1]$ and $E[\xi_2]$) with different number of neighbours. Each plot shows $E[\xi_1]$ and $E[\xi_2]$ for different combinations of neighbours of each type (shown below x-axis in the form (n_1,n_2)) obtained both with simulations and numerical evaluation. Note

that the results for $E[\xi_1]$ in Fig. 7.3(b) and $E[\xi_1]$ in Fig. 7.3(a) correspond to the case of a homogeneous WSN scenario while the rest are for heterogeneous WSN scenarios.

It can be seen in all the figures that the expected redundancy degree calculated with simulation, matches closely with that evaluated using Eq. 7.8 thereby validating our analysis. The results show that the expected redundancy degree of any sensor increases with the number of neighbouring sensors making it a potential candidate for being redundant. However, on comparing Figs. 7.3(a) and 7.3(b), we can see that $E[\xi_1]$ increases sharply with an increase in type 2 neighbours because the type 2 sensors have larger communication and sensing ranges. The higher utility of type 2 sensors for redundancy degree can also be concluded from Fig. 7.3(c) in which both $E[\xi_1]$ and $E[\xi_2]$ increase sharply with the number of neighbours, because there are larger number of type 2 sensors among the neighbours when compared to the scenario used in Fig. 7.3(d) where most of the neighbours are type 1 sensors.

7.5 Sleep Scheduling Protocol for Partial Coverage

In this section, we use the analysis in the previous section to propose a protocol that helps each sensor to determine if it is redundant and go to sleep without compromising the desired coverage ratio. We propose a distributed protocol for this purpose which does not use any geographical information but only gathers periodic information about the number of neighbours, their type, and their current state with short control messages.

7.5.1 Description of the scheduling protocol

We assume that the sink or base station which is a powered node computes the expected redundancy degree for a type i sensor, given the number of neighbours of each type, and their ranges for sensing and communication. The expected redundancy degree corresponding to a given number of neighbours of different types is stored in

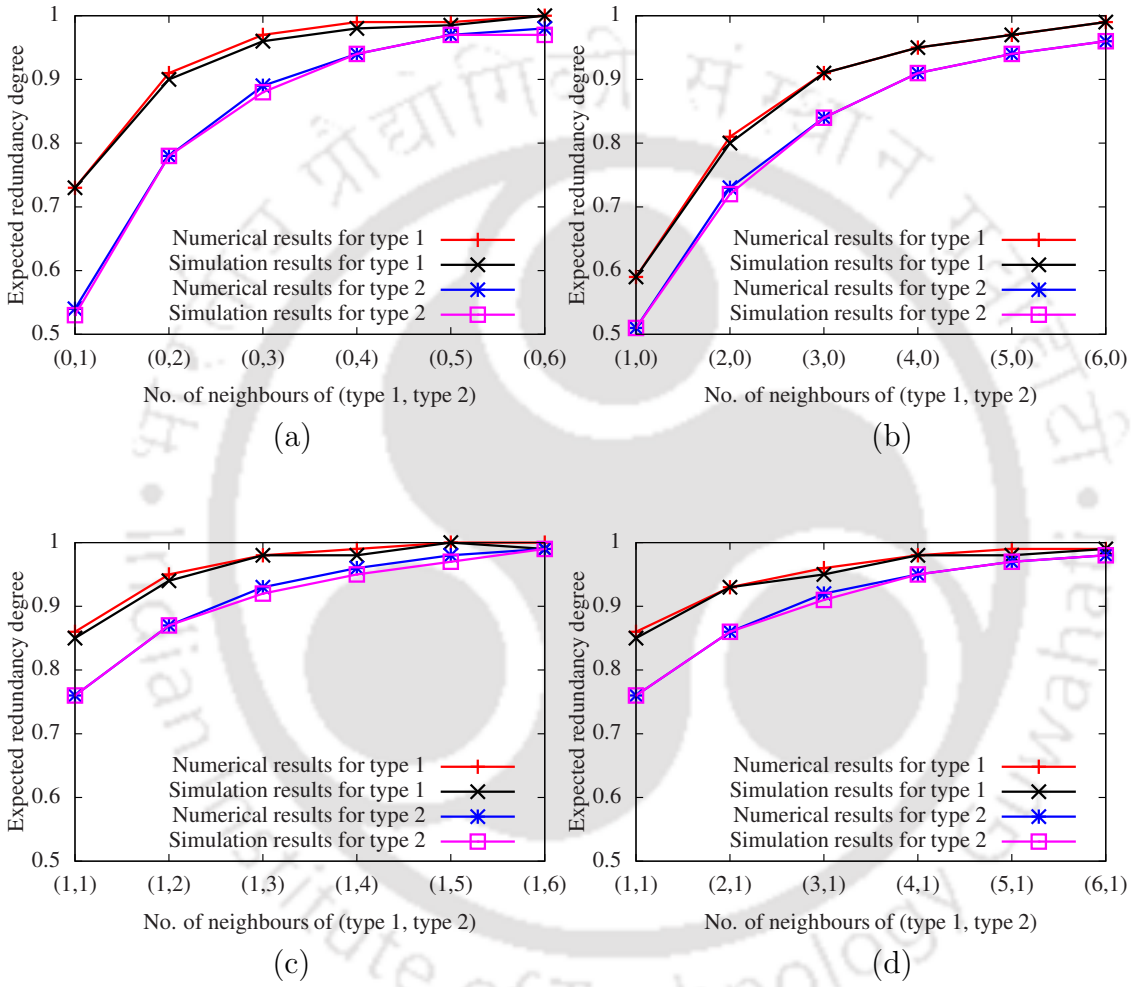

Figure 7.3 Variation in the expected redundancy degree of a sensor for different number of neighbours.

a table called *Redundancy Table* (format shown in Table 7.1(b)). Computation of this table is facilitated by Eq. 7.8. The *Redundancy Table* is either stored in each sensor off-line or can be sent by the base station initially at the time of deployment. Once a sensor knows the information about its neighbours, it can lookup the expected redundancy degree from this table, compare it with the desired coverage ratio and determine if it is redundant. We explain the protocol used to gather information about the neighbours and sleep scheduling in detail below.

In the sleep scheduling protocol, the operation time of the WSN is divided into successive rounds. Each round consists of two phases: the decision phase and the sensing phase. In the decision phase, all sensors decide on their activity for the current round. During the sensing phase, all active sensors are responsible for sensing until the beginning of the next round. After each round, all sensors become active to participate in the decision phase of the next round. The duration of each round is chosen such that it is much longer than the decision phase but much shorter than the average lifetime of the WSN.

At any given point of time, a sensor can be in one of these states: ACTIVE, WAIT, and SLEEP. In ACTIVE state, a sensor is responsible to cover its sensing region and communicate with its neighbours. At the beginning of each round, all sensors are in ACTIVE state and independently execute the scheduling protocol. In SLEEP state, the sensor is put to sleep in order to conserve energy. Sensors in this state are not required to maintain the desired QoC during the round. A sensor goes into WAIT state if it determines itself to be redundant but is in the process of asserting its transition to SLEEP state with its neighbours. The state transition diagram of this protocol is similar to that in previous proposals like [77, 78].

The scheduling protocol uses two messages HELLO and SLEEP to disseminate information among all the neighbours. Each sensor turns active at the beginning of a round (*i.e.*, during the decision phase) and broadcasts a HELLO message with its

ID, type, and current state to all its neighbours. A sensor that receives the HELLO message stores information about its neighbours in a *Neighbour Table* in the format shown in Table 7.1(a). The table stores the unique ID of each neighbour, its type, and the current state of the neighbour. This information is updated with periodic HELLO messages between the sensors.

From the information in the *Neighbour Table*, each sensor knows the number of neighbours of each type and their state. It then looks up the expected redundancy degree corresponding to the number of different types of neighbours from the *Redundancy Table*. Table 7.1(b) shows the format of the *Redundancy Table* for a type 1 sensor. The first two columns in the table show the number of neighbours of each type while the third column shows the expected redundancy degree. For example, if this sensor has two type 2 sensors in the neighbourhood (in ACTIVE or WAIT state), the expected redundancy degree is 0.91. Since the *Redundancy Table* can be computed offline and stored at the time of deployment, determining the expected redundancy degree of a sensor is simplified to only periodically refreshing the information in the *Neighbour Table* and looking up the *Redundancy Table*.

Table 7.1 Data stored at a type 1 sensor.

ID	Type	State
1	type 1	ACTIVE
2	type 2	WAIT
3	type 2	WAIT
4	type 1	ACTIVE
5	type 1	ACTIVE

(a) Neighbour Table.

n_{11}	n_{12}	$E[\xi_1]$
0	0	0
0	1	0.73
0	2	0.91
⋮	⋮	⋮
6	6	1

(b) Redundancy Table.

Each sensor compares the expected redundancy degree with the desired coverage ratio of the field (a constant QoC requirement) to determine if it is redundant. If the sensor is potentially redundant, it switches to WAIT state. Otherwise it remains in the ACTIVE state. In WAIT state, a sensor starts a random back-off timer and keeps

track of its SAC neighbours with HELLO messages. The motive behind back-off time is to avoid a black-hole when several sensors try to go to SLEEP state simultaneously. If the sensor has sufficient number of active neighbours at the end of back-off time, it sends SLEEP messages to a selected number of neighbours (greater than or equal to the number of neighbours required for its redundancy), and switches to the SLEEP state until the next round. To send the SLEEP messages, a neighbour already in the ACTIVE state is given higher priority either because it does not have sufficient neighbours for redundancy, or it just switched from WAIT state to the ACTIVE state. A SLEEP message consists of the IDs of the sender and all the selected neighbours. When a sensor receives the SLEEP message, it switches to ACTIVE state or stays in the same state until the next round. This is because the receiving sensor is made responsible for the area covered by the sender of the SLEEP message. If SLEEP message is received by a sensor whose ID is not listed in the message the receiving sensor uses it to update its *Neighbour Table*.

7.5.2 Performance Evaluation

In this subsection, we discuss the results from a simulation study of the proposed scheduling protocol implemented in the ns 2.34 simulator [73]. We consider the same scenario described in Section 7.4.2 for the simulations. Since the control messages used by the protocol namely, HELLO and SLEEP messages are very short and their frequency is low, we assume that their collision can be neglected. We assume that the power consumption in sensors during transmission, reception, idle, and sleep modes is 60mW, 12mW, 12mW, and 0.03mW, respectively [76]. The initial energy of a sensor is assumed to be 60J, which allows the sensor to operate for about $5,000$ seconds in reception/idle mode. The simulations are conducted by varying the ratio of the number of sensors of each type (shown as $n_1 : n_2$), area of the FoI, number of sensors deployed, and the desired coverage ratio (η_{th}). For each simulation, we conduct ten

runs with different seeds, and average the results. The results presented here are with 95% confidence level though the error bars are not visible in the plots.

• **Coverage ratio of the FoI:** We first verify if the scheduling protocol always ensures that the desired coverage ratio is maintained during the simulation. Since the scheduling protocol helps each sensor to identify if it is redundant for a given η_{th} and lets it go to sleep, it is important to verify if the actual coverage ratio, $\eta \geq \eta_{th}$. Table 7.2 shows the actual coverage ratio maintained during the simulation with different number of sensors deployed. It can be seen that the condition $\eta \geq \eta_{th}$ is always satisfied by the scheduling protocol. We will see in other results that while ensuring the desired coverage ratio, the protocol also reduces the number of active sensors and thereby prolongs the network lifetime.

Table 7.2 Coverage ratio obtained with the protocol.

η_{th}	**Actual coverage ratio** Initial number of sensors		
	100	200	300
0.60	0.65	0.66	0.66
0.80	0.85	0.87	0.87
0.95	0.98	0.99	0.99

• **Impact of desired coverage ratio:** Next, we study the impact of desired coverage ratio on the number of sensors used in the deployment. For three values of η_{th}, we measure the number of active sensors used to satisfy the condition $\eta \geq \eta_{th}$. For this simulation, the sensors (with different ratios) are deployed in $10,000m^2$ area. Fig. 7.4 shows the number of active sensors required to satisfy the desired coverage ratio as the number of sensors deployed in the FoI is increased. It can be observed that when there is higher QoC requirement (larger η_{th}), the number of active sensors is larger but fairly remains constant irrespective of the number of sensors deployed in the FoI. This shows that with the proposed scheduling protocol, the number of sensors required in practice to cover the FoI is small.

By comparing Fig. 7.4(a) with parts (b)-(d) of Fig. 7.4 it can be observed that for the same η_{th}, the number of active sensors required is smaller when only type 2 sensors are used (*i.e.*, $n_1 : n_2$=0 : 1) compared to the other three cases. This is because type 2 sensors have larger radii for sensing and communication and therefore have higher utility for coverage. Using larger number of type 2 sensors in the FoI also makes larger number of sensors redundant (see the results in Fig. 7.3), reducing the number of active sensors. However, often the cost of such sensors may be higher prohibiting the use of only sensors with larger ranges. If we assume type 2 sensors to be costlier than type 1 sensors, then instead of deploying the sensors in the ratio of 1 : 3, deploying them in the ratio of 1 : 1 gives the desired level of coverage with slightly larger number of active sensors as seen from parts (b)-(d) of Fig. 7.4.

From the results in Fig. 7.4, it may appear that the number of active sensors remains almost constant irrespective of the number of sensors deployed. But these results are for a fixed area of $100 \times 100m^2$. Next, we study the impact of the size of the FoI on the number of active sensors. We deploy around 600 sensors with different ratios of the two types of sensors and increase the area of the FoI. Fig. 7.5 shows that the number of active sensors required increases as the area of the FoI is increased from $100 \times 100m^2$ to $900 \times 100m^2$ for a given coverage ratio. Similar to the results in the previous simulation, the number of active sensors is smallest when all the sensors are of type 2 (*i.e.*, $n_1 : n_2 = 0 : 1$).

• **Lifetime of network:** Next, we study the impact of the scheduling protocol on the lifetime of the WSN. We measure the network lifetime with the number of rounds of simulation time till all the sensors drain their energy completely. For this simulation, 100 sensors (with different ratios) are deployed in $10,000m^2$ area and the number of rounds for which the network survives is measured. Fig. 7.6 shows the actual coverage ratio obtained for the entire duration of the simulation for different values of η_{th}. The results also show the network lifetime when no scheduling protocol is used. It can

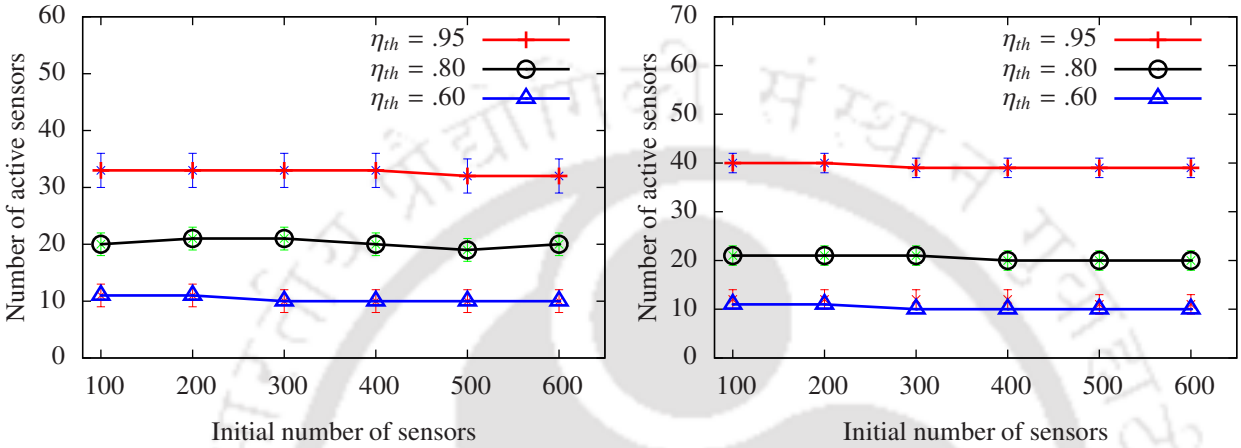

(a) $n_1 : n_2 = 0 : 1$ (b) $n_1 : n_2 = 1 : 3$

(c) $n_1 : n_2 = 1 : 1$ (d) $n_1 : n_2 = 1 : 0$

Figure 7.4 Relationship between the number of active sensors and desired coverage ratio.

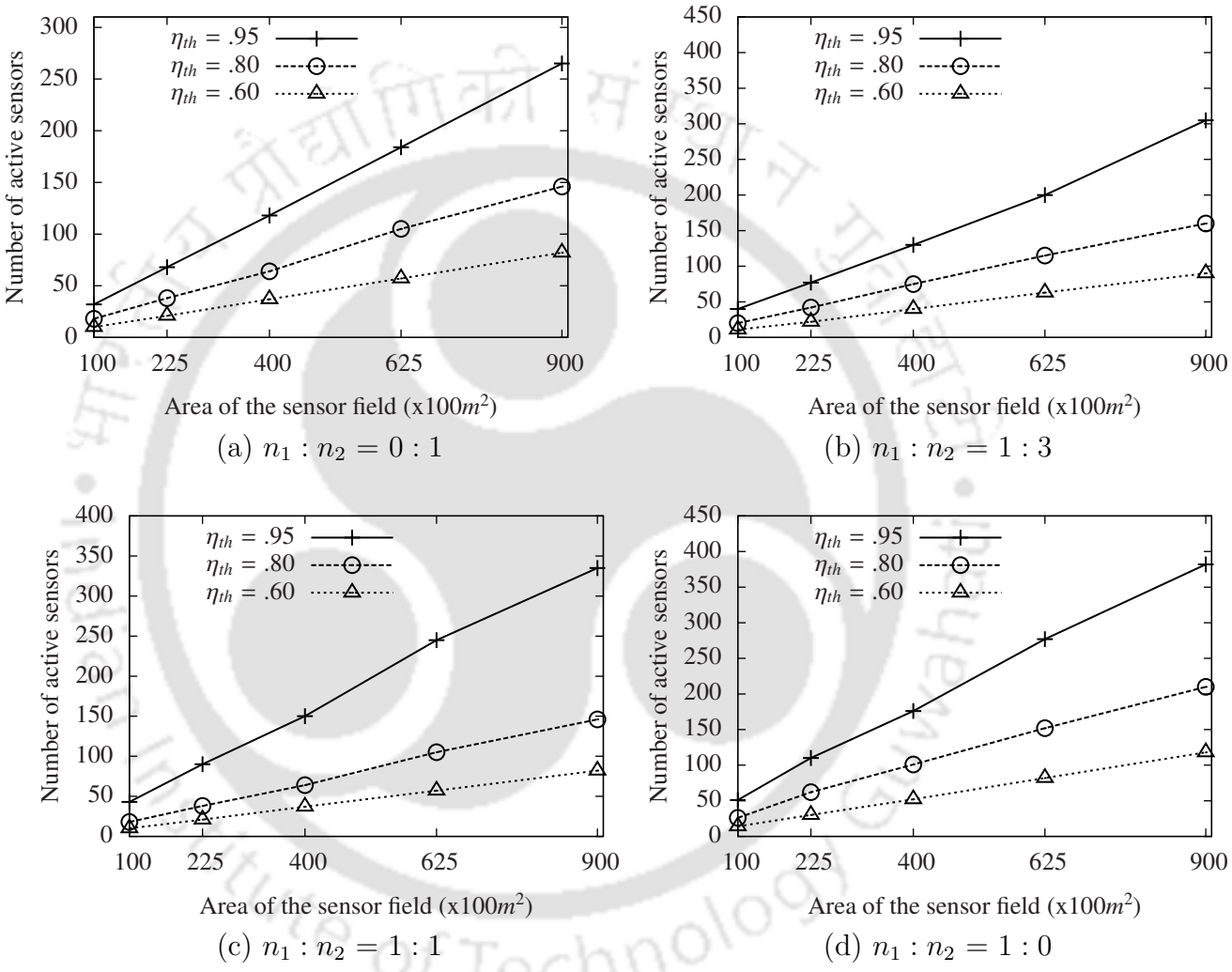

Figure 7.5 Relationship between the number of active sensors and the area of the FoI for different coverage ratios.

be concluded from all the results in Fig. 7.6 that when the scheduling protocol is not used, all the sensors remain active to provide complete coverage of the FoI for a short duration and then their energy drains out. This can be observed by a sudden drop in the actual coverage ratio after a few rounds. When the desired coverage ratio is only 0.6, the sensors continue to cover the FoI for much longer duration and the reduction in the QoC is also gradual. As sensors lose their energy, the actual coverage ratio goes below the desired level but the network is still active till all the sensors drain their energy. This gradual fall in the coverage ratio is absent if no scheduling protocol is used because even the redundant sensors consume their energy.

Next, we study if the network lifetime is prolonged by increasing the number of deployed sensors. For different coverage ratios, we increase the number of sensors deployed in $10,000m^2$ area and study the lifetime of the network in units of simulation rounds. The results are shown in Fig. 7.7. As expected, without scheduling protocol the network lifetime is unaffected by the number of sensors deployed since all the sensors remain active. On the other hand, the lifetime increases when the scheduling protocol is used to put redundant sensors to sleep because, only some of the sensors remain in active state (as observed in Fig. 7.4 and Fig. 7.5). The active sensors take turns in maintaining the desired coverage ratio and hence the energy of the sensors is evenly consumed.

• **Comparison with other protocols:** Finally, we compare the scheduling protocol proposed in this work with two of the existing protocols in the literature *viz.*, CCP [30] and PCP [66]. To the best of our knowledge, most of the existing sleep scheduling protocols [77, 76] rely on geographical information and work for homogeneous WSNs. This makes a direct comparison between the proposed protocol and the existing ones unfair. To make the comparison fair, we only use homogeneous WSN scenarios for this simulation. We use 600 sensors of the same type in $10,000m^2$ area and assume that the $\eta_{th} = 0.95$. Fig. 7.8(a) shows the number of active type 2 sensors required

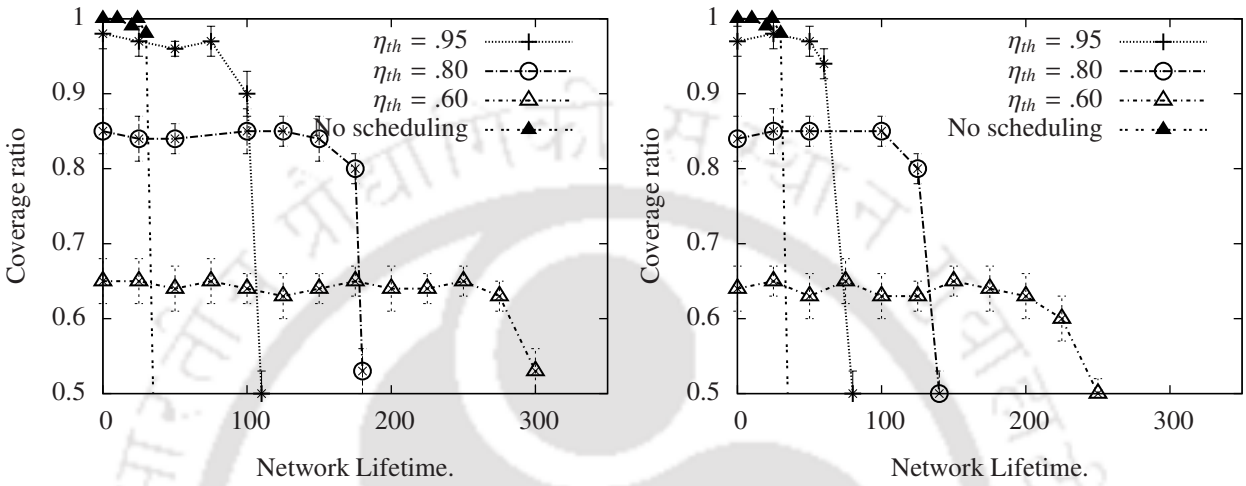

(a) $n_1 : n_2 = 0 : 1$ (b) $n_1 : n_2 = 1 : 3$

(c) $n_1 : n_2 = 1 : 1$ (d) $n_1 : n_2 = 1 : 0$

Figure 7.6 Demonstration of network lifetime for different values of desired coverage ratio.

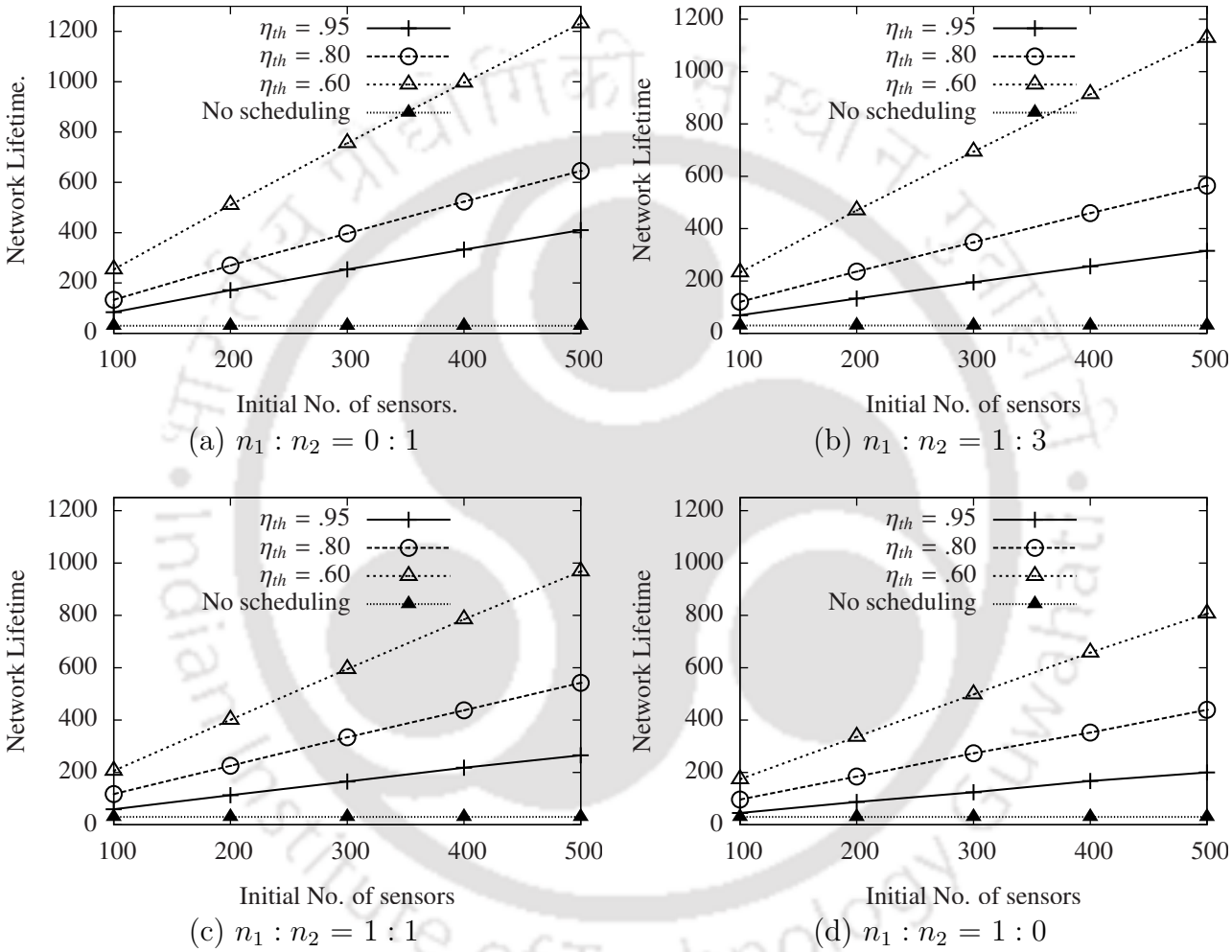

(a) $n_1 : n_2 = 0 : 1$ (b) $n_1 : n_2 = 1 : 3$

(c) $n_1 : n_2 = 1 : 1$ (d) $n_1 : n_2 = 1 : 0$

Figure 7.7 Relationship between coverage ratio and network lifetime with increasing number of sensors deployed.

at different times of the simulation for all the three protocols. The protocol proposed in this work requires the least number of active sensors for a desired coverage ratio throughout the duration of the simulation. Similarly, Fig. 7.8(b) shows that the number of active sensors is lowest in the proposed protocol with only type 1 sensors deployed. Thus, it can be concluded that the proposed protocol consumes lesser energy and prolongs the network lifetime when compared to CCP and PCP even in a homogeneous WSN scenario.

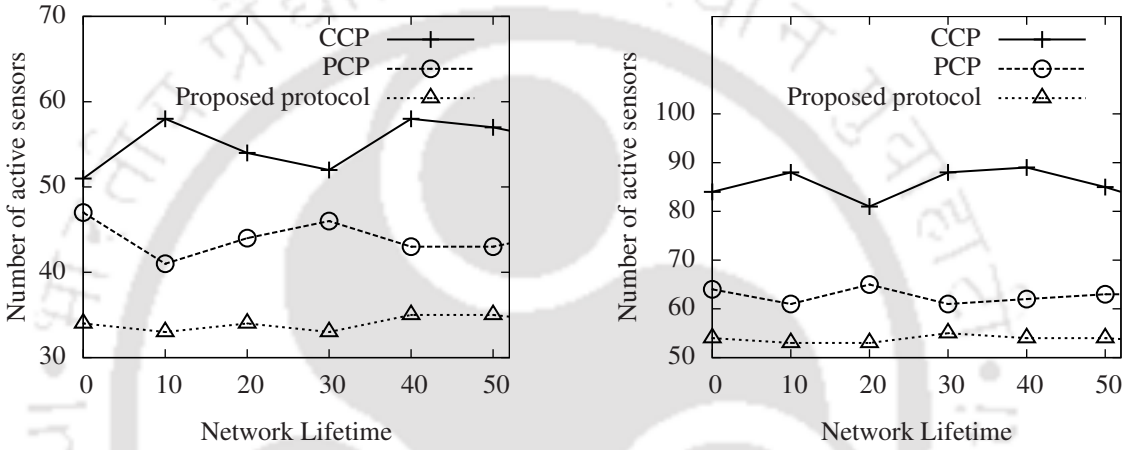

(a) $n_1 : n_2 = 0 : 1$ (b) $n_1 : n_2 = 1 : 0$

Figure 7.8 Comparison of the number of active sensors scheduled by the proposed protocol with two other protocols.

7.6 Conclusion

In this chapter, we proposed a probabilistic approach to determine the redundancy of sensors while satisfying partial coverage requirements for a heterogeneous WSN. We derived an expression to evaluate the expected redundancy degree of a sensor and used it to determine if a sensor is redundant for a desired coverage ratio of the FoI. We proposed a scheduling protocol to identify all the redundant sensors and schedule them to sleep while ensuring the QoC. The proposed protocol is completely distributed, does not use any geographic information, and uses only the information gathered about the neighbours with a few control messages. We validated the expression for expected

redundancy degree with numerical evaluation and simulations. We simulated the scheduling protocol for different network scenarios and demonstrated that the number of active sensors is reduced by the protocol and hence the network lifetime is increased.

Chapter 8

Conclusions and Discussion

This thesis has made five major research contributions to coverage and connectivity problems in heterogeneous WSNs with stochastic deployment of sensors. The main focus in the study was to estimate the critical sensor density for coverage and connectivity, and to prolong the network lifetime with sleep scheduling protocols.

In Chapter 3, we calculated the CSD required for a desired level of coverage of a FoI under border effects. Rather than using the area and the perimeter of the FoI (as in [1]), we used the exact geometry of FoI to compute the effective sensing area of uniformly deployed sensors. With this analysis, we could compute the sensing area that effectively contributes to the coverage of the FoI. Our results demonstrate the impact of border effects on CSD and clearly show that the geometry of the FoI should be considered to compute the CSD, particularly for a large area with a low density of sensors.

Chapter 4 studied the issue of k-coverage and connectivity in WSNs with stochastic deployment of sensors outside the FoI near the boundary. This work would be applicable for applications like canal water surface, railway track, and a road surface monitoring system where the sensors cannot be deployed directly inside the FoI to be monitored. Beyond this benefit, we also demonstrated an application of this work to

develop a traffic information acquisition system. The system can easily be deployed along the roadside for vehicle counting, classification, and direction detection. We believe that the proposed work can motivate further research in intelligent transport systems where the sensors are not required to be embedded at exact positions but can be deployed randomly along the edges.

In Chapter 5, we considered the directional sensing model and heterogeneity in the sensors to estimate the expected k-coverage and m-connectivity probability in 3D WSNs. We demonstrated an application in identifying the exact number of sensors of different types required for a desired level of coverage and connectivity such that the network cost is minimised. To this end, we showed that different types of sensors have different utility in coverage and connectivity which can be exploited to design 3D heterogeneous WSNs. We also considered the probability of the sensors being alive in a heterogeneous WSN and showed its impact on designing better WSNs.

In Chapter 6, we studied the coverage problem in 3D heterogeneous WSNs where each point in a FoI is covered by at least k sensors, $k \geq 1$. We derived an expression for the probability of a sensor, with a set of neighbours of different types, being redundant for k-coverage of the FoI. We observed that the number of neighbours required for redundancy of a sensor is lesser if the neighbours have larger sensing and communication ranges. We proposed a distributed scheduling protocol to put the redundant sensors to sleep yet maintain the desired level of coverage of the FoI. This protocol does not require the sensor to have any information about its geographical location/relative position to discover its redundancy. The proposed protocol out performed the existing protocols in prolonging network lifetime.

Finally, in Chapter 7, we focused on the problem of determining if a sensor is redundant in satisfying the partial coverage requirements. We used a probabilistic approach to determine the degree of redundancy in the coverage and proposed a scheduling protocol to identify the redundant sensors and put them to sleep. This

work showed that different types of sensors have different utility in coverage redundancy which can be used to design a heterogeneous WSN. For example, given the number of sensors of each type and the desired coverage ratio, the ratio of the number of sensors of different types to be deployed in the network can be determined with an objective of minimising the overall cost of the network or prolonging the network lifetime.

Future Directions

This thesis gives rise to a number of important research directions for coverage and connectivity of WSNs. Here we list some extensions to the work in this thesis.

- We have only considered the coverage problem for convex-shaped polygonal FoI while considering the border effects. Connectivity is complementary to coverage and it indicates how well the sensory data can be communicated by the sensors to the sink. The CSD required for both the coverage and connectivity in a polygon-shaped FoI could be a part of the future work.

- The application of traffic monitoring in campus considered in the work is very simple. In the future, sensors deployed outside the edges of the road could be considered for other ITS systems. The impact of heterogeneity in terms of sensing range, communication range, and/or probability of being alive could be studied.

- We estimated the expected k-coverage ratio and m-connectivity probability in 3D heterogeneous directional WSNs without considering the border effects in this work. Estimation of the CSD required for the coverage and connectivity in a regular-shaped 3D FoI is a challenging problem to be addressed in the future.

- We proposed scheduling protocols to identify all the redundant sensors and

schedule them to sleep while ensuring the desired level of coverage in heterogeneous WSNs. We did not consider connectivity in this work. Future work could include the design of scheduling protocols to identify all the redundant sensors and schedule them to sleep while ensuring the desired level of coverage and connectivity in heterogeneous WSNs. We also ignored the border effects. These could be addressed in the future to improve the design of energy-efficient WSNs.

Bibliography

[1] L. Lazos and R. Poovendran, "Stochastic coverage in heterogeneous sensor networks," *ACM Transactions on Sensor Networks*, vol. 2, no. 3, pp. 325–358, 2006.

[2] H. M. Ammari and S. K. Das, "Joint k-coverage and hybrid forwarding in duty-cycled three-dimensional wireless sensor networks," in *Proc. of SECON*, 2008, pp. 170–178.

[3] C.-F. Huang, Y.-C. Tseng, and L.-C. Lo, "The coverage problem in three-dimensional wireless sensor networks," *Journal of Interconnection Networks*, vol. 8, no. 3, pp. 209–227, 2007.

[4] B. Wang, "Coverage problems in sensor networks: A survey," *ACM Computing Surveys*, vol. 43, no. 4, pp. 32:1–32:53, 2011.

[5] X. Bai, Z. Yun, D. Xuan, B. Chen, and W. Zhao, "Optimal multiple-coverage of sensor networks," in *Proc. of INFOCOM*, 2011, pp. 2498–2506.

[6] H. M. Ammari and S. K. Das, "A study of k-coverage and measures of connectivity in 3D wireless sensor networks," *IEEE Transactions on Computers*, vol. 59, no. 2, pp. 243–257, 2010.

[7] Y. Li, C. T. Vu, C. Ai, G. Chen, and Y. Zhao, "Transforming complete coverage algorithms to partial coverage algorithms for wireless sensor networks," *IEEE*

Transactions on Parallel and Distributed Systems, vol. 22, no. 4, pp. 695–703, 2011.

[8] H. Jin, L. Wang, J.-Y. Jo, Y. Kim, M. Yang, and Y. Jiang, "EECCR:An energy-efficient m-coverage and n-connectivity routing algorithm under border effects in heterogeneous sensor networks," *IEEE Transactions on Vehicular Technology*, vol. 58, no. 3, pp. 1429 – 1442, 2009.

[9] L.-H. Yen, C. W. Yu, and Y.-M. Cheng, "Expected k-coverage in wireless sensor networks," *Ad Hoc Networks*, vol. 4, no. 5, pp. 636–650, 2006.

[10] H. Zhang and J. C. Hou, "On deriving the upper bound of α-lifetime for large sensor networks," in *Proc. of MobiHoc*, 2004, pp. 121–132.

[11] ——, "Is deterministic deployment worse than random deployment for wireless sensor networks?" in *Proc. of INFOCOM*, 2006, pp. 1–13.

[12] G. Paillard and V. Ravelomanana, "Limit theorems for degree of coverage and lifetime in large sensor networks," in *Proc. of INFOCOM*, 2008, pp. 2011–2019.

[13] "Surface water," http://www.ysi.com/.

[14] "Railway track," http://metrom-rail.com/track-monitoring-systems.

[15] "Country border," http://www.ultra-ccs.com/details/4.

[16] "Hardware survey," http://www.cse.unsw.edu.au/sensar/hardware/hardware_survey.html.

[17] "Tinyos," www.tinyos.net/.

[18] "Liteos," http://www.liteos.net/.

[19] "Contiki," www.sics.se/ contiki .

[20] "Large simulations in ns-2.34," http://www.isi.edu/nsnam/ns/ns-largesim.html.

[21] "Tossim," http://tinyos.stanford.edu/tinyos-wiki/index.php/TOSSIM.

[22] "Glomosim," http://pcl.cs.ucla.edu/projects/glomosim/.

[23] I. Chatzigiannakis, C. Koninis, G. Mylonas, S. Fischer, and D. Pfisterer, "WISEBED: an open large-scale wireless sensor network testbed," in *Proceedings of the 1st International Conference on Sensor Networks Applications, Experimentation and Logistics*, Sep. 2009. [Online]. Available: http://www.springerlink.com/content/l11255074h700524/

[24] "Senslab," http://www.senslab.info.

[25] "Indriya," indriya.comp.nus.edu.sg/.

[26] M. Cardei and J. Wu, "Coverage in wireless sensor networks." in *Handbook of sensor networks*. CRC Press, chapter 19, 2004.

[27] J. Rourke, "Open problem from art gallery solved," *International Journal of Computational Geometry & Applications*, vol. 2, pp. 215–217, 1992.

[28] J. Xiao, C. Qi, and L. Shu, "Research of coverage control algorithm in three-dimensional wireless sensor network based on energy efficiency," in *Proc. of CCDC*, 2012, pp. 3363–3368.

[29] M. K. Watfa and S. Commuri, "An energy efficient and self-healing 3-dimensional sensor cover," *IJAHUC*, vol. 3, no. 1, pp. 33–47, 2008.

[30] G. Xing, X. Wang, Y. Zhang, C. Lu, R. Pless, and C. Gill, "Integrated coverage and connectivity configuration for energy conservation in sensor networks," *ACM Transactions on Sensor Networks*, vol. 1, no. 1, pp. 36–72, 2005.

[31] V. Ravelomanana, "Extremal properties of three-dimensional sensor networks with applications," *IEEE Transactions on Mobile Computing*, vol. 3, no. 3, pp. 246–257, 2004.

[32] L. F. M. Vieira, M. G. Almiron, and A. A. F. Loureiro, "3D MANETs: Link probability, node degree, network coverage and applications," in *Proc. of WCNC*, 2011, pp. 2042–2047.

[33] L. Liao, W. Chen, C. Zhang, L. Zhang, D. Xuan, and W. Jia, "Two birds with one stone: Wireless access point deployment for both coverage and localization," *IEEE T. Vehicular Technology*, vol. 60, no. 5, pp. 2239–2252, 2011.

[34] P. Hall, *Introduction to the Theory of Coverage Processes.* John Wiley & Sons, 1988.

[35] R. Szewczyk and et. al., "Habitat monitoring with sensor networks," *ACM Commun*, vol. 47, no. 6, pp. 34–40, 2004.

[36] V. Dyo and et. al., "WILDSENSING: Design and deployment of a sustainable sensor network for wildlife monitoring," *ACM Transactions on Sensor Networks*, vol. 8, no. 4, pp. 29:1–29:33, 2012.

[37] Y. E. Aslan, I. Korpeoglu, and Ö. Ulusoy, "A framework for use of wireless sensor networks in forest fire detection and monitoring," *Computers, Environment and Urban Systems*, vol. 36, no. 6, pp. 614–625, 2012.

[38] P.-J. Wan and C.-W. Yi, "Coverage by randomly deployed wireless sensor networks," *IEEE/ACM Transactions on Information Theory*, vol. 52, no. 6, pp. 2658–2669, 2006.

[39] B. Wang, K. C. Chua, V. Srinivasan, and W. Wang, "Information coverage in randomly deployed wireless sensor networks," *IEEE Transactions on Wireless Communications*, vol. 6, no. 8, pp. 2994–3004, 2007.

[40] K.-S. Hung and K.-S. Lui, "On perimeter coverage in wireless sensor networks," *IEEE Transactions on Wireless Communications*, vol. 9, no. 7, pp. 2156–2164, 2010.

[41] J.-W. Lin and Y.-T. Chen, "Improving the coverage of randomized scheduling in wireless sensor networks," *IEEE Transactions on Wireless Communications*, vol. 7, no. 12, pp. 4807–4812, 2008.

[42] L. Mo and et. al., "Canopy closure estimates with greenorbs:Sustainable sensing in the forest," in *Proc. of ACM SenSys*, Nov. 2009, pp. 99–112.

[43] F. de Goes, D. Cohen-Steiner, P. Alliez, and M. Desbrun, "An optimal transport approach to robust reconstruction and simplification of 2D shapes," *Comput. Graph. Forum*, vol. 30, no. 5, pp. 1593–1602, 2011.

[44] P. Gritzmann and V. Klee, "Inner and outer j-radii of convex bodies in finite-dimensional normed spaces," *Discrete & Computational Geometry*, vol. 7, pp. 255–280, 1992.

[45] C. Zhang, X. Bai, J. Teng, D. Xuan, and W. Jia, "Constructing low-connectivity and full-coverage three dimensional sensor networks," *IEEE Journal on Selected Areas in Communications*, vol. 28, no. 7, pp. 984–993, 2010.

[46] C.-H. Ou and K.-F. Ssu, "Sensor position determination with flying anchors in three-dimensional wireless sensor networks," *IEEE Transactions on Mobile Computing*, vol. 7, no. 9, pp. 1084–1097, 2008.

[47] H. M. Ammari and S. K. Das, "Critical density for coverage and connectivity in three-dimensional wireless sensor networks using continuum percolation," *IEEE Transactions on Parallel and Distributed Systems*, vol. 20, no. 6, pp. 872–885, 2009.

[48] S.-Y. Cheung and P. Varaiya, "Traffic surveillance by wireless sensor networks: Final report," *Institute of Transport Studies, University of California, Berkeley, Tech. Rep.*, 2007.

[49] B. W. and et. al., "Road surface networks technology enablers for enhanced ITS," in *Proc. of IEEE VNC*, 2010, pp. 152–159.

[50] D. Tacconi and et. al., "Using wireless sensor networks to support intelligent transportation systems," *Ad Hoc Networks*, vol. 8, no. 5, pp. 462–473, 2010.

[51] P. A. and et. al., "Wireless sensor networks for traffic management and road safety," *IET Intell. Transp. Systems*, vol. 6, no. 1, pp. 67–77, 2012.

[52] S. Taghvaeeyan and R. Rajamani, "Portable roadside sensors for vehicle counting, classification, and speed measurement," *IEEE Transactions on Intel. Trans. Systems*, vol. 15, no. 1, pp. 73–83, Feb 2014.

[53] R. Wang and et. al., "Easisee: Real-time vehicle classification and counting via low-cost collaborative sensing," *IEEE Transactions on Intel. Trans. Systems*, vol. 15, no. 1, pp. 414–424, Feb 2014.

[54] X. Ta, G. Mao, and B. D. O. Anderson, "On the phase transition width of k-connectivity in wireless multihop networks," *IEEE Transactions on Mobile Computing*, vol. 8, no. 7, pp. 936–949, 2009.

[55] M. D. Penrose, "On k-connectivity for a geometric random graph," *Random Struct. Algorithms*, vol. 15, no. 2, pp. 145–164, 1999.

[56] G. Zhou, T. He, S. Krishnamurthy, and J. A. Stankovic, "Impact of radio irregularity on wireless sensor networks," in *Proc. of Mobisys*, 2004, pp. 125–138.

[57] "xbow," http://www.xbow.com/.

[58] L. Selavo, G. Zhou, and J. Stankovic, "Seemote: In-situ visualization and logging device for wireless sensor networks," in *BROADNETS*, 2006, pp. 1–9.

[59] S. Cho, C.-B. Yun, J. P. Lynch, A. Zimmerman, B. S. Jr., and T. Nagayama, "Smart wireless sensor technology for structural health monitoring of civil structures," *International Journal of Steel Structures*, vol. 8, no. 4, pp. 267–275, 2008.

[60] I.F.Akyildiz, D.Pompili, and T.Melodia, "Underwater acoustic sensor networks: Research challenges," *Ad Hoc Networks*, vol. 3, no. 3, pp. 257–279, 2005.

[61] H. Ma, X. Zhang, and A. Ming, "A coverage-enhancing method for 3D directional sensor networks," in *Proc. of INFOCOM*, 2009, pp. 2791–2795.

[62] X. Luo, M. Dong, and Y. Huang, "On distributed fault-tolerant detection in wireless sensor networks," *IEEE Transactions on Computers*, vol. 55, no. 1, pp. 58–70, 2006.

[63] M. Ding, D. Chen, K. Xing, and X. Cheng, "Localized fault-tolerant event boundary detection in sensor networks," in *Proceedings of INFOCOM*, vol. 2, 2005, pp. 902–913.

[64] G. Yang and D. Qiao, "Critical conditions for connected-k-coverage in sensor networks," *IEEE Communications Letters*, vol. 12, no. 9, pp. 651–653, 2008.

[65] C. Bettstetter, "On the minimum node degree and connectivity of a wireless multihop network," in *Proc. of MOBIHOC*, 2002, pp. 80–91.

[66] M. Hefeeda and H. Ahmadi, "Energy-efficient protocol for deterministic and probabilistic coverage in sensor networks," *IEEE Transactions on Parallel and Distributed Systems*, vol. 21, no. 5, pp. 579–593, 2010.

[67] L. Wang and Y. Xiao, "A survey of energy-efficient scheduling mechanisms in sensor networks," *Mobile Networks and Applications*, vol. 11, no. 5, pp. 723–740, 2006.

[68] F. Meng, H. Wang, G. Wei, and Z. Fan, "Energy-efficient and coverage-specific node scheduling for wireless sensor networks," in *Proceedings of MSWIM*, New York, NY, USA, 2010, pp. 368–375.

[69] X. Bai, C. Zhang, D. Xuan, and W. Jia, "Full-coverage and k-connectivity (k=14,6) three dimensional networks," in *Proc. of INFOCOM*, 2009, pp. 388–396.

[70] E. W. Weisstein, "Sphere-sphere intersection," 2012, [Online] Available: http://mathworld.wolfram.com/Sphere-SphereIntersection.html.

[71] R. Durrett, "Elementary probability for applications," *Cambridge University Press*, 2009.

[72] E. Bulut and I. Korpeoglu, "Sleep scheduling with expected common coverage in wireless sensor network," *Wireless Networks*, vol. 17, no. 1, pp. 19–40, 2011.

[73] "The network simulator - ns-2.34," http://www.isi.edu/nsnam/ns.

[74] Z. Zhou, S. R. Das, and H. Gupta, "Variable radii connected sensor cover in sensor networks," *ACM Transactions on Sensor Networks*, vol. 5, no. 1, pp. 89–124, 2009.

[75] C.-F. Huang, Y.-C. Tseng, and H.-L. Wu, "Distributed protocols for ensuring both coverage and connectivity of a wireless sensor network," *ACM Transactions on Sensor Networks*, vol. 3, no. 1, pp. 1–24, 2007.

[76] H. M. Ammari and S. K. Das, "Centralized and clustered k-coverage protocols for wireless sensor networks," *IEEE Transactions on Computers*, vol. 61, no. 1, pp. 118–133, 2012.

[77] K. Wu, Y. Gao, F. Li, and Y. Xiao, "Lightweight deployment-aware scheduling for wireless sensor networks," *Mobile Networks and Applications*, vol. 10, no. 6, pp. 837–852, 2005.

[78] Y. Li, C. Ai, Z. Cai, and R. Beyah, "Sensor scheduling for p-percent coverage in wireless sensor networks," *Cluster Computing*, vol. 14, no. 1, pp. 27–40, 2011.

[79] X. Wang, X. Wang, and J. Zhao, "Impact of mobility and heterogeneity on coverage and energy consumption in wireless sensor networks," in *Proceedings of IEEE ICDCS*, 2011, pp. 477–487.

List of Publications

Refereed Journal Papers

- **Hari Prabhat Gupta**, S.V. Rao, and T. Venkatesh, "Critical Sensor Density for Partial Coverage under Border Effects in Wireless Sensor Networks", IEEE Transactions on Wireless Communications, vol. 13, no. 5, pp. 2374-2382, March 2014. [Chapter 3]

Refereed Conference Papers

- **Hari Prabhat Gupta**, S.V. Rao, and T. Venkatesh, "Analysis of Stochastic k-Coverage in Wireless Sensor Networks with Boundary Deployment", In Proc. of IEEE WCNC, Istanbul, Turkey, April 2014. [Chapter 4]

- **Hari Prabhat Gupta**, S.V. Rao, and T. Venkatesh, "Critical Sensor Density for Fault-tolerant Coverage in 3D Heterogeneous Wireless Sensor Networks", In Proc. of IEEE ANTS, Chennai, India, December 2013. [Chapter 5]

- **Hari Prabhat Gupta**, S.V. Rao, and T. Venkatesh, "Analysis of the Redundancy in Coverage of A Heterogeneous Wireless Sensor Network", In Proc. of IEEE ICC, pages 1904 - 1909, Budapest, Hungary, June 2013. [Chapter 6]

- **Hari Prabhat Gupta**, S.V. Rao, and T. Venkatesh, "Sleep Scheduling for Partial Coverage in Heterogeneous Wireless Sensor Networks", In Proc. of COMSNETS, pages 1-10, Bangalore, India, January 2013. [Chapter 7]

Poster Presentations

- **Hari Prabhat Gupta**, S.V. Rao, and T. Venkatesh, "Minimum Sensor Density for Coverage in Sensor Networks", In ACM MobiHoc, Bangalore, July 2013 (Recent Results poster). [Chapter 3]

- **Hari Prabhat Gupta**, S.V. Rao, and T. Venkatesh, "Critical Sensor Density for Connectivity in Heterogeneous Wireless Sensor networks", In ACM MobiHoc, Bangalore, July 2013 (Recent Results poster). [Chapter 4]

- **Hari Prabhat Gupta**, S.V. Rao, and T. Venkatesh, "Analysis on the Redundancy of A Heterogeneous Wireless sensor Network", In 8^{th} TCS Technical Architects Global Conference, Delhi, India, May 2012 (Poster). [Chapter 3]

Journals Papers Under Review

- **Hari Prabhat Gupta**, S.V. Rao, and T. Venkatesh, "Analysis of Stochastic k-Coverage and Connectivity in Sensor Networks with Boundary Deployment". [Chapter 4]

- **Hari Prabhat Gupta**, S.V. Rao, and T. Venkatesh, "Analysis of Stochastic Coverage and Connectivity in 3D Heterogeneous Directional Sensor Networks". [Chapter 5]

- **Hari Prabhat Gupta**, S.V. Rao, and T. Venkatesh, "Sleep Scheduling Protocol for k-Coverage of Three-Dimensional Heterogeneous Wireless Sensor Networks". [Chapter 6]